



AD-E300 451

DNA 4590F

00 **い** こ AO

WIND-TUNNEL SHOCK-TUBE SIMULATION AND EVALUATION OF BLAST EFFECTS ON AN **©** ENGINE INLET

Kaman AviDyne 83 Second Avenue Burlington, Massachusetts 01803

15 March 1978

FILE 当

Final Report for Period October 1975-December 1977

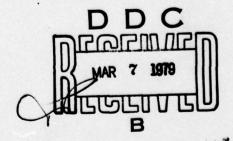
CONTRACT No. DNA 001-76-C-0107

APPROVED FOR PUBLIC RELEASE; DISTRIBUTION UNLIMITED.

THIS WORK SPONSORED BY THE DEFENSE NUCLEAR AGENCY UNDER RDT&E RMSS CODE 8342076464 N99QAXAE51014 H2590D.

Prepared for

Director **DEFENSE NUCLEAR AGENCY** Washington, D. C. 20305



79 01 22

Destroy this report when it is no longer needed. Do not return to sender.

PLEASE NOTIFY THE DEFENSE NUCLEAR AGENCY, ATTN: TISI, WASHINGTON, D.C. 20305, IF YOUR ADDRESS IS INCORRECT, IF YOU WISH TO BE DELETED FROM THE DISTRIBUTION LIST, OR IF THE ADDRESSEE IS NO LONGER EMPLOYED BY YOUR ORGANIZATION.

UNCLASSIFIED SECURITY CLASSIFICATION OF THIS PAGE (When Date Entered) READ INSTRUCTIONS REPORT DOCUMENTATION PAGE BEFORE COMPLETING FORM 3. RECIPIENT'S CATALOG NUMBER OVT ACCESSION NO. 459 DE 5. TYPE OF REPORT & PERIOD COVERED Final Reports for Briod WIND-TUNNEL SHOCK-TUBE SIMULATION AND EVALUATION OF BLAST EFFECTS ON AN ENGINE INLET Oct 75-Dec 77 KA-TR-147 AUTHOR(s CONTRACT OR GRANT NUMBER(S) DNA 901-76-C-0107 J. Ray Ruetenik Robert F. Smiley ERFORMING ORGANIZATION NAME AND ADDRESS PROGRAM ELEMENT, PROJECT, TASK Kaman AviDyne N990AXAE510-14 83 Second Avenue Burlington, Massachusetts 01803 11. CONTROLLING OFFICE NAME AND ADDRESS 12. REPORT DATE 15 March 2078 Director Defense Nuclear Agency 13. NUMBER OF PAGES 236 Washington, D.C. 20305 4. MONITORING AGENCY NAME & ADDRESS(if different from Controlling Office) 15. SECURITY CLASS (of this report) UNCLASSIFIED 15a. DECLASSIFICATION DOWNGRADING SCHEDULE 16. DISTRIBUTION STATEMENT (of this Report) Approved for public release; distribution unlimited. 17. DISTRIBUTION STATEMENT (of the abstract entered in Block 20, if different from Report) 18. SUPPLEMENTARY NOTES This work sponsored by the Defense Nuclear Agency under RDT&E RMSS Code B342076464 N99QAXAE51014 H2590D. 19. KEY WORDS (Continue on reverse side if necessary and identify by block number) Shock Tube Aircraft Computer Studies Inlet Pressure Subsonic Blast Engine Experimental Test Shock Wind Tunnel B-1This report describes 20. ABSTRACT (Continue on reverse side if necessary and identify by block number) A development and test program is described for simulation of blast wave intercepts with a scaled aircraft engine in subsonic flight, using the shock tube technique for firing the blast-type waves. The program initially consisted of preliminary theoretical calculations and tests with two-inchdiameter shock tubes fired into the AEDC IT transonic tunnel, followed by the design, construction and testing of three large 22.6 inch-diameter shock

DD FORM 1473 A EDITION OF 1 NOV 65 IS OBSOLETE

tubes. These shock tubes were installed in the AEDC 16T (16 foot square)

UNCLASSIFIED .

UNCLASSIFIED

of deg and 5 deg

SECURITY CLASSIFICATION OF THIS PAGE(When Date Entered)

20. ABSTRACT (Continued)

aircraft model. Forty-five firings were made, covering tunnel speeds of Mach 0, 0.55, 0.70, 0.85 and 0.90, blast overpressures (scaled to 1 atm. ambient pressure) from 2 to 6 psi, 6° and 5° yaw, and inlet flow rates representative of cruise and maximum power conditions. The model inlets were instrumented with 40 combination steady-state and dynamic total-pressure probes at each engine face section and other dynamic transducers to measure incident blast wave properties and inlet internal ramp and cowl pressures. The test data were digitized and used to determine time histories of inlet distortion during the blast encounter.

Calculations of blast pressures in the inlets made with the KA BID code satisfactorily reproduced the principal features of the observed inlet duct and engine face pressures.,

Blast-induced distortions during the time of definite blast-type flow in the inlet were generally smaller than but did sometimes exceed normal inlet allocation levels for the B-l aircraft. Distortions at later times greatly exceeded this allocation.

Four potentially adverse effects to engine operation from blast interaction were identified: blast-induced distortion, fan choking, afterburner blow-out and shock-boundary layer induced distortion.

A

UNCLASSIFIED

SECURITY CLASSIFICATION OF THIS PAGE(When Data Entered)

PREFACE

This work was performed by the AviDyne Division of the Kaman Sciences Corporation for the Defense Nuclear Agency under Contract DNA-001-76-C-0107. MAJ David W. Garrison of the DNA Shock Physics Directorate served as technical monitor to July 31, 1977, and CAPT Michael Rafferty from August 1, 1977, through the remainder of the program.

Dr. J. Ray Ruetenik of Kaman AviDyne was the project leader under Dr. Norman P. Hobbs, Technical Director of KA. Mr. Robert F. Smiley performed engineering functions. Professor Jack L. Kerrebrock, Professor and Director of the Gas Turbine and Space Propulsion Laboratories, MIT, served as technical consultant on propulsion.

Appreciation is expressed to MAJ Garrison and CAPT Rafferty for their continuing interest and significant support of this program. Appreciation is also expressed to CAPT William Tuck, AEDC, for test coordination, and the ARO personnel for their dedicated work, in particular Mr. H. Eldon McDill and Mr. Richard J. Christenson, Test directors of the 1T and 16T tests, respectively, and Mr. Karl F. Thormaehlen, mechanical engineer. Appreciation is also extended to Rockwell International personnel, particularly Mr. Ray L. Noonan, Mr. W. Robert Haagenson and Mr. Clarence E. Mitchell, for their contributions to the test program.

NTIS	White Section
DDC	Edif Section 🗖
UNAMMOUR	CED
JUSTIFICAT	ION
BY	
	SA/AVALASASTY CODES
BISTRIBUT	CODES SPECIAL

Conversion factors for U.S. customary to metric (SI) units of measurement.

To Convert From	То	Multiply By
angstrom	meters (m)	1. 000 000 X E -10
atmosphere (normal)	kilo pascal (kPa)	1.013 25 X E +2
bar	kilo pascal (kPa)	1.000 000 X E +2
barn	meter ² (m ²)	1.000 000 X E -28
British thermal unit (thermochemical)	joule (J)	1.054 350 X E +3
calorie (thermochemical)	joule (J)	4. 184 000
cal (thermochemical)/cm ²	mega joule/m ² (MJ/m ²)	4. 184 000 X E -2
curie	*giga becquerel (GBq)	3.700 000 X E +1
degree (angle)	radian (rad)	1. 745 329 X E -2
degree Fahrenheit	degree kelvin (K)	$t_{\mu} = (t^{\circ} f + 459.67)/1.8$
electron volt	joule (J)	1.602 19 X E -19
erg	joule (J)	1. 000 000 X E -7
erg/second	watt (W)	1.000 000 X E -7
foot	meter (m)	3. 048 000 X E -1
foot-pound-force	joule (J)	1. 355 818
gallon (U. S. liquid)	meter ³ (m ³)	3. 785 412 X E -3
inch	meter (m)	2. 540 000 X E -2
jerk	joule (J)	1.000 000 X E +9
joule/kilogram (J/kg) (radiation dose absorbed)	Gray (Gy)	1.000 000
kilotons	terajoules	4. 183
kip (1000 lbf)	newton (N)	4. 448 222 X E +3
kip/inch ² (ksi)	kilo pascal (kPa)	6. 894 757 X E +3
ktap	newton-second/m ²	0.004 101 A E +0
	(N-s/m ²)	1.000 000 X E +2
micron	meter (m)	1 000 000 X E -6
mil	meter (m)	2. 540 000 X E -5
mile (international)	meter (m)	1.609 344 X E +3
ounce	kilogram (kg)	2. 834 952 X E -2
pound-force (lbs avoirdupois)	newton (N)	4. 448 222
pound-force inch	newton-meter (N·m)	1. 129 848 X E -1
pound-force/inch	newton/meter (N/m)	1. 751 268 X E +2
pound-force/foot ²	kilo pascal (kPa)	4. 788 026 X E ~2
pound-force/inch ² (psi)	kilo pascal (kPa)	6. 894 757
pound-mass (lbm avoirdupois)	kilogram (kg)	4. 535 924 X E -1
pound-mass-foot ² (moment of inertia)	kilogram-meter ² (kg·m ²)	4. 214 011 X E -2
pound-mass/foot ³	kilogram/meter ³ (kg/m ³)	1. 601 846 X E +1
rad (radiation dose absorbed)	**Gray (Gy)	1.000 000 X E -2
roentgen	coulomb/kilogram (C/kg)	2. 579 760 X E -4
shake	second (s)	1.000 000 X E -8
slug	kilogram (kg)	1. 459 390 X E +1
torr (mm Hg, 0° C)	kilo pascal (kPa)	1, 333 22 X E -1

^{*}The becquerel (Bq) is the SI unit of radioactivity; 1 Bq = 1 event/s. **The Gray (Gy) is the SI unit of absorbed radiation.

A more complete listing of conversions may be found in "Metric Practice Guide E 380-74," American Society for Testing and Materials.

TABLE OF CONTENTS

			Page
1.	INTR	CODUCTION	11
2.	PREL	IMINARY INVESTIGATIONS FOR DEVELOPMENT OF TEST TECHNIQUE	13
	2.1	THEORETICAL STUDIES - REFLECT/S2D	13
	2.2	SHOCK TUBE FIRINGS IN AEDC 1T WIND TUNNEL	13
3.	DEVE	CLOPMENT OF 16T BLAST TEST FACILITY	21
		GENERAL DESIGN CRITERIA	21
		SHOCK TUBE DESIGN AND TESTING	22
		BLAST INPUT INSTRUMENTATION	30
	3.4	TUNNEL WALL MODIFICATIONS	30
4.	16T	WIND TUNNEL BLAST TEST PROGRAM	32
		GENERAL TEST SETUP	32
		MODEL AND INSTRUMENTATION DETAILS	32
	4.3	16T WIND TUNNEL TESTS	37
		4.3.1 Unyawed steady-state tests	39
		4.3.2 Yawed steady-state tests	39
		4.3.3 Shock tube firings	39
		DATA REDUCTION	42
	4.5	SAMPLE TEST RESULTS	42
	4.6		55
		4.6.1 Blast Input to the Inlets	55
		4.6.2 Shock Tube Location Effects on Blast Input and Inlet Response	61
5.	ANAL	YSIS OF 16T TEST RESULTS	66
	5.1	GENERAL PHENOMENA 5.1.1 Differences Between Shock Tube and	66
		Nuclear Blast Flows	76
	5.2		77
		ANALYSIS OF INLET DISTORTION	81
		5.3.1 Data Presentation	91
		5.3.2 Effects at low mass flow rates	91
		5.3.3 Effects at high mass flow rates	117
		5.3.4 Mach number effects	119
		5.3.5 Effects of yaw angle	119
		5.3.6 Long Duration Distortion Effects	119
		5.3.7 Concluding Remarks on Distortion Effects	121

TABLE OF CONTENTS (CONCL'D)

		Page
6.	COMPARISON OF THEORY AND EXPERIMENT	123
7.	SHOCK ORIENTATION EFFECTS	132
8.	INTERACTION OF BLAST SHOCK WITH THE ENGINE FAN	138
	8.1 QUASI-STEADY BLAST SHOCK INTERACTION WITH A FAN 8.2 BLAST SHOCK AT ENGINE FACE 8.3 ENGINE FAN CHARACTERISTICS	138 141 141
	8.4 BLAST EFFECT ON FAN OPERATION	141
	8.5 FAN REFLECTED SHOCK	147
9.	REFLECTED SHOCK-BOUNDARY LAYER INTERACTION WITHIN INLET	155
	9.1 SHOCK-BOUNDARY LAYER CALCULATION 9.2 SHOCK-BOUNDARY LAYER RESULTS	155 157
10.	DISCUSSION	164
	10.1 BLAST GENERATORS 10.2 16T WIND TUNNEL TESTS AND ANALYSIS	164 165
11.	CONCLUSIONS	170
REFE	RENCES	172
APPE	NDIX A - THEORETICAL STUDIES OF THE FLOW FIELD PRODUCED BY FIRING A SHOCK TUBE INTO A STATIONARY FLUID	175
	A.1 INTRODUCTION	175
	A.2 S2D CODE STUDIES	175
	A.3 REFLECT2 CODE STUDIES	177
	A.4 CONCLUSIONS	179
APPE	NDIX B - STEADY-STATE PRE-BLAST TEST CONDITIONS IN THE AEDC 16T TUNNEL	181
APPE	NDIX C - LIST OF COMMON SYMBOLS AND CONVENTIONS	231

LIST OF ILLUSTRATIONS

Figure		Page
2.1	Test setup for blast tests in the AEDC 1T transonic wind tunnel.	14
2.2	Shadowgrams of blast field produced by firing a shock tube into air at rest, $\Phi=90^{\circ}$.	16
2.3	Shadowgrams of blast field produced by firing a shock tube into a wind tunnel at Mach 0.80, Φ =90°.	17
2.4	Transient blast pressures for a firing of a shock tube into a Mach 0.75 wind tunnel flow, $\Phi=90^{\circ}$.	19
3.1	Top view of test installation in AEDC wind tunnel.	23
3.2	Blast test setup in the AEDC 16T transonic wind tunnel.	24
3.3	23-inch-diameter shock tube setup for testing.	28
3.4	Typical diaphragm rupture pattern.	29
3.5	Oblique view of a claw probe mounted above the inlet model.	31
4.1	Details of inlet model and engine simulation.	33
4.2	Closeup view of engine inlet and claw probes in the AEDC 16T wind tunnel.	34
4.3	Engine face transducer locations.	35
4.4	Inlet instrumentation.	36
4.5	Sample test results for Run 8 (Part 573), Mach 0.70, florate ≈ 303 lb/sec, tube 2, $\Delta p \approx 5.0$ psi.	w44
4.6	Typical blast pressure measurements for firings from three shock tubes, Mach 0.85, flow rate ≈ 300 lb/sec.	57
4.7	Comparison of engine face pressures for firings from shock tubes 2 and 3.	62
4.8	Comparison of blastward inlet ramp pressure time histories for Mach 0.85 firings from two shock tubes.	65
5.1	Variation of blast-induced side-slip angle with intercepangle and overpressure.	ot 67

LIST OF ILLUSTRATIONS (Cont'd)

Figure		Page
5.2	Variation of blast-induced total pressure with intercept angle and overpressure.	71
5.3	Inlet time-distance relationships.	78
5.4	Typical shock wave pattern in the inlets.	79
5.5	Distortion time histories for Run 8 (Part 573), Mach 0.70, $\Delta p=5.0$ psi; $\varphi=98^{\circ}$, flow rate ≈ 303 lb/sec, tube 2.	82
5.6	Range of distortion indices for B-1 inlet at subsonic cruise.	92
5.7	Distortion time histories for two overpressures at Mach 0.70, flow rate \approx 300 lb/sec, tube 2.	93
5.8	Distortion time histories for four overpressures at Mach 0.70 for the blastward inlet, flow rate $\approx 350~\text{lb/sec}$, tube 2.	94
5.9	Distortion time histories for three overpressures at Mach 0.70 for the leeward inlet, flow rate $\approx 350~\text{lb/sec}$, tube 2.	97
5.10	Distortion time histories for four overpressures at Mach 0.85 for the blastward inlet, flow rate $\approx 300~\rm lb/sec$, tube 1.	100
5.11	Distortion time histories for four overpressures at Mach 0.85 for the leeward inlet, flow rate $\approx 300~\rm lb/sec$, tube 1.	103
5.12	Distortion time histories for two overpressures at Mach 0.85, flow rate \approx 350 lb/sec, tube 2.	104
5.13	Distortion time histories for four Mach numbers for the blastward inlet, flow rate \approx 350 lb/sec, tube 2.	107
5.14	Distortion time histories for four Mach numbers for the leeward inlet, flow rate ≈ 350 lb/sec, tube 2.	110
5.15	Distortion time histories for four Mach numbers for the blastward inlet, flow rate $\approx 350~\text{lb/sec}$, tube 1.	113
5.16	Distortion time histories for four Mach numbers for the leeward inlet, flow rate \approx 350 lb/sec, tube 1.	114
5.17	Distortion time histories for three yawed runs at Mach 0.70, yaw = 5° , flow rate ≈ 350 lb/sec.	115

LIST OF ILLUSTRATIONS (CONT'D)

Figure		Page
5.18	Outboard inlet total pressure contours for a large blast-induced distortion condition.	118
5.19	Comparison of ramp pressure time histories for four Mach numbers, tube 2, flow rate $\approx 350~\text{lb/sec.}$	120
6.1	Comparison of theoretical and experimental time histories of ramp and cowl pressures at Mach 0.70, flow rate $\approx 350~\text{lb/sec}$.	125
6.2	Comparison of theoretical and experimental time histories of ramp pressures in the blastware inlet at Mach 0.85, tube 1 data, flow rate ≈ 350 lb/sec.	126
6.3	Comparison of theoretical and experimental time histories of ramp pressures in the blastward inlet at Mach 0.85, tube 2 data, flow rate \approx 350 lb/sec.	127
6.4	Comparison of theoretical and experimental time histories of cowl pressures at Mach 0.85, flow rate \approx 350 lb/sec.	128
6.5	Comparison of theoretical and experimental total pressure time histories at the engine face for the blastward inlet.	129
7.1	Comparison of engine face total pressure time histories for three blast intercept angles.	133
7.2	Comparison of engine face total pressure ratio time histories for three blast intercept angles.	135
8.1	Shock interaction with fan.	139
8.2	Configuration of NASA two-stage axial-flow fan.	143
8.3	Performance maps for NASA two-stage axial-flow fan.	144
8.4	Two-stage-fan overall performance map.	146
8.5	Variation of fan reflected shock properties with incident shock pressure ratio.	148
8.6	Variation of fan transmitted shock properties with incident shock pressure ratio.	153
9.1	Boundary layer separation and distortion from fan reflected shock wave.	156
9.2	Effect of fan reflected shock on boundary layers	158

LIST OF ILLUSTRATIONS (CONCL'D)

Figure		Page
9.3	Inlet time-distance relationships for a flight Mach number of 0.85 and a mass flow rate of 350 lb/sec.	162
A.1	Problem of a shock tube firing into a stationary fluid.	176
A.2	Theoretical blast pressures outside of a shock tube.	178
A.3	Variation of overpressure with distance from shock tube.	180

LIST OF TABLES

<u>Table</u>		Page
4.1	Locations of dynamic pressure transducers	38
4.2	Nominal test conditions	40
4.3	Steady-state yaw conditions	41
4.4	16T wind tunnel test conditions	43
5.1	Equations for calculating distortion parameters IDC, IDR, IDL, IDA and IDT.	89
8.1	Inlet data of Run 40 (Part 619) pertinent to blast shock-fan interaction.	142

and the second of the second o

SECTION I INTRODUCTION

This study is concerned with the simulation of the situation where an aircraft inlet is subjected to a blast wave of sufficient strength and long enough duration to produce significant distortion of the flow field at the engine face. For critically designed engine-inlet systems, such blasts, produced by nuclear explosions, might cause severe engine stall or flameout problems.

The objective of the test program reported here was to develop a test technique for measuring blast interaction with an aircraft inlet and to conduct a series of tests for the development of prediction methods.

Wind tunnels provide a well-developed means for the simulation of flight flow conditions for an engine inlet. A technique for the simulation of blast waves in a supersonic wind tunnel by employing a shock tube mounted in the wind tunnel wall has been demonstrated by Pierce (Ref. 1.1).

A development and test program, conducted at the Arnold Engineering Development Center (Ref. 1.2), is reported here for the simulation of blast wave intercepts with a scaled aircraft inlet in subsonic flight using the shock-tube technique for firing the blast-type waves. Pilot tests of the technique were performed in a 1-ft wind tunnel during August 1975, followed by "bench" tests of a prototype shock tube during August 1976. A wind tunnel test program then was conducted in the AEDC 16T wind tunnel with a 0.1-scale B-1 inlet during September 24-28, 1976.

This report is concerned primarily with documentation of the development of the facility to test the response of engine-inlet systems to blast waves in high speed wind tunnels, with the presentation of test results from the facility for a 0.1-scale aircraft inlet, and with the discussion and application of associated analytical techniques to predict inlet behavior in a blast environment.

Section 2 of the report describes preliminary analytical studies and small model wind tunnel tests performed to assess the feasibility of performing well controlled inlet blast tests in a high speed wind tunnel with blast waves produced by shock tubes fired into the tunnel. Section

3 describes the subsequent development of a large shock tube facility for use in the AEDC 16T (16 foot square) transonic wind tunnel (Ref. 1.2). Section 4 describes and presents sample results of a blast test program performed in this facility, using three 23 in.-diameter shock tubes and a 0.1-scale B-1 inlet model. Section 5 presents a general analysis of the test results, pointing out some basic characteristics of the inlet blast interaction process and presenting an analysis of the inlet distortion measurements obtained during the tests.

Section 6 presents a comparison of experimental blast pressure time histories with theoretical calculations made with the BID computer code. Section 7 supplements the test results by presenting some blast calculations made with the BID code to illustrate some blast-inlet interaction effects over a greater range of blast intercept angles than were covered by the tests.

Section 8 discusses the interaction of a blast-induced inlet shock with an engine fan and Section 9 discusses blast-induced boundary layer interactions in an inlet.

The overall study results are discussed in Section 10 and conclusions are given in Section 11.

Appendix A discusses some theoretical studies of the firing of a shock tube into a stationary fluid. Appendix B presents the steady-state pre-blast measurements made during the 16T tests.

SECTION II

PRELIMINARY INVESTIGATION FOR DEVELOPMENT OF TEST TECHNIQUE

As the first stage of the development of a wind-tunnel shock-tube blast test facility, a program of preliminary theoretical calculations and model tests was undertaken to establish the feasibility of the test concept and to provide design information for construction of a full-scale installation.

2.1 THEORETICAL STUDIES-REFLECT/S2D

The first development step consisted of theoretical calculations for the problem of a circular shock tube fired into stationary air. These calculations, made with the Kaman AviDyne REFLECT-2 and S2D computer codes (see Appendix A) indicated that useful shock wave patterns simulating nuclear blast wave patterns in the 2 to 5 psi overpressure range could be obtained at distances 3 to 10 diameters downstream of the end of a shock tube. In particular, these calculation results, summarized in Appendix A, indicated that, at a distance of about 4.5 diameters downstream of the end of a shock tube, a blast duration of nearly constant overpressure could be obtained for about 2.5 milliseconds per foot of tube diameter.

2.2 SHOCK TUBE FIRINGS IN AEDC 1T WIND TUNNEL

Using the results of the above theoretical calculations as a guideline, a small 2 in.-dia shock tube was constructed and was fired into the AEDC 1T (one-foot-square) transonic wind tunnel for a wide range of flow and shock tube conditions, during which pressure measurements were made for a large number of locations inside the wind tunnel.

The geometric setup used in the AEDC 1T tunnel is indicated in Figure 2.1. Three shock tube configurations were tested, about 14 inches long, with ratios of the driven-tube lengths to driver-tube lengths of about 0.5, 2 and 8. The end of each shock tube protuded into the tunnel by about one inch (perpendicular to the floor) where it was terminated by a 8 in-dia. circular flange (Fig. 2.1). Firings were made with the angle of the shock tube axis to the tunnel axis, Φ , (see Figure 2.1), being 90° , 60° and 45° . Tunnel ambient pressures were in

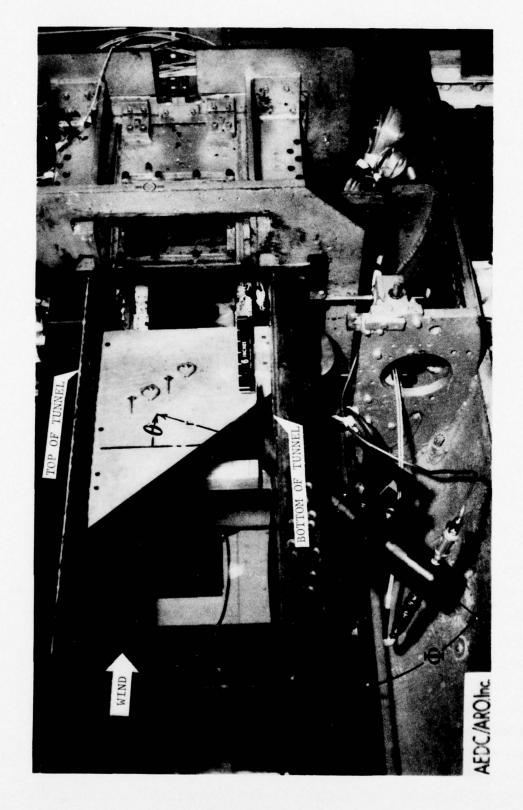


Figure 2.1. Test setup for blast tests in the AEDC 1T transonic wind tunnel (tunnel side walls removed).

the range 11 to 16 psia and shock tube driver pressures ranged from about 60 to 380 psia.

Transient blast pressure measurements were made inside the wind tunnel by means of pressure transducers imbedded in the surface of a thin plate placed in the plane of symmetry, as shown in Figure 2.1. Measurements were made of local blast pressure time histories for radial distances from the shock tube exit of 2.5, 3.5 and 4.5 tube diameters (r/d) and for polar angle locations (θ in Fig. 2.1) of -15° , 0° , 15° , 30° , 45° , 60° and 75° . Also, for several locations, measurements of transient total pressure and flow velocities were made with two total-pressure and two claw probes mounted about a half inch from the face of the thin plate, as shown in the figure. Kulite XCQL-093-025 pressure transducers were used in the plate and probes.

Sample shadowgrams showing the blast field produced by firing the 2-in shock tube into the wind tunnel are presented in Figures 2.2 and 2.3. Figure 2.2 shows three shadowgrams of one firing into still air and Figure 2.3 shows two shadowgrams for a firing into a Mach 0.8 tunnel flow. The shadowgrams are taken looking into the side of the tunnel, with the tunnel flow proceeding from left to right, and with the shock tube being fired into the tunnel vertically up $(\Phi=90^{\circ})$ through the bottom wall of the tunnel.

In Figure 2.2, the lowest shadowgram was taken first (before blast exit from the tubes) and the upper one last. The blast front can be clearly seen in these shadowgrams and becomes essentially a circular arc after the front of the blast wave has moved several tube diameters away from the tube exit. In the upper shadowgram of Figure 2.2, between the top of the blast front and the shock-tube exit is seen a nearly horizontal dark line which roughly delineates the contact surface between the "hot" tunnel air (above) and the "cold" expanded air (below) from the driver section of the shock tube. This cold gas can also be more clearly seen as the dark jet core in Figure 2.3. From the viewpoint of simulating a nuclear blast or other long-duration blast wave, it should be noted that only that portion of the blast wave lying between the blast front and the hot-cold gas contact surface is of interest.

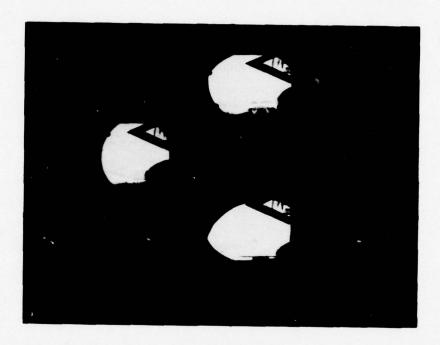


Figure 2.2. Shadowgrams of blast field produced by firing a shock tube into air at rest, $\phi = 90^{\circ}$.

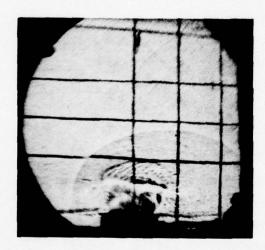


Figure 2.3. Shadowgrams of blast field produced by firing a shock tube into a wind tunnel at Mach 0.80, ϕ = 90°.

The effect of the tunnel flow on the shape of the blast shock front was found to be relatively small in the sense that the blast front shape remained essentially circular for all Mach numbers tested (up to 0.9), but, of course, the pattern is convected downstream more with increasing tunnel speed. The central cold-gas core also tends to be convected downstream (Fig. 2.3), but less so than the blast front.

Pressure time histories obtained from all transducers were digitized by ARO and were subsequently provided in the form of plots, tabulations and magnetic tapes (Ref. 2.1).

Sample pressure measurements in the blast field are shown in Figure 2.4 for the shock tube normal to the tunnel axis, $\Phi=90^{\circ}$, measured at a radial distance of 4.5 tube diameters from the tube exit, at a tunnel Mach number of 0.8 and a ratio of tube driver pressure to driven pressure of about 10. It should be noted that for a polar angle (θ in Figure 2.1) of 15° a blast wave is produced with a nearly constant pressure level for about 0.2 milliseconds. In the polar angle range - 15° to 30° useful nearly-constant blast durations of at least 0.1 millisecond are seen to have been produced; but for larger angles ($\theta \geq 45^{\circ}$) the pressure has an initial spike-behavior which makes it of little value for simulating blast shocks of long duration.

Similar results to those shown in Figure 2.4 were obtained for most conditions tested, covering shock-tube angles (Φ) of 45, 60 and 90 degrees to the tunnel axis, tunnel Mach numbers of 0, 0.6, 0.75 and 0.9 and driver/driven-tube pressure ratios between about 4 and 30. Useful nearly-constant pressure blast durations up to a maximum of about 0.3 millisecond were obtained for some conditions.

In order to provide a more quantitative index of the obtained duration of nearly constant pressure, estimates were made for the 90° tube angle ($\Phi = 90^{\circ}$) from curves like Figure 2.4 of the time, t_{30} , required for the blast overpressure to decay (or increase) 30 percent from the initial shock value. For blast overpressures between 2 and 5 psi at a radial distance of 4.5 diameters (r/d = 4.5), the 30-percent-

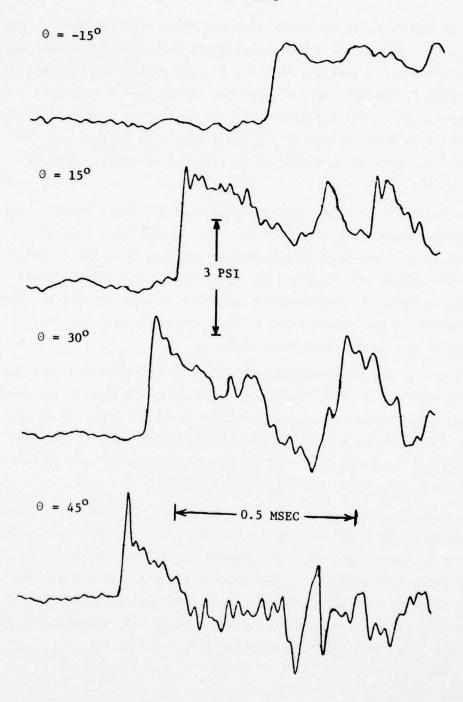


Figure 2.4. Transient blast pressures for a firing of a shock tube into a Mach 0.75 wind tunnel flow, ϕ = 90°.

A STANDARD OF THE STANDARD OF

decay time was found to generally increase about linearly with increasing overpressure. In the 4 - 5 psi overpressure range the decay time was about 0.16 msec or 1 msec/ft. dia. for a polar angle (θ) of 0° and about 0.09 msec or 0.5 msec/ft for 30° , and did not appear to vary much with Mach number. For a polar angle of 15° the decay time decreased considerably with increasing Mach number; at the 5 psi level, it appeared to vary from about 0.3 msec or 2 msec/ft at Mach 0.6 to about 0.18 msec or 1.1 msec/ft at Mach 0.9.

The angle of the tubes to the tunnel axis (Φ) had a marked effect on the blast waves that were produced. As the angle was reduced, causing the blast to be fired more in the downstream direction, the resulting shock overpressure was lower and the overpressure at a fixed point decayed more rapidly. Satisfactory results were obtained for the tube at 90 degrees to the tunnel axis, so this angle was selected for later development of a large shock tube facility.

Blast pressure waveforms were found to be relatively insensitive to the shock-tube driven-tube/driver length ratio in the useful early-time (hot-gas) part of the flow period. Hardly any difference was observed between the waveforms for the length ratios of 0.5 and 2.0, but some waveforms for the length ratio of 8 had somewhat shorter nearly-constant durations than those for the other length ratios.

To summarize the test results, it appeared that useful long duration blast waves could be obtained by firing shock tubes into a wind tunnel operating at speeds up to at least Mach 0.9. Nearly constant pressure blast durations lasting up to a maximum of about 2 milliseconds per foot of tube diameter were obtained for some firing conditions and the longest duration of nearly constant pressure blast waves was obtained at polar angles (θ) from the shock tube of about 15° .

SECTION III DEVELOPMENT OF 16T BLAST TEST FACILITY

Having established the feasibility of shock tube-wind tunnel blast tests by small model tests in the 1T tunnel, a program was undertaken to develop and apply a similar large shock tube facility for engine inlet testing in the AEDC 16T (sixteen foot square) transonic wind tunnel (Ref. 2.1). Development of this facility consisted of selection and modification of a inlet model, shock tube design, construction and testing, selection of dynamic instrumentation for measuring the blast field, and tunnel modifications.

The test installation was designed to take as much advantage as possible of existing hardware and fixtures.

3.1 GENERAL DESIGN CRITERIA

The inlet model selected for blast testing in the AEDC 16T tunnel is designated as the 0.1-scale B-1 Inlet Development Model II. This model was selected as having a representative transonic inlet of modern design which was already well instrumented with dynamic pressure engine face transducers of high enough frequencies to respond to blast induced transients. The model required only small modifications to strengthen it for blast testing and it was compatible with existing mounting fixtures for the 16T tunnel.

The important features of the model with respect to shock tube design are the size of the inlet opening, which is about 5.5" long by 4.4" wide by 3.3" high for each inlet, and the length of the inlet, about 25".

Other model characteristics are discussed in Section 4.2.

The shock tubes had to be designed to produce a sufficiently small variation of incident shock pressure across the above inlet opening. Also the duration of the blast wave produced had to be at least long enough so that the blast wave does not decay significantly before its front has had time enough to pass down the inlet into the engine and to be reflected back past the engine face.

It appeared that the most cost-effective facility design satisfying the above requirements was to position the test model near the center of the tunnel, permitting use of existing fixtures, and to mount shock tubes in both tunnel walls, two in one wall and one in the other, as indicated in Figures 3.1 and 3.2. This design concept, using three shock tubes, permitted the firing of three blast waves at the model before the tunnel had to be shut down to change shock tube diaphragms, thus saving considerable time and expense. Dimensions and orientations of the three shock tubes were chosen to conform as close as practical to the optimum conditions obtained from the 1T model tests, namely, ratio of tube-to-inlet distance to tube diameter of about 4.5, polar angles from shock tube to inlet (θ) between -15° and +30°, with about 15° being optimum, and shock tube axis perpendicular to tunnel wall $(\Phi=90^{\circ})$. A common inside diameter of 22.6 inches appeared to be the best choice, which gave distance/diameter ratios of 4.3, 3.8 and 4.3 for shock tubes 1, 2, and 3, respectively. The resulting geometrical arrangement of tunnel, shock-tubes and model is shown schematically in Figure 3.1 and photographs of the setup are presented in Figure 3.2.

With respect to the question as to how uniform the blast pressure would be across the inlet opening, the results of the 1T tests indicated that for the above-selected model and shock tube geometry, the intensity of the blast wave would generally vary across one inlet not more than \pm 2 percent from the mean value and at worst not exceeding \pm 4 percent.

3.2 SHOCK TUBE DESIGN AND TESTING

Using the guidelines discussed in Section 3.1, ARO designed and constructed three similar 22.6 in-dia shock-tube blast generators for

when the spine or will

A necked down shock tube driven section having a 13.1-inch exit diameter was also designed as an insert for any of the three shock tubes. This smaller diameter insert was constructed and several static firings were made with it to explore the possibility of obtaining a better blast waveform at low blast pressures than could be obtained with the large diameter tubes. This insert was also intended to provide more flexibility in the range of blast overpressures which could be obtained with a particular pair of diaphrams. However, the few firings made with this insert produced no obviously improved waveforms and the time required to install and remove the insert from a shock tube when installed in the 16T wind tunnel proved to be too long to be tolerated for the limited test time available. Consequently, no wind tunnel firings were made with the small diameter driven section insert.

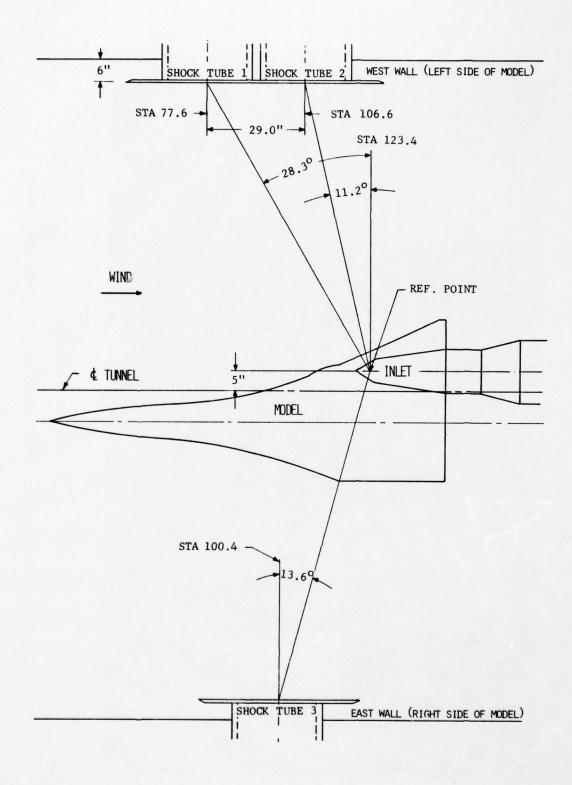
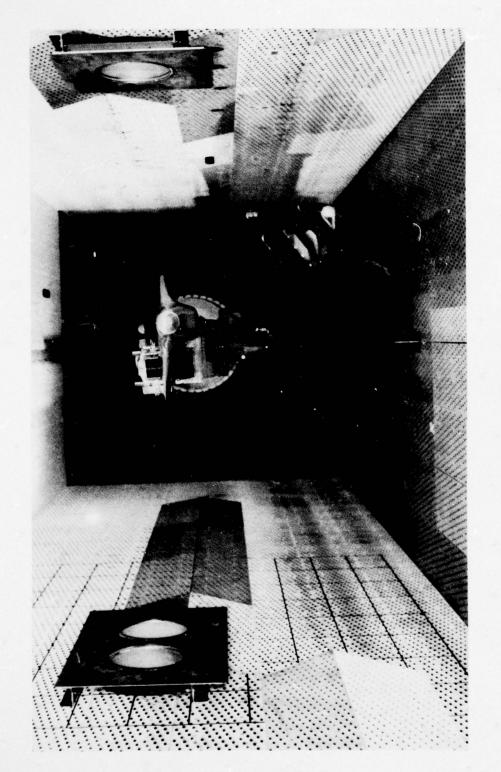
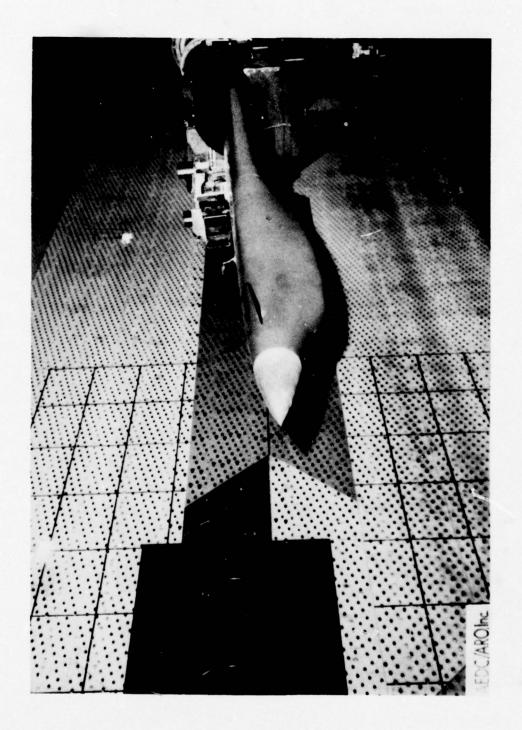


Figure 3.1. Top view of test installation in AEDC wind tunnel.



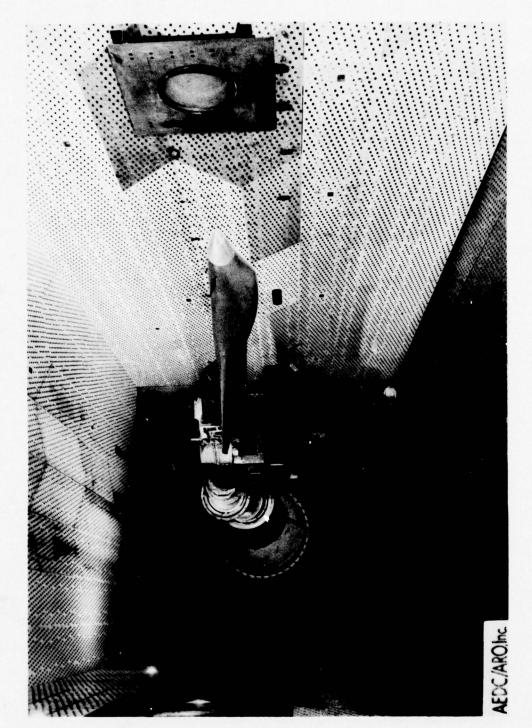
(a) View looking downstream.

Figure 3.2. Blast test setup in the AEDC 16T transonic wind tunnel.



(b) View showing model forebody and west wall.

Figure 3.2. Continued.



(c) View showing model, supports and east wall.

Figure 3.2. Concluded.

firing shock waves into the AEDC 16T tunnel. Some details of one of these tubes can be seen in Figure 3.3. The shock tube is about 17 feet long. The driven-tube length is about twice the driver tube length. The tube has a double diaphragm construction, and uses pre-scored pre-stressed 24 in-dia diaphragms. Diaphragms are constructed either of aluminum, nickel steel or 316 stainless steel, depending on the firing pressure level.

All three shock tubes had essentially the same design dimensions except that the ratio of the length of the driven section to that of the driver section had to be varied somewhat to permit close mounting of two of the tubes side by side in the 16T tunnel without interference. Judging from the results of the 1T tests (Sec. 2.2), these differences in lengths would not be expected to produce any significant differences between the blast waves generated by the three tubes.

Considerable effort was devoted to the design and operational use of the diaphragms. A series of 17 static firings was run to establish the range of loading pressures and other requirements for achievement of satisfactory diaphragm bursts in respect to the blast wave produced and avoidance of ejecta. A typical diaphragm break pattern is shown in Figure 3.4. The diaphragms generally broke cleanly on the pre-scored lines, forming four petals, and never produced any observable flying metallic debris.

Shock-tube operations were automated as much as possible in order to obtain a maximum number of firings in the few test days available for wind tunnel testing. Semi-automated diaphragm removal and replacement required less than 15 minutes per diaphragm pair and nearly fully automated pressurization and firing of a shock tube generally took less than 5 minutes.

The above-mentioned 17 static firings, made in the AEDC 16S wind tunnel facility at an ambient pressure of 0.5 atmosphere at driver pressures from 62 to 233 psia, were also utilized to obtain measurements of blast overpressures and impact pressures produced by the shock tube flow, both for protective design of wind tunnel equipment to be in the path of the jet from the shock tube and for providing a guide for diaphram

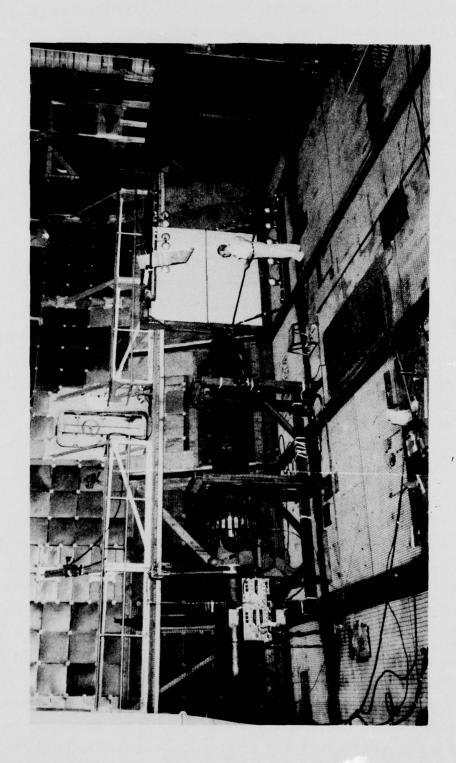


Figure 3.3. 23-inch-diameter shock tube setup for testing.

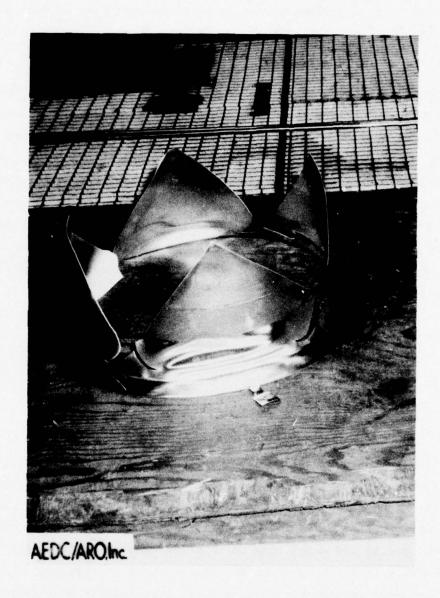


Figure 3.4. Typical diaphragm rupture pattern.

The state market of the state of the

selection to achieve desired levels of blast overpressure at the test model during wind tunnel firings.

3.3 BLAST INPUT INSTRUMENTATION

In order to provide measurements of blast wave intensity and direction as the blast wave strikes the inlet, three similar claw probes were designed to be mounted on or near the test model. Figure 3.5 shows a photograph of one of these probes mounted above the tested inlet. Each probe consists basically of two 45°-swept claw arms (90° apart) with Kulite series XCQL-093-025 type dynamic pressure transducers at the tips, to measure total pressure and flow direction, and of a flat plate surface toward the rear of the probe with one static pressure orifice and one imbedded Kulite LQ series wafer pressure transducer to measure the pre-blast and transient "static" blast pressures, respectively. The three claw probes were calibrated in the AEDC 16T tunnel for sideslip angles from about -50 to +50 degrees at Mach numbers of 0.6, 0.7, 0.85 and 0.95. The calibration data indicated that the probes could provide reasonable estimates of flow characteristics for sideslip angles between about -30 and +30 degrees.

3.4 TUNNEL WALL MODIFICATIONS

Preliminary KA estimates of the forces which would be imposed on the 16T wind tunnel wall opposite a firing shock tube indicated that the local wall pressures could greatly exceed the tunnel wall design criterion of 3 psi differential pressure. To obtain design information on such wall loads, during the shock tube calibration test (Sec. 3.2), ARO fired one of the 22.6 in-dia shock tube at a large plate instrumented with an array of pressure transducers. Using these test results as a guideline, the tunnel walls were strengthened in critical areas. In the subsequent test program in the wind tunnel, no damage was experienced to the tunnel walls during any shock tube firing.

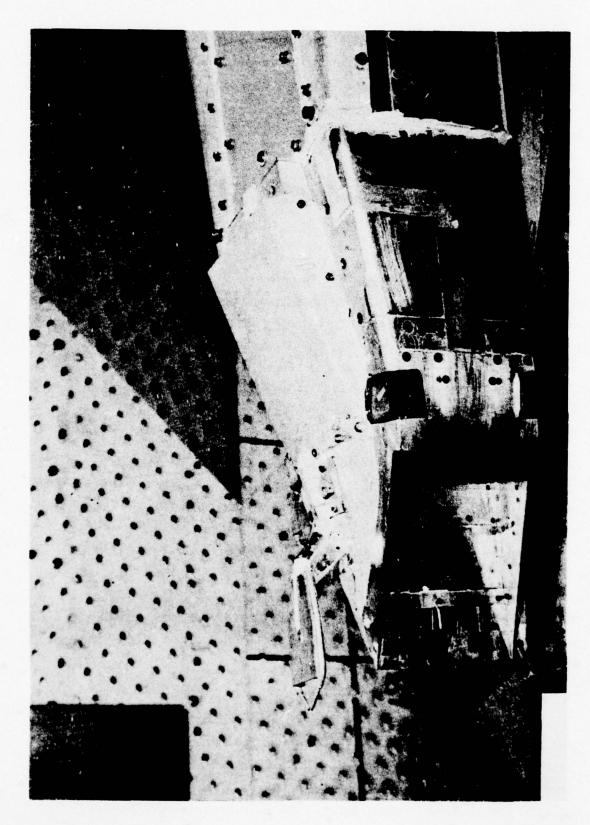


Figure 3.5. Oblique view of a claw probe mounted above the inlet model.

SECTION IV

16T WIND TUNNEL BLAST TEST PROGRAM

Following development of the 16T wind tunnel blast test facility, a series of 45 wind tunnel shock tube firings were performed with the 0.1-scale B-l inlet model. This section presents a discussion of the details of the test setup, instrumentation, and firing conditions and presents and discusses some aspects of sample data obtained from the tests.

4.1 GENERAL TEST SETUP

As was mentioned in Section 3, the test setup consisted of a 0.1-scale B-1 model installed in an inverted position near the center of the AEDC 16T transonic tunnel, with three shock tubes projecting through the tunnel side walls (Fig. 3.1). Figure 3.2 presents photographs of the model and shock tube setup inside the tunnel. Various details of model construction are shown in Figures 3.5, 4.1 and 4.2. During all tests the model was maintained at an angle of attack of +3 degrees.

Blast waves can be fired at the model inlet from any of the three 22.6 in-dia shock tubes seen projecting into the tunnel about 6 inches from the side walls in Figure 3.2. The shock-tube axes are perpendicular to the side walls $(\Phi=90^{\circ})$ and the axis of each tube is located at a fixed location between 1 and 4 feet upstream of the inlet opening, so that, for all three shock tubes, the inlet is located within the polar angle range (θ) 12 to 29 degrees from the shock-tube exit (Figure 3.1), the angles being 28.3° , 11.2° and 13.6° for tubes 1, 2 and 3, respectively. These locations were chosen to give blast waves of as long duration as practical, whose fronts would generally strike the inlet roughly side-on or slightly from the rearward.

4.2 MODEL AND INSTRUMENTATION DETAILS

The most important features of the inlet model used for the blast test are illustrated in Figures 4.1 through 4.4 (see also Ref. 4.1). The model is a 0.1-scale representation of the forward part of the B-1 aircraft fuselage with a left-hand stub wing set at the 67.5°- sweep position and a left-hand dual inlet. The normally variable geometry

5

Figure 4.1. Details of inlet model and engine simulation. (Rockwell arawing)

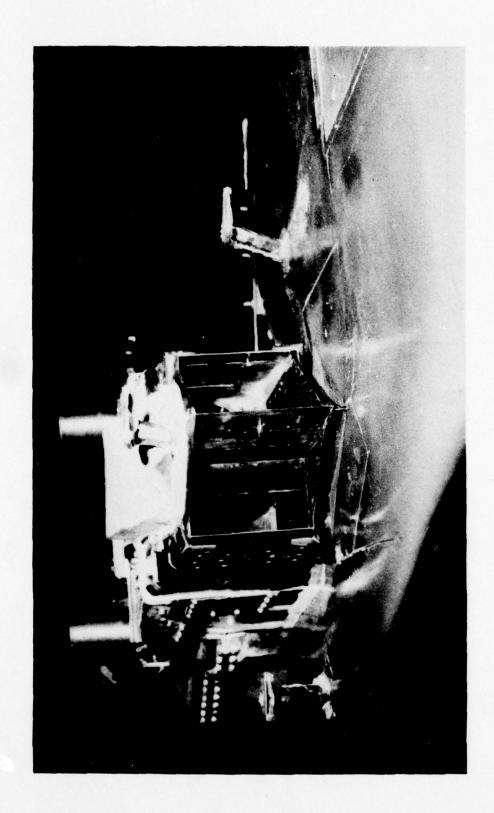


Figure 4.2. Closeup view of engine inlet and claw probes in the AEDC 16T wind tunnel.

The second of the second

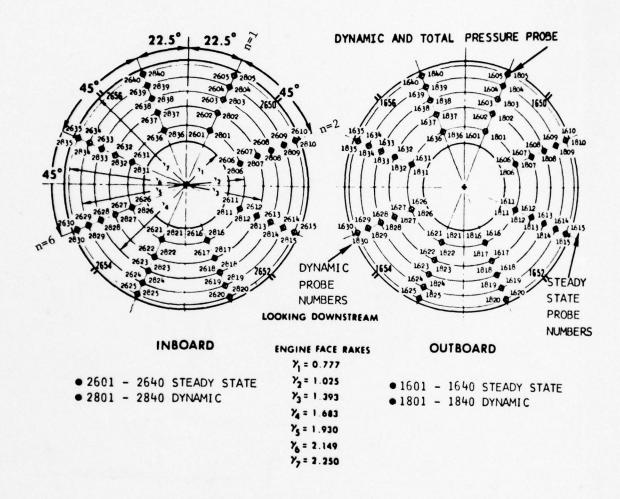
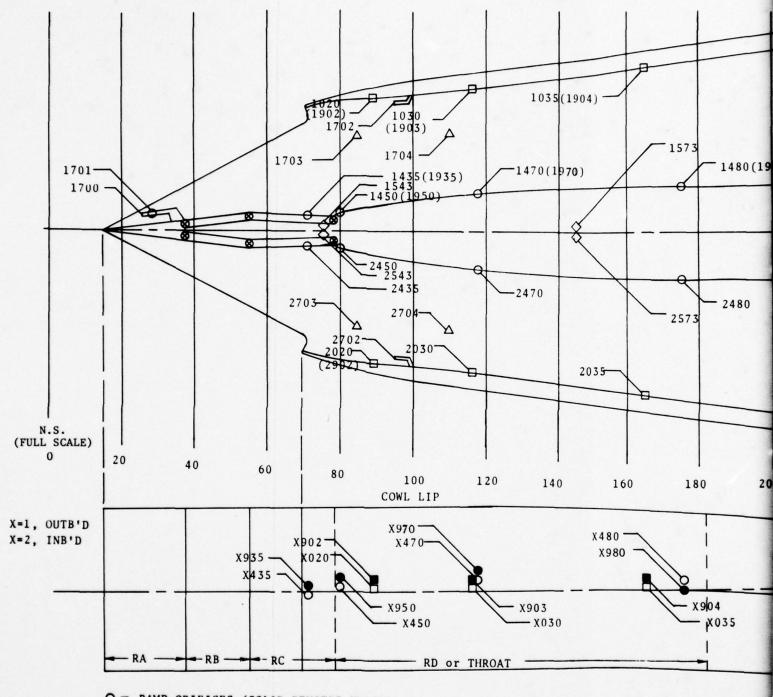


Figure 4.3. Engine face transducer locations. (Rockwell drawing)



O - RAMP ORIFICES (SOLID DENOTES KULITE)

COWL ORIFICES (" " ") Δ - UPR. SIDEPLATE ORIFICES

Figure 4.4.

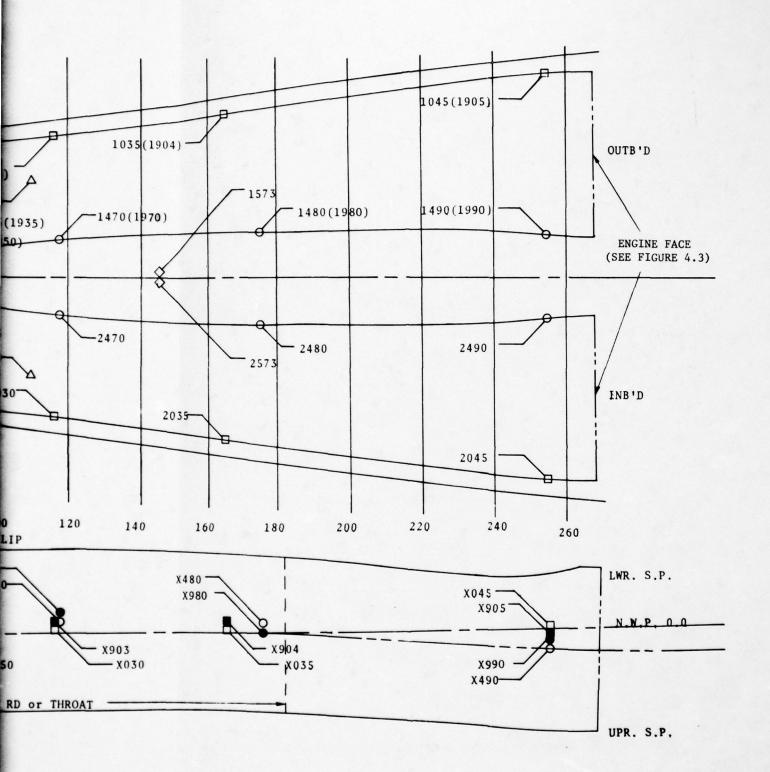


Figure 4.4. Inlet instrumentation. (Rockwell drawing)

inlet ramp system for the model was fixed for these tests in the normal subsonic cruise position. The engine face is located at Nacelle Station 269.5. The aircraft engine is simulated by an engine hub structure and by remotely actuated hydraulically operated flow control vanes which produce prescribed choked flow rates in the simulated engine at a position about 4.5 inches downstream of the engine face.

Forty combination steady-state and dynamic total-pressure probes are located in each inlet at the engine face section, located as indicated in Figures 4.3 and 4.4 and in Table 4.1. The dynamic probes used Kulite type CQL-080-25 transducers, which were found, from pre-test shock tube calibrations, to generally have response times to transient pulses of about 25 microseconds or less. These Kulite transducers had a 25-psi range, 0.080-in diameter and about 125 kHz natural frequency.

Other model instrumentation consisted of 54 static-pressure orifices and 10 dynamic Kulite transducers whose locations are described in Reference 4.1 (some indicated in Fig. 4.4). The 10 Kulite transducers, each accompanied by a static-pressure orifice, were mounted inside and flush with the inlet wall in the locations indicated in Figure 4.4 (also Fig. 5.4) and Table 4.1. These transducers were used to monitor inlet ramp and cowl pressures. All but one of these transducers were mounted in the outboard inlet.

Also mounted on the model were three claw probes, described in Section 3.3, to measure the characteristics of the blast wave at the model. Figures 3.5 and 4.2 indicate the locations of these three probes. Probe 2 was located just above the forward tip of the inlet; Probes 1 and 3 were located just above the wing surface, about 9.3 inches outboard and inboard of the inlet centerline, respectively, with their tips located at the same longitudinal station as the inlet cowl tips.

4.3 16T WIND TUNNEL TESTS

The 16T wind-tunnel blast test program was designed to obtain data on the blast response of the test model for a range of overpressures from 2 to 5 psi (scaled to 1 atmosphere ambient pressure) for tunnel

TABLE 4.1
LOCATIONS OF DYNAMIC PRESSURE TRANSDUCERS⁺

Engine face pressures (see Figure 4.3)

TYPE	RADIUS (Inches)	ORIFICE NUMBER							
		Ø=22.5	67.5°	112.5°	157.5°	202.5°	247.5°	292.5°	337.5°
Total	1.025 1.393 1.683 1.930 2.149	801 802 803 804 805	806 807 808 809 810	811 812 813 814 815	816 817 818 819 820	821 822 823 824 825	826 827 828 829 830	831 832 833 834 835	836 837 838 839 840

Add 1000 to tube number for outboard inlet; add 2000 to tube number for inboard inlet.

Cowl unsteady-state pressures (see Figure 4.4 or 5.4)

Transducer Number			Location		
Outboard	Inboard	Туре	N.S.*	Remarks	
1902	2902	Static	8.90	Buzz indicator	
1903	-	"	11.60	Cowl static	
1904	-	"	16.50	Cowl static	
1905	-	. "	25.45	Cowl static	

Ramp unsteady-state pressures outboard inlet (see Figure 4.4 or 5.4)

1935	Static	6.90	Third ramp
1950	"	7.91	Aft ramp
1970	"	11.70	Aft ramp
1980	"	17.42	Aft ramp
1990		25.45	Aft ramp

^{*}Nacelle station in inches (model scale).

⁺This page modified from Reference 4.1.

Mach numbers from 0.55 to 0.90 and for inlet flow rates representative of cruise and maximum power conditions. Table 4.2 outlines the test matrix which was followed to cover these conditions.

Tunnel testing was performed over a three night period, on 24 September and 27-28 September 1976. Testing consisted of calibrations, steady-state runs and a series of blast firings as described below. All tests were performed at below one atmosphere ambient pressures (usually 0.5 atmosphere) to minimize blast loads on the model and equipment, subject to the limit of a minimum Reynolds number per foot of 2.5 X 10⁶.

4.3.1 Unyawed Steady-State Tests

Prior to the blast tests, a series of unyawed steady-state runs were made covering all Mach number and inlet mass flow rate ranges of interest. These runs were made partly as a calibration of the inlet model vanes to control mass flow rate and partly to verify that the inlet steady-state distortion properties were the same as were found in previous tests of the model.

Steady state runs were also made immediately before each shock tube firing to provide reference (pre-blast) pressures at all dynamic pressure transducer locations. (The dynamic pressure transducers measure only changes of pressure; absolute pressures are obtained by adding pre-blast (steady-state) pressures to the dynamic pressures). Results of these pre-blast steady-state tests are presented in Appendix B.

4.3.2 Yawed Steady-State Tests

A few steady-state runs were made with the model at various yawed positions in the range -10 to +10 degrees, according to the schedule given in Table 4.3. These runs were made partly to calibrate the inlet flow controls under yawed conditions and partly to aid in assessing the quasi-steady late-time response of the inlet to the side-slip effects of blast waves of very long duration.

4.3.3 Shock Tube Firings

Forty-five shock tube firings were performed in the AEDC 16T tunnel at tunnel Mach numbers of 0, 0.55, 0.70, 0.85 and 0.90. Tests were

TABLE 4.2

NOMINAL TEST CONDITIONS

Mach No.	Flight conditions	Mass flow (1b/sec)	Overpressure * (psi)	Yaw (deg)
0	Parked	0	4	0
0.55	Cruise	235	4	0
0.55	Max. power	350	4	0
0.70	Cruise	300	2,3,4	0
0.70	Max. power	350	2,3,4,5	0,5
0.85	Cruise	300	2,3,4,5	0
0.85	Max. power	350	4,5	0
0.90	Max. power	350	4	0

⁺Full scale values (divide by 100 to obtain model values)

^{*}Scaled to ambient pressure of one atmosphere

TABLE 4.3
STEADY-STATE YAW CONDITIONS

Mach no.	Flow rate (1b/sec)	Yaw angle range (deg)		
0.55	352	-10 to +10		
0.70 0.70	303 352	-10 to +10 -10 to +10		
0.85	350	-10 to +7.5		

generally performed with the tunnel static pressure set at about 1/2 atmosphere, except for the Mach 0.55 runs, for which about 2/3 atmosphere was used. The inlet mass flow rate was generally set to simulate both cruise and maximum power flight conditions for each Mach number condition according to the schedule in Table 4.2. This schedule required testing at mass flow rates of about 235, 300, and 350 lb/sec (full scale)*.

Tunnel steady-state pre-blast conditions are tabulated in Table 4.4 and Appendix B. Tunnel total temperature was 569° (\pm 1°) for all firings with the tunnel turned on and was 534° R for the one static firing. Firings were made over a range of overpressures from about 2 to 6 psi, scaled to a tunnel ambient pressure of one atmosphere.**

Also presented in Table 4.4 are estimated values of the blast overpressure (Δp) and the blast intercept angle (ϕ) as the blast wave strikes the inlet. The source and accuracy of these values is discussed subsequently in Section 4.6.

4.4 DATA REDUCTION

The test data obtained from each shock tube firing were digitized by ARO at time intervals of 10.45 microseconds for a total of 2048 samples per firing. The resulting digital data were provided to KA in the form of magnetic tapes and time history plots of most of the basic data and derived quantities (Ref. 4.2). Tabular time history printouts of a few variables were also provided by ARO.

4.5 SAMPLE TEST RESULTS

Pressure time histories for typical pressure transducers are presented in Figure 4.5 for a typical shock tube firing (Run 8/Part 573) to illustrate the major features of the test data. In general, in this figure, the ordinate label designates the variable measured and the vertical scale is always either pressure/p_t or pressure/p_o (the latter

All mass flow rates in this report are scaled to full scale conditions. Model values are 1/100 of these values.

^{**} It should be noted that all blast pressure values designated as Δp in this report are all scaled to a tunnel ambient pressure of one atmosphere. Pressures not specifically designated as Δp , such as shock tube driver pressures in Table 4.4 and all pressure values in Appendix B are actual test pressures.

TABLE 4.4

16T WIND TUNNEL TEST CONDITIONS

	Part Point	Mach		(lb/sec)	Tube	Tube Pressure	Nominal Shock Overpressure	Intercept Angle	Yaw Ang
Run	No.	No.	OB Inlet	IB Inlet	No.	(psia)	(psi)	(deg)	(deg
1	501.01	0	0	0	2	69	2.7	79	0
2	615.03	.552	235	235	3	186	4.7	91	1
3	591.03	.550	351	348	1	157	3.7	76	
4	589.03	.551	351	348	2	115	3.8	97	
5	590.02	.549	351	349	3	124	4.0	94	
6	602.02	.700	302	300	1	72	2.6	86	
7	600.04	.701	302	302	²	58	2.6	106	
8	573.04	.700	304	302	+	112	5.0	98	
9	601.03	.701	302	300	3	69	3.0	104	
10	574.03	.701	303	300	+	132	4.4	97	
11	621.03	.700	351	351	1	73	3.0	84	
12	519.02	.699	348	344		103	3.8	88	
13	527.02	.700	349	344	+	135	4.8	78	
14	626.02		352	352		142	4.8	79	
15	512.03	.700	351	344	2	59	2.8	103	
16	517.02	.700	349	344	1	85	3.8	103	
17	525.02	.701	348	344	+	113	5.0	100	
18	624.02	.700	350 .	350		139	5.2	99	
19	513.03	.700	351	344	3	70	3.0	102	
20	518.02	.700	348	343		102	4.2	99	
21	526.02	.700	349	344	1	133	4.8	98	
22	625.02	.701	350	350	•	155	5.6	92	+
23	570.03	.699	351	350	1	144	3.6	87	+5.
24	568.04	.700	350	349	2	132	5.8	103	+5.
25	569.03	.703	350	349	3	143	4.2	105	-5.
26	559.02	.850	300	298	1	61	2,2	89	0
27	598.03	.848	299	299		90	3.0	85	1
28	584.03	.847	294	293	•	122	5.0	82	
29	608.04	.850	299	299		142	4.4	82	
30	557.04	.850	300	298	2	55	-	-	
31	596.05	.848	300	300	1	73	3.8	108	
32	582.03	.847	300	297	1	94	4.4	105	
33	606.03	.849	300	299	•	120	-	-	
34	558.03	.850	303	301	3	60	>2	-	
35	597.03	.848	300	300		85	4.0	104	
36	583.03	.847	298	296		114	4.4	102	
37	607.03	.850	299	298		140	4.8	108	
38	546.02	.847	348	347	1	121	3,6	84	
39	544.04	.847	348	347	2	94	4.0	107	
40	619.02	.850	352	351	+	120	5.8	110	
41	545.03	.847	348	347	3	113	4.4	105	
42	620.02	.850	351	350	+	139	5.6	100	
43	553.03	.900	327	329	1	117	3.0	86	
44	550.02	.899	349	354	2	86	4.0	107	+
45	551.01	.900	349	354	3	104	4.2	105	

FIGURE 4.5.

SAMPLE TEST RESULTS

FOR RUN 8 (PART 573), MACH 0.70,

FLOW RATE ≈ 303 LB/SEC, TUBE 2, Δp = 5.0 PSI

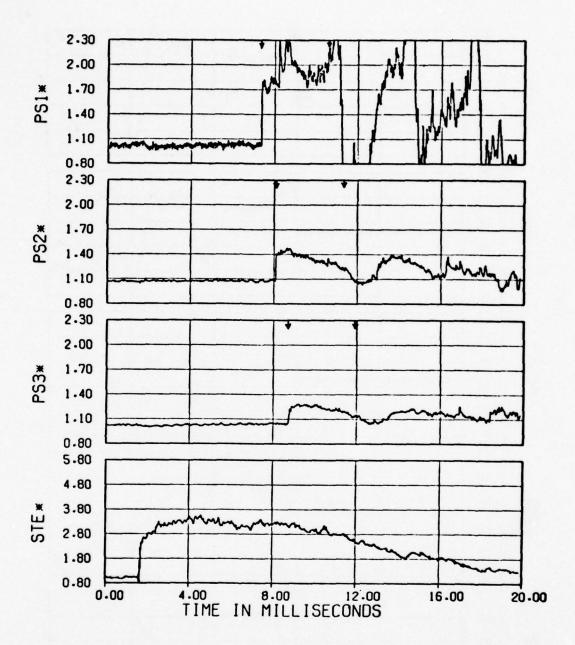


Figure 4.5a. Blast and shock tube pressures.

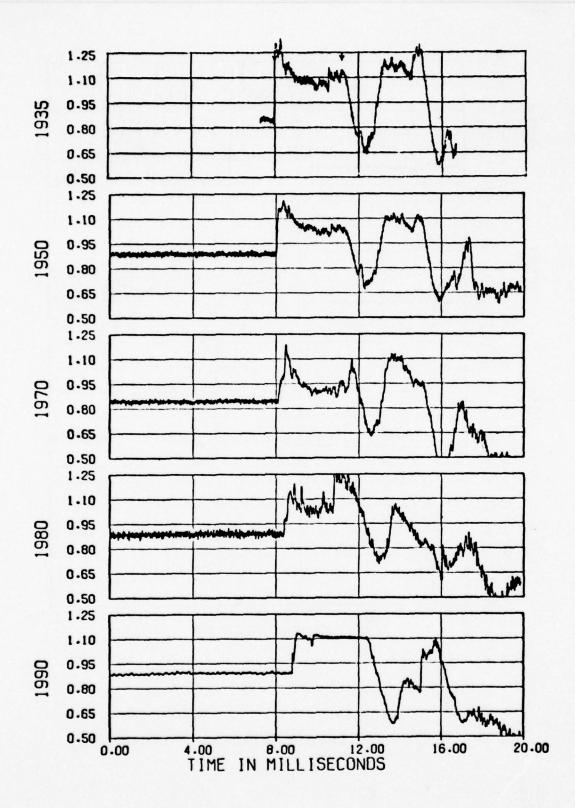


Figure 4.5b. Ramp pressures.

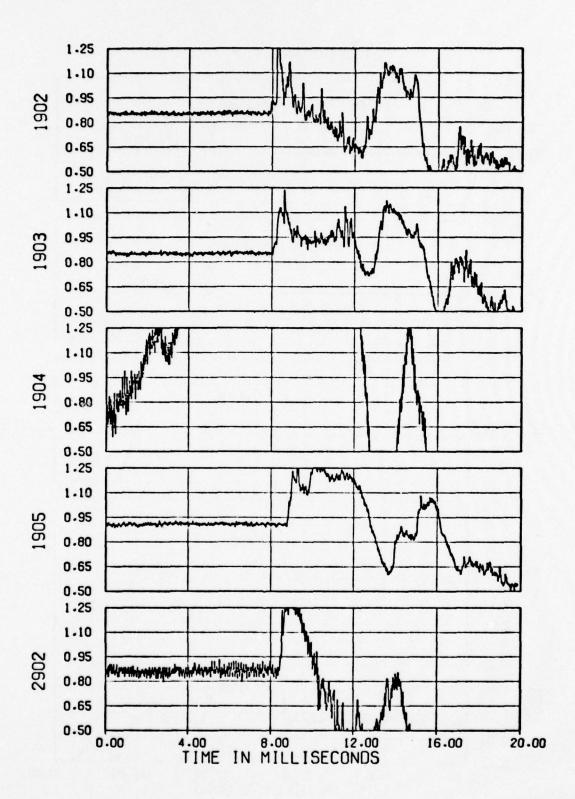


Figure 4.5c. Cowl pressures.

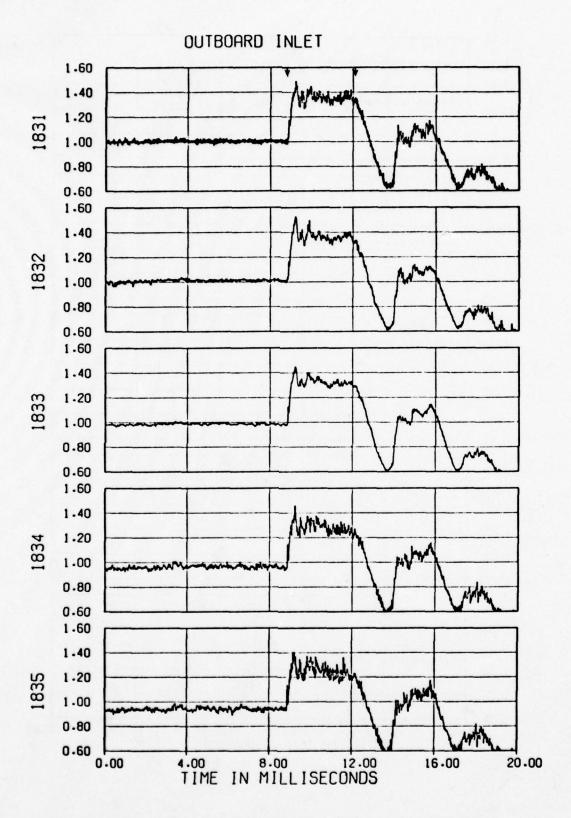


Figure 4.5d. Blastward inlet engine face total pressures.

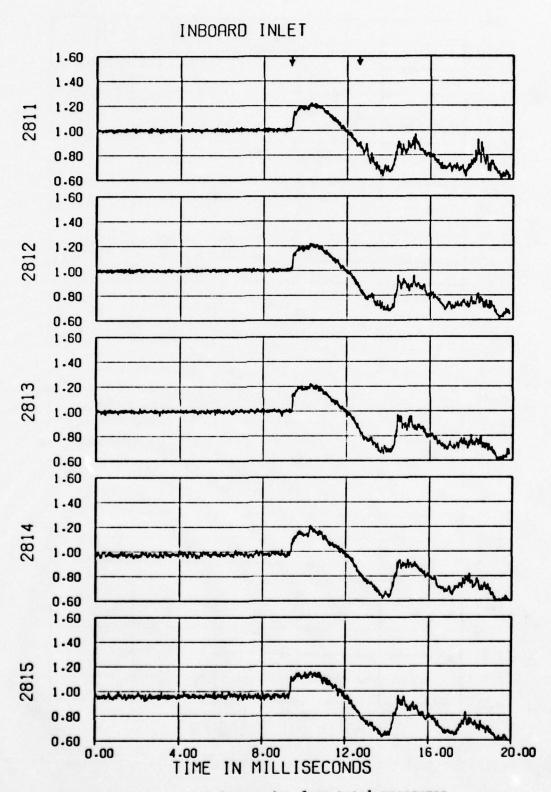


Figure 4.5e. Leeward inlet engine face total pressures.

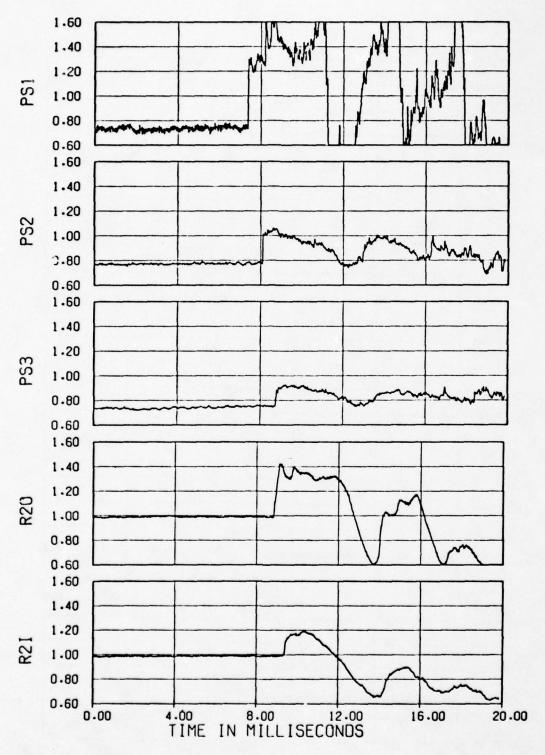


Figure 4.5f. External blast pressures and average engine face total pressures.

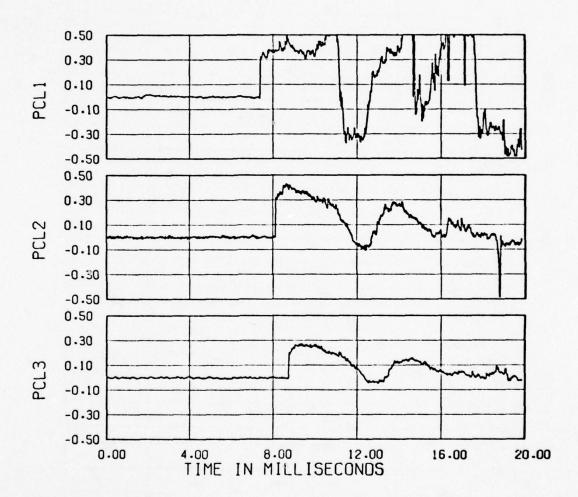


Figure 4.5g. Left claw arm pressures.

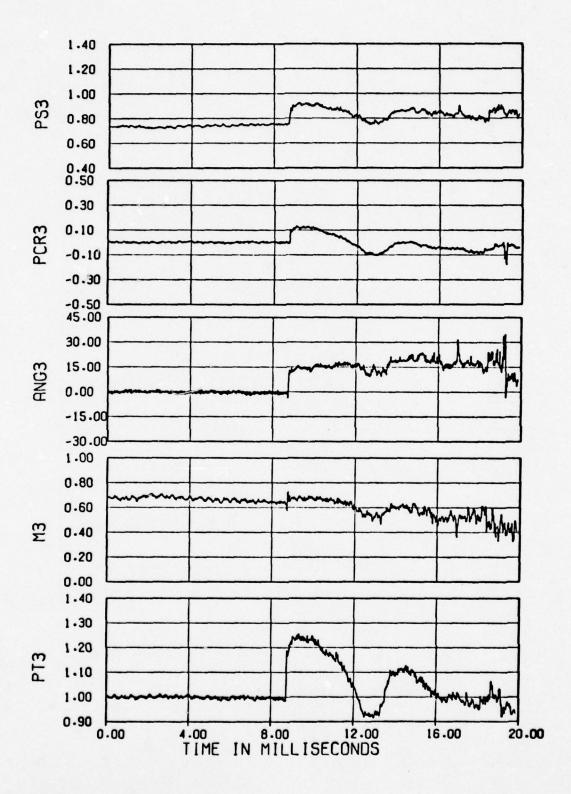


Figure 4.5h. Claw 3 parameters.

being designated by an asterisk after the label), where p_t is the steady-state (pre-blast) tunnel total pressure and p_0 is the steady-state tunnel ambient static pressure.

The lowest part of Figure 4.5a shows the blast pressure inside the firing shock tube 14 inches from the muzzle end (STE). The pressure variation consists of a initial shock, followed by a slight rise and a nearly constant level for about 8 milliseconds, after which a slow decay follows.

The upper parts of Figure 4.5a give the (static) local blast pressures (PS) measured on the three claw probes, which provide an indication of the strength of the blast wave as it strikes the inlets. Looking first at PS2, which is near to the forward tip of the inlet, it may be noted that the pressure rises immediately on blast arrival to a large shock value, appears to increase slightly more over a period of about one millisecond, decays slowly until a time typically of about 3.3 milliseconds after initial blast arrival and then decays more rapidly. Similar variations are seen for the other two probes (PS1 and PS3), except that the signal for PS1, on the blastward side of the inlet, is complicated by the appearance of the reflection of the shock wave from the blastward blunt side of the inlet at about one millisecond after blast arrival.

It should be noted that for nuclear blast wave simulation purposes only the part of the signal from shock arrival to the rapid pressure change, starting at about 3.3 msec after blast arrival for PS2 in Figure 4.5a, is directly of interest. This rapid change can appear either as a rapid pressure drop usually at about 3.3 msec., as for PS2, or it may take the form of a rapid increase in pressure at about the same time followed by an abrupt pressure drop at a slightly later time, as for PS1 (Fig. 4.5a). At later times (after about the 3.3 msec) the flow pattern is more like a quasi-steady flow where the shock tube exit flow can be considered similar to a nozzle or jet flow. More specifically, from our two-dimensional REFLECT2 theoretical calculations (Appendix A), it appears that the rapid change in the blast pressure (at about 3.3 msec) corresponds generally to the arrival of the contact surface between the

"hot" tunnel gas and the "cold" gas jet from the shock tube. In most figures hereafter, the time of blast arrival at the transducer and a time 3.3 msec tater are indicated as a pair of vertical arrows in order to permit the reader to focus his attention more easily on the range of primary significance for nuclear blast simulations (between the arrows). While the test results for larger times may also be of some significance for blast simulations, this remains to be demonstrated.

Time histories of ramp and cowl pressures are presented in Figures 4.5b and 4.5c. (See Fig. 4.4 and Table 4.1 for transducer locations). It may be noted that there is considerable variation of waveform for the different locations for reasons to be discussed later. (It should be noted that transducer 1990 generally appears to be truncated, 1904 is generally unreliable and the calibration constant used for 2902 appears generally unreliable).

Typical time histories of blast-induced total pressure at the blastward engine face location are shown in Figure 4.5d. Roughly, the same variations are seen to be experienced for all locations and the general trends are similar to those of the input blast pressure (e.g., PS2 in Figure 4.5a).

Typical time histories of blast total pressure at the leeward engine face location are shown in Figure 4.5e. The leeward pressures are somewhat similar to those for the blastward side (Fig. 4.5d) but are clearly different from those for the blastward side in two significant respects. First the initial pressure rise is more rapid for the leeward side (essentially a single shock) whereas for the blastward side the rise time is relatively large (say about 0.3 msec), and generally appears to involve a sequence of several small shocks. Secondly, the blast pressure appears to decay more rapidly for the leeward side at late times.

For a few firings the onset of this cold gas effect appeared to occur somewhat later, but for most cases where a definite onset could be estimated, it appeared to occur at between about 3.2 and 3.5 milliseconds after blast intercept.

Figure 4.5f presents times histories of the already presented three blast pressure measurements PS1, PS2 and PS3 as a fraction of pre-blast free stream total pressure (Pt) and also presents the average engine face total pressures R20 and R2I, for the outboard (blastward) and inboard (leeward) inlets, respectively. As would be expected, these last two variables correspond closely to the corresponding variations for the individual transducers in Figures 4.5d and 4.5e, respectively.

Typical claw probe results are shown in Figure 4.5g and 4.5h. Directly measured parameters are the "static" pressure PSi and the left and right claw arm pressures, PCLi and PCRi, where i designates the probe number. Derived quantities are the resultant flow (sideslip) angle, ANG, the local Mach number, Mi, and the total pressure, PTi.

4.6 OBSERVATION ON BLAST INPUT CONDITIONS

Before proceeding to an analysis of the significance of the test results in Section 5 it is important to first indicate briefly the source and reliability of the blast input overpressure (Δp) and intercept angle (φ) data presented in Table 4.4 and to indicate what differences in blast input and inlet response behavior may be attributed to the different locations of the three firing shock tubes.

4.6.1 Blast Input to the Inlets

The strength and orientation of the initial blast wave incident on the inlets and its subsequent time history variations must be known in order to evaluate the significance of any test firing. However, insomuch as the blast waves for these tests were not simple constant strength plane waves it is not a simple task to deduce the blast strength from the test data. More specifically, the orientation of the blast wave at the inlet depends on the tunnel flow conditions (Mach number), on the location of the shock tube, and on the shock tube firing conditions (tube driver pressure/tunnel pressure) and may be time dependent. The intensity of the blast depends on the radial distance and polar angle of the inlet from the shock tube axis and on the tunnel flow conditions and the shock tube firing conditions. Furthermore the strength of the blast wave striking the inlet and the blast measurement probes can be significantly modified by interferences between the blast wave, the

model wing and fuselage and the inlet, particularly at late times after arrival of the blast at the inlet.

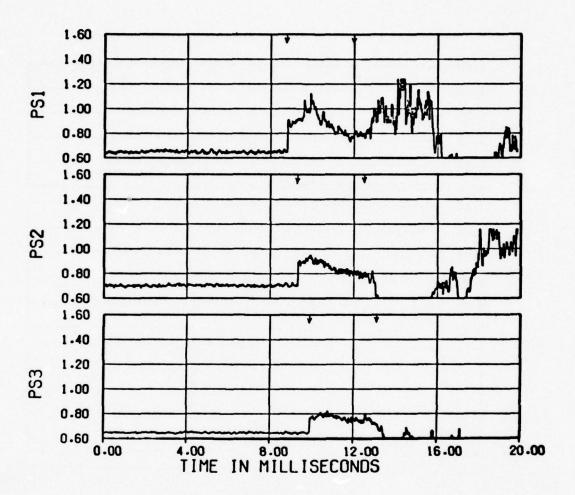
4.6.1.1 Blast Strength

A first approximation for the blast input to the inlet is given by the static pressure transducers mounted on the claw probes as indicated in Figure 4.2. Typical time histories of the blast signal seen by these static transducers are shown in Figure 4.6 for firings from the three shock tubes.

Referring first to the firing from tube No. 1 (Fig. 4.6a), probe 1 (PS1) is struck first by the blast wave, probe 2 second, and probe 3 last. Probe 1 defines the blast wave as it is seen from a position slightly downstream of the inlet cowl lip and about 6 inches outboard of the cowl lip. This record should provide a reasonable estimate of the incident blast strength at the probe location for a time duration of about one millisecond, at the end of which time the blast wave has reflected from the blunt side of the inlet model and returned to the probe, thereby providing the second shock pressure increase observed on that probe at that time. In view of this reflection effect it is difficult to determine the late time history of the incident blast wave for tube 1 firings from probe 1 measurements. (The same argument applies to probe 3 measurements for firings from tube 3, as can be seen from Figure 4.6c).

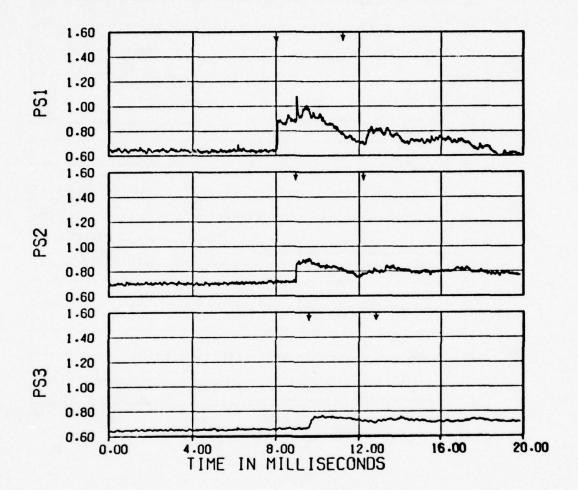
The blast strength time history obtained from probe 2, located above and near the forward end of the inlet appears to generally give the best representation of the blast wave input that can be obtained without a detailed analysis of the claw probe data. There are no obvious strong interference reflections in the probe 2 data (at least up to about 3.3 milliseconds after blast arrival), although there certainly must be some interferences due to diffraction of the blast wave about the inlet structure.

The blast strength record obtained from probe 3 for firings from tube 1 or 2 (or from probe 1 for tube 3 firings) is considered only qualitatively representative of the true blast input to the inlet because the blast wave experiences substantial diffraction about the inlet structure before reaching this probe.



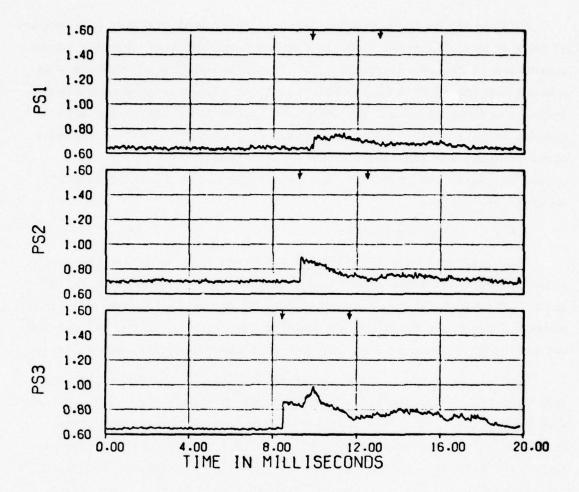
(a) Shock tube 1 firing, Run 29 (Part 608)

Figure 4.6. Typical blast pressure measurements for firings from three shock tubes, Mach 0.85, flow rate ≈ 300 lb/sec.



(b) Shock tube 2 firing, Run 31 (Part 596)

Figure 4.6. Continued.



(c) Shock tube 3 firing, Run 35 (Part 597)

Figure 4.6. Concluded.

In view of the above observations and in view of frequent malfunctions of many of the claw probe elements, it was concluded that the best representations of the blast strength that is available from the test data at present are the probe 2 static data and these data were generally used to define the (nominal) blast strength data presented in the tables and figures of this report. A more accurate evaluation of the true incident blast strength and its time history derived from the claw probe data would, of course, be desirable, but insufficient time was available to develop this subject.

4.6.1.2 Blast Orientation

The blast incidence angle, ϕ , at which the blast wave strikes the inlet is of considerable importance in determining blast effects on the inlet. The blast intercept angle is defined as the angle between a line normal to the blast front and the axis of the inlet, with 0° , 90° and 180° representing head-on, side-on and tail-on blast intercepts, respectively.

Initial estimates of blast intercept angles for the 16T tests were made from the shadowgram studies made in the 1T tunnel (Sec. 2.2). Attempts were made to take similar shadowgrams during the 16T tests, but these were generally unsuccessful. Instead, estimates of the blast intercept angles for the 16T test conditions were generally obtained by observing the differences in arrival times of the blast wave at claw probe 2 and at the transducers 1935, 1902 and 2902 located near the inlet mouth, under the assumption that the blast wave could be considered to be locally a plane shock wave, travelling with respect to the local pre-blast fluid at a shock speed corresponding to the shock overpressure in Table 4.4. The resulting intercept angle estimates are presented in Table 4.4. Generally these angles are in reasonable agreement with estimates from the 1T test shadowgrams, for cases of comparable test conditions.

^{*}See Figure 4.4.

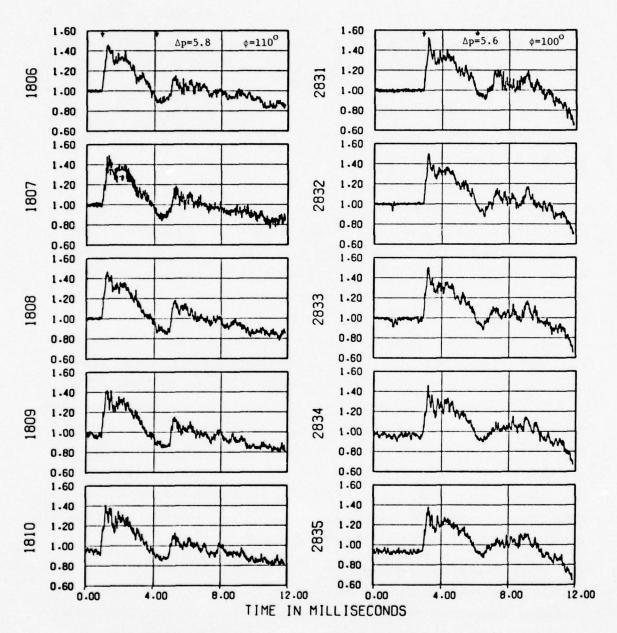
4.6.2 Shock Tube Location Effects on Blast Input and Inlet Response

The blast waves produced at the inlet by firings from different shock tubes can produce somewhat different effects on the inlet response due to factors other than obvious differences in intercept angles and overpressures. It is the purpose of this section to clarify this question somewhat by examination of some of the test data before proceeding to a more extensive analysis of the data in Section 5.

Consider the effects of firing at the inlet from opposite sides of the tunnel. The blast waves fired at the model from shock tubes 1 and 2 encounter the inlet essentially without any initial interferences from the model wing and fuselage body (see Fig. 3.1), whereas the blast wave from shock tube 3, which must cross the wing before reaching the inlet, may be substantially modified before striking the inlet. Consequently, some differences might be expected for the inlet response conditions to firings from the different sides of the tunnel. In order to indicate the extent of these differences, Figure 4.7 presents a comparison of inlet engine face total pressure time histories for firings from shock tubes 2 and 3 for roughly comparible overpressure and blast intercept conditions. The left-hand side of this figure presents inlet pressure for a firing from tube 2 and the right hand side presents the corresponding inlet pressure for a firing from tube 3. For example, transducer 1806 (in the outboard inlet) for a tube 2 firing would be expected to have the same type of response as the symmetrically located transducer 2831 (in the inboard inlet) would have for a firing from tube 3.

It is evident from Figure 4.7a that the inlet response pressures are about the same for firings from the two tubes, certainly for the estimated duration of the blast event, say to about 3.3 msec after blast arrival. For much later times, there are appreciable differences, but this is not of great importance for the present study.

For the leeward inlet, Figure 4.7b indicates the same general shape of pressure histories for the two firings but does indicate an appreciably more rapid decay of pressure for the firing from tube 3. This more rapid

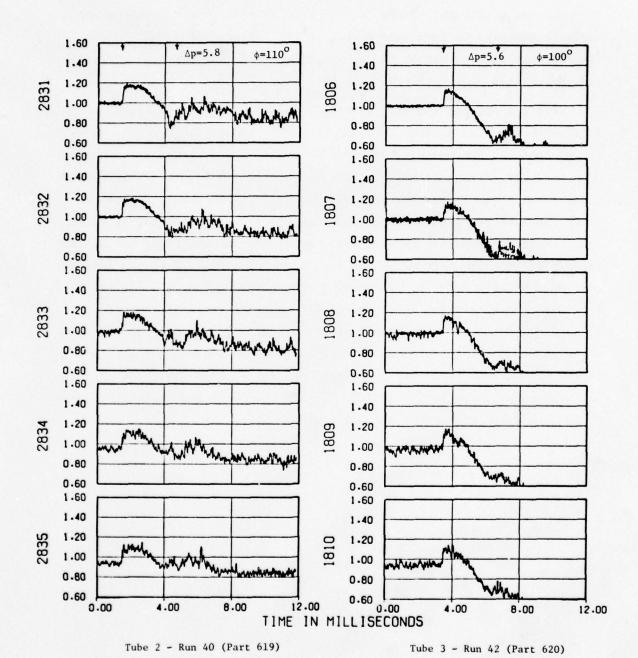


Tube 2 - Run 40 (Part 619)

Tube 3 - Run 42 (Part 620)

(a) Blastward inlet

Figure 4.7. Comparison of engine face pressures for firings from shock tubes 2 and 3.



(b) Leeward inlet

Figure 4.7. Concluded.

decay can be attributed partly to wing-fuselage-inlet interference, which would be expected to have more effect on the leeward inlet than on the blastward inlet, and partly to the 10° difference in intercept angles for the two firings.

Some differences are also observable between the blast inputs and inlet responses for firings from the two tubes located on the same side of the tunnel. For example, Figure 4.8 compares inlet ramp pressure time histories for firings at similar overpressure levels from the side-by-side shock tubes 1 and 2 (see Fig. 4.4 for transducer locations). It may be noted that the two sets of time histories are quite similar during the blast event (between the two arrows), especially for the first two milliseconds after blast arrival. Then the pressures tend to decrease for the rest of the blast event for the tube 2 firing and to increase for the tube 1 firing, and after the end of the blast event the two sets of time histories are considerably different. The greater pressures and fluctuations observed toward the end of and after the blast event for the tube 1 firing may be attributed partly to its much lower blast incidence angle, 84° here compared to 110° (see Sec. 7), and partly to the greater closeness of the jet from tube 1 to the inlet mouth.

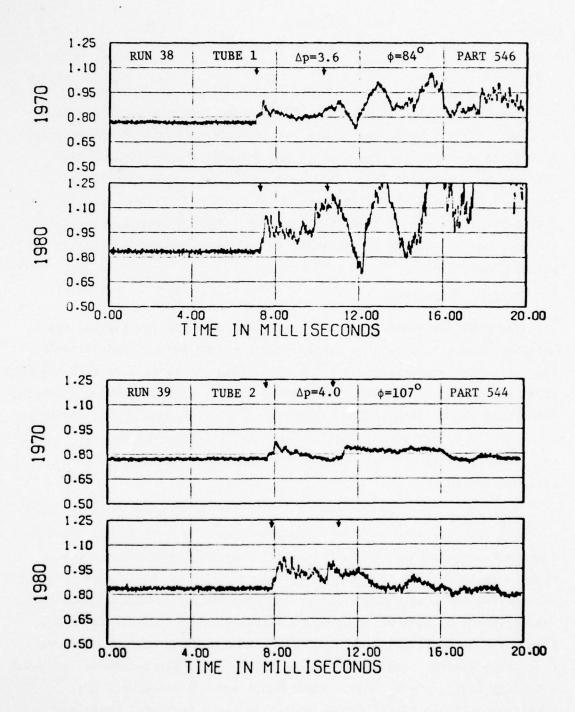


Figure 4.8. Comparison of blastward inlet ramp pressure time histories for Mach 0.85 firings from two shock tubes.

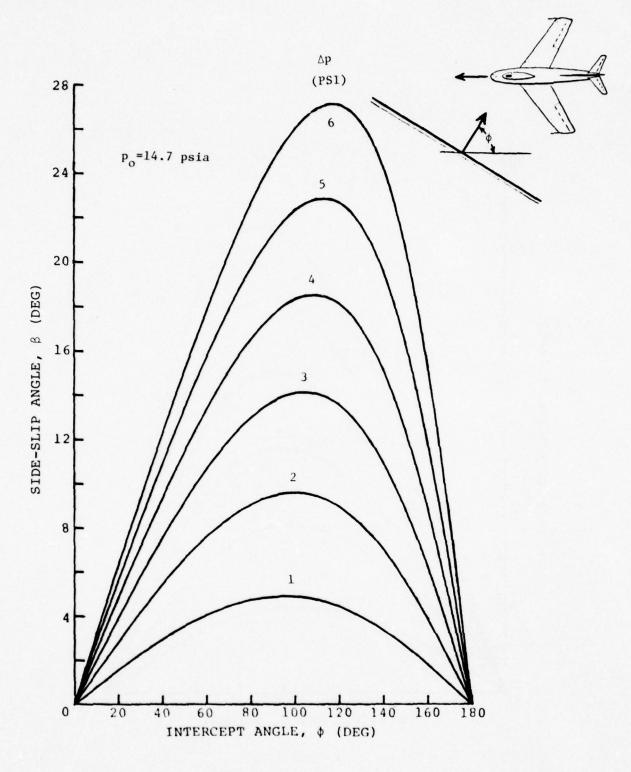
SECTION V ANALYSIS OF 16T TEST RESULTS

This section presents a general discussion and analysis of some of the principal effects relevant to and observed from the 16T blast test results. First a brief discussion is given of the basic characteristics of a blast wave interacting with an inlet-engine system (Sec. 5.1), followed by a more specific discussion of the transient shock wave pattern in an inlet after blast encounter (Sec. 5.2). Next are discussed distortion effects in the inlet (Sec. 5.3). Finally some observations are made on the ability of the inlet to endure long-duration blast effects (Sec. 5.4).

5.1 GENERAL PHENOMENA

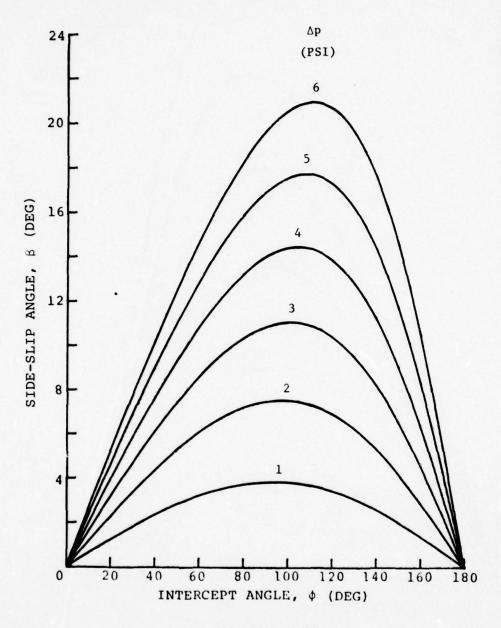
The physical characteristics of a blast wave and its initial interactions with an inlet-engine system are discussed below. The initial discussion deals primarily with the case where the blast wave is considered as a simple plane shock wave of constant or very slowly decaying strength, resembling the blast wave from a nuclear weapon. Subsequently, attention is given to the differences in phenomena which are associated with the more complex blast wave produced by the shock tubes as used in the present studies.

As a blast wave travels toward an aircraft moving in space it produces changes in the ambient atmosphere behind its front which are imposed on the aircraft as it is enveloped by the blast field. The blast wave is defined essentially by two characteristics, the overpressure, Δp , and the intercept angle, φ , between a normal to the blast front and the direction of aircraft motion. With reference to the aircraft, the flow field behind the blast front will have a greater ambient pressure, $P_0 + \Delta p$, a greater total pressure, $P_t + \Delta p_t$, and a blast-induced increased side-slip angle, $\psi = \psi_0 + \Delta \psi$. Figures 5.1 and 5.2 illustrate the magnitude of these blast-induced side-slip angle and total pressure changes for several Mach numbers. For example, it is seen from



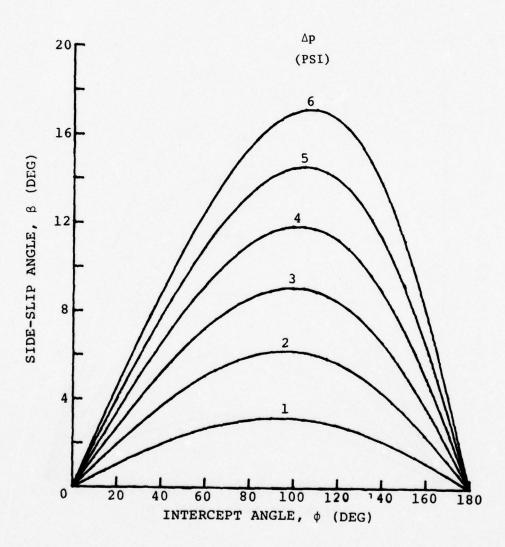
(a) MACH 0.55

Figure 5.1. Variation of blast-induced side-slip angle with intercept angle and overpressure.



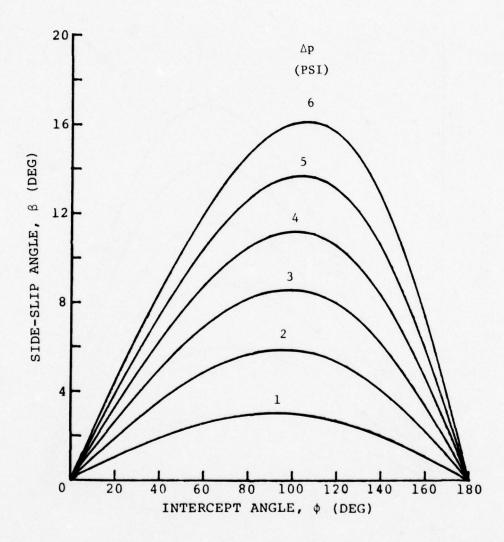
(b) MACH 0.70

Figure 5.1. Continued



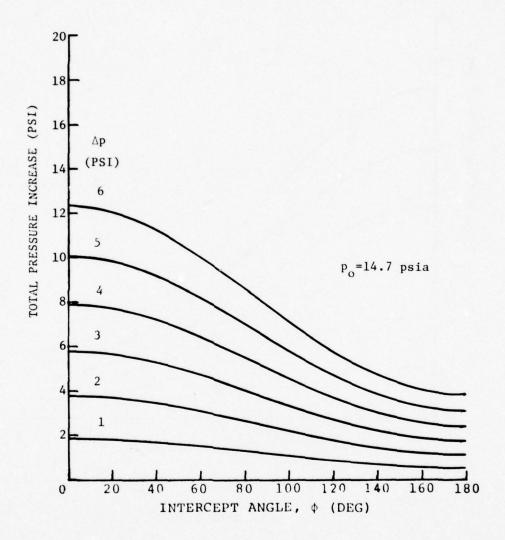
(c) MACH 0.85

Figure 5.1. Continued



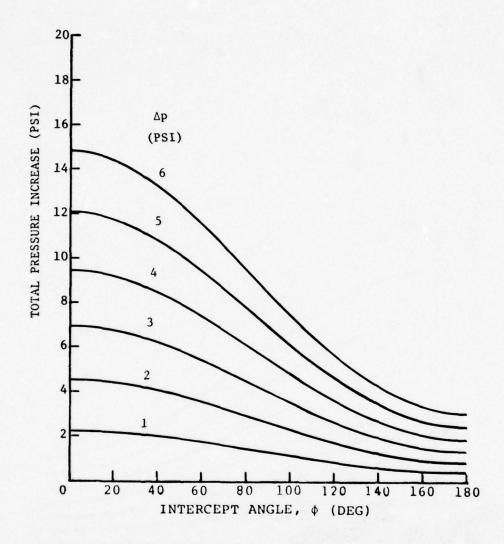
(d) MACH 0.90

Figure 5.1. Concluded.



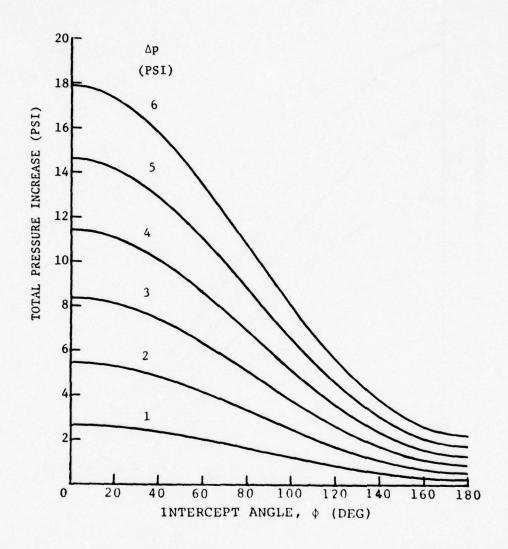
(a) MACH 0.55

Figure 5.2. Variation of blast-induced total pressure with intercept angle and overpressure.



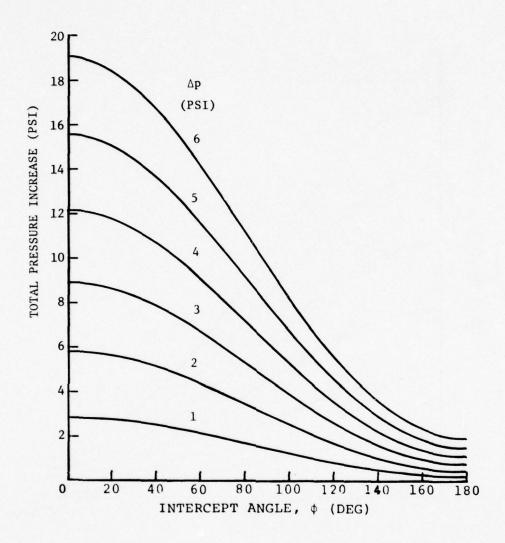
(b) MACH 0.70

Figure 5.2. Continued



(c) MACH 0.85

Figure 5.2 Continued



(d) MACH 0.90

Figure 5.2. Concluded

Figure 5.1 that the greatest blast-induced yaw angles are produced by intercept angles somewhat over 90° (i.e., slightly from the rear). Blast-induced total pressure changes in Figure 5.2 are seen to be largest for zero intercept angle and to decrease subsequentially to relatively small values for tail-on $(\phi=180^{\circ})$ intercepts.

As a blast wave envelopes an aircraft these blast properties may be substantially modified by diffraction and reflections from various parts of the structure before and after the wave encounters the engine inlet.

As the wave proceeds into an engine inlet it may experience a sequence of reflections from the walls of the inlet (as discussed in Sec. 5.2) and from engine components, and may penetrate in part completely through the engine system.

Eventually, if the blast wave is of sufficient duration, these blast reflection effects will be resolved and the inlet-engine system will come to a quasi-steady equilibrium condition consistent with the blast-induced overpressure, total pressure and side-slip angle, characterized by an engine mass flow rate which can be different from that for the pre-blast condition.

In discussing the effects of a blast wave on inlet-engine performances it is convenient to think of the phenomena in terms of the following somewhat overlapping three stages of the blast encounter.

The first or initial stage consist of the time during which the blast wave moves down the inlet into the engine, reflects in part from the engine structure or fan of a turbofan engine and subsequently moves upstream and out the mouth of the inlet. In the case of the present 0.1-scale model the time required for these events up to the time when the reflected shock wave has moved upstream of the simulated engine face section is on the order of 2 milliseconds. (Time zero is defined here as the time when the blast wave first strikes the cowl lip of the blastward inlet.)

The second stage of the blast flow encounter is associated with the inception and convection of boundary-layer disturbances down the inlet. In particular, boundary-layer separation and vortex formations may be

produced at the cowl lip by large blast-induced side-slip angles and will be convected downstream at speeds comparable to or lower than the particle velocity in the inlet, which is generally much smaller than the rate at which a blast wave moves down the inlet. In the case of the tested inlet, it would take on the order of 3 milliseconds (after cowl lip blast encounter) for such particle velocity effects to reach the engine face. Other boundary layer effects which might be expected in this same time period would be boundary layer instabilities excited by the reverse flow reflected upstream from the engine throat. For the present inlet, such effects would not be expected to begin at the engine face before times of about 2 milliseconds after blast intercept.

The third stage of the blast flow consists of the late time stage when all significant internal shock wave systems have been dissipated or reflected from the inlet-engine system and boundary layer effects have reached a quasi-steady equilibrium condition. This stage was not reached in the present tests because of the limited duration of the blast waves used.

5.1.1 Differences Between Shock Tube and Nuclear Blast Flows

The initial flow from the shock tubes used in the present tests generally resembles the essential features of a nuclear blast wave at least for part of the blast-type flow period described (in Section 4.5) of about 3.3 milliseconds. However there are some noteworthy features, which should be borne in mind, where the shock tube flow differs from that for a nuclear blast. First the strength of the shock tube blast wave remains relatively constant for only one or two milliseconds, after which its strength generally tends to decrease toward zero at 4 to 6 seconds after initial shock arrival. Also, in the late decay stage, "cold" air blown out of the shock tube produces a high velocity jet with a complex spatial variation of fluid properties which bears little resemblance to a nuclear blast field. As a general rule of thumb for the present tests, it appears that this "cold" jet does not strongly influence the test results for times after blast arrival less than about 3.3 milliseconds (see Sec. 4.5).

A sketch illustrating the above-discussed sequence of events in the blastward inlet is presented as Figure 5.3 in the form of a time distance plot for an inlet mass flow rate of 350 lb/sec. The time origin is the time when the blast wave first arrives at the cowl lip. The initial blast wave moves down the inlet to the simulated engine throat vane system and is reflected back upsteam as indicated by the "shock" curve. The "particle velocity" curve indicates the convective speed of material in the inlet; "vortex" motions are indicated here as travelling at speeds between 1/2 and 1 times the particle velocity and are indicated to reach the engine face at times on the order of 3-6 milliseconds, depending on the vortex speed. The cold gas motion is indicated by the two upper curves, starting at time 3.3 msec. This cold gas effect might be expected to travel down the inlet at some speed between the particle velocity and the sound(+ particle) velocity, depending on how close the inlet mouth is to the jet from the shock tube. It is important to note here that large shock-type cold gas effects (see lower cold gas curve) can arrive at the engine face before vortex effects arrive, hence making it difficult to unambiguously evaluate vortex effects at the engine face by simple inspection of test records.

5.2 SHOCK PATTERN IN THE INLETS

As a guide to the discussion in later sections of blast-induced distortion and its effects on engine performance, this section briefly discusses some details of the character of the blast-induced shock flow pattern in the inlet.

Figure 5.4 presents a sketch of the tested inlet configuration and shows the shock wave pattern inside the inlet for a time when the blast shock has penetrated down the blastward (outboard) inlet to slightly beyond the engine face location. In this figure, the blast is assumed to have struck the inlet about perpendicular to the inlet axis (ϕ =90°) from the outboard side of the inlet. After encountering the lip of the outboard cowl, the blast shock wave begins to diffract about the cowl lip and to penetrate into the inlet at a downstream speed about equal

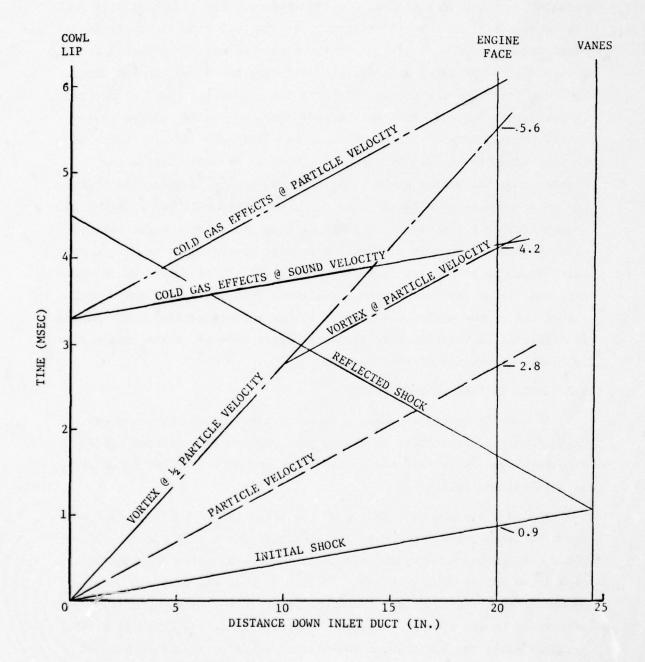


Figure 5.3. Inlet time-distance relationships.

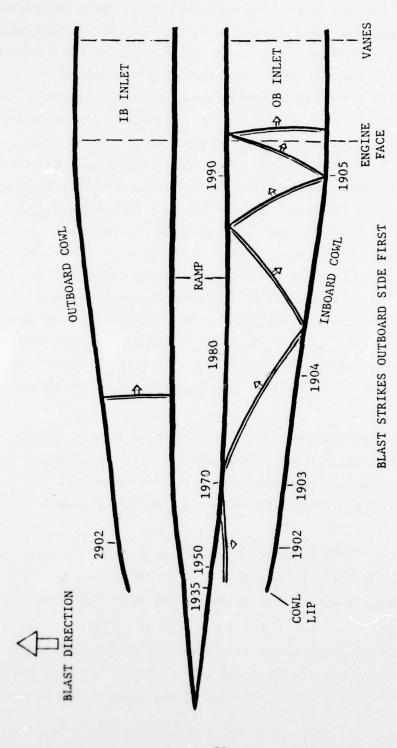


Figure 5.4. Typical shock wave pattern in the inlets.

to the sum of the (pre-blast) flow velocity in the inlet plus the speed of sound in the inlet. At the same time the part of the shock wave upstream of the cowl lip proceeds to the outboard ramp surface, experiences essentially normal reflection there, with about doubling of its intensity, and then tends to bounce back and forth between the ramp and cowl surfaces while being at the same time convected downstream into the inlet. The resulting overall blast front pattern at any time can be constructed graphically by assuming the shocks to travel at essentially the speed of sound relative to the local ambient inlet velocity and the accuracy of the construction can be checked or improved by adjusting these constructions slightly to conform to the experimentally observed times of blast arrivals at the various transducer stations along the ramp and cowl indicated in Figure 5.4. (Generally the first two or three shock arrival times can be clearly distinguished in the transducer time histories.) It should be noted that the shock pattern in Figure 5.4 is rather simplified in that it assumes regular reflection of the waves at the cowl and ramp surfaces and it does not consider the interference effects of the engine hub structure (Figure 4.1). Actually Mach stems will tend to form for some reflected waves and additional reflections will occur from the hub; however, Figure 5.4 does illustrate the overall pattern well enough for the present discussions.

The shock pattern on the leeward side of the inlet is much simpler. Here, the shock wave simply diffracts about the tip of the ramp and tends to enter the leeward inlet essentially as a one-dimensional disturbance having a single shock with its front essentially normal to the inlet side walls.

The shock patterns shown in Figure 5.4 were based partly on test data for Run 39 (Part 544) conditions, Mach 0.85 at 350 lb/sec, but would be expected to apply rather well to any of the other test Mach numbers as well.

Now, to indicate the significance of the type of shock pattern seen in Figure 5.4, consider first the blastward inlet. It is seen that the shock waves are generally not at all parallel to the inlet walls, except

State of the second state of the second

for the initial blast front. Hence, there is generally an appreciable time-varying spatial variation of blast pressure across any section of the inlet, which lasts from the time of first blast arrival until that time when all of the incident blast front and its reflections will have been either convected downstream through the engine or reflected from the engine throat back upstream and out the mouth of the inlet. This spatial pressure variation across any section of the inlet will, of course, produce flow distortion in the section, the intensity of which will be related to the intensity of the shock or shocks passing through or near to that section at the time in question.

Another consequence of the complex shock pattern in the blastward inlet is its effect on the rate at which the shock pressure builds up. Essentially, for the blastward inlet, the pressure buildup consists of a sequence of separated shocks adding to each other, so that the resultant effect is a relatively slow staircase type buildup of pressure, taking on the order of 0.3 millisecond for typical cases. On the leeward inlet, however, where there is essentially a single shock front, the pressure buildup is essentially instantaneous.

5.3 ANALYSIS OF INLET DISTORTION

A primary objective of the test program was to obtain time histories of the inlet distortion parameters resulting during blast wave inlet interactions. In this study, time histories of the following inlet distortion parameters were calculated from the test data for both inlets for all runs and were plotted as illustrated in Figure 5.5 for Run 8 (Part 573): IDCi, IDRi, IDC12, IDC45, IDR, IDC, IDL, IDA and IDT, where i designates the ith instrumented engine face ring (i = 1 to 5). These particular distortion parameters, defined in Table 5.1, were selected because they are standard for the analysis of the B-1 inlet and engine system. The discussion of distortion in this report is, however, restricted to the parameters IDC, IDR and IDL, and primarily to IDL. IDC is the total circumferential distortion index, IDR is the total radial distortion index and IDL is the fan stall margin ratio. IDL is an overall measure of the inlet distortion, which depends on IDC,

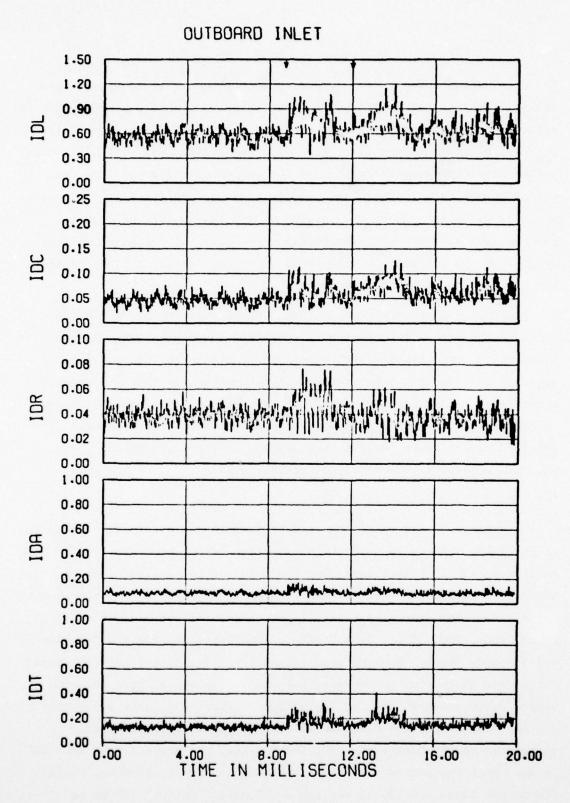


Figure 5.5. Distortion time histories for Run 8 (Part 573), Mach 0.70, $\Delta p = 5.0$ psi, $\phi = 98^{\circ}$, flow rate ≈ 303 lb/sec, tube 2.

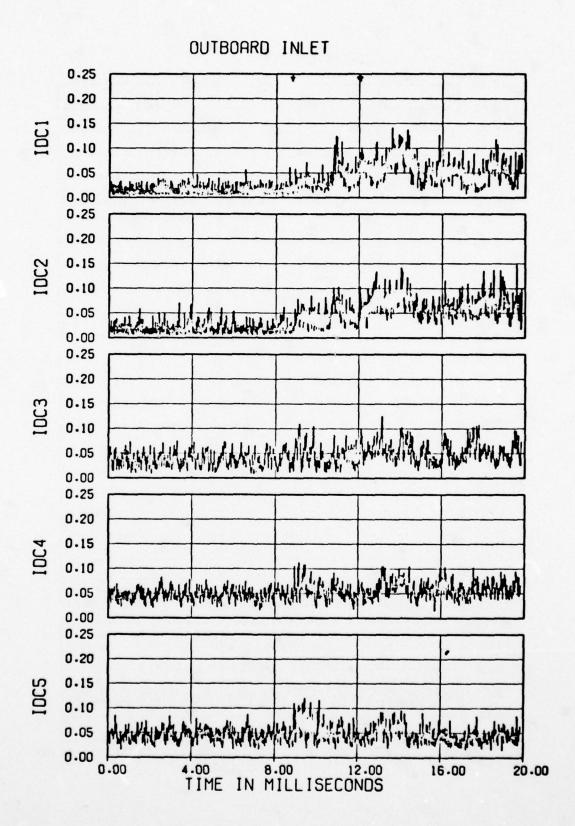


Figure 5.5. Continued.

and the service of th

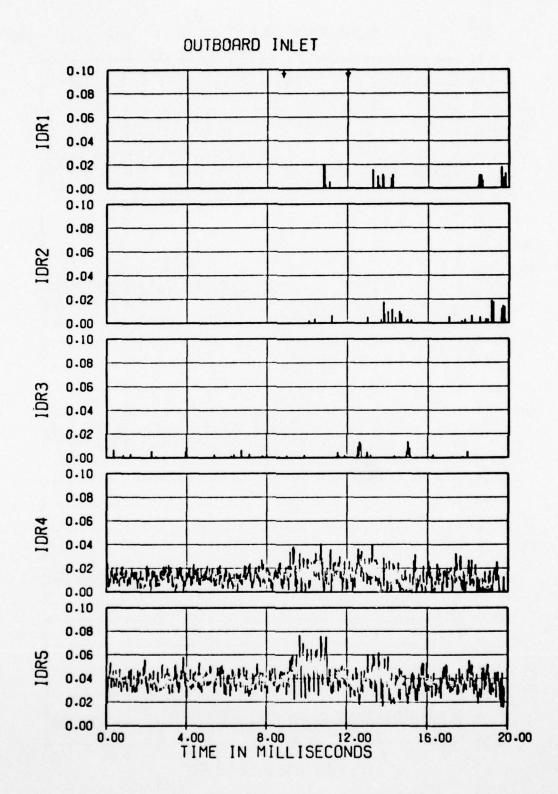


Figure 5.5. Continued.

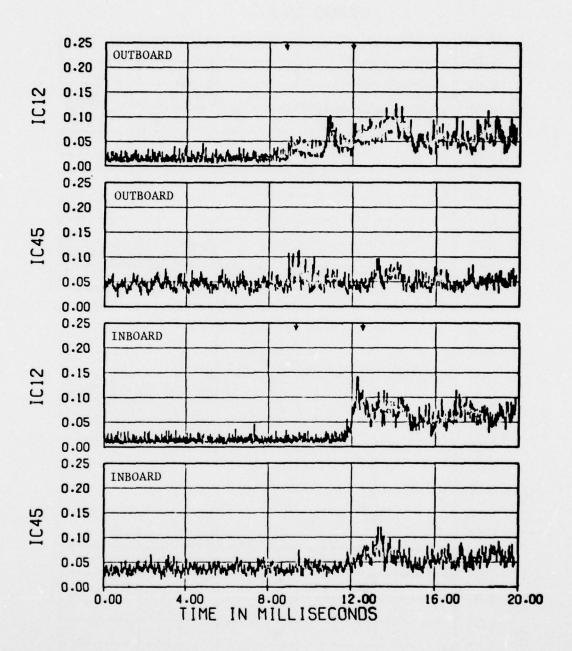


Figure 5.5. Continued.

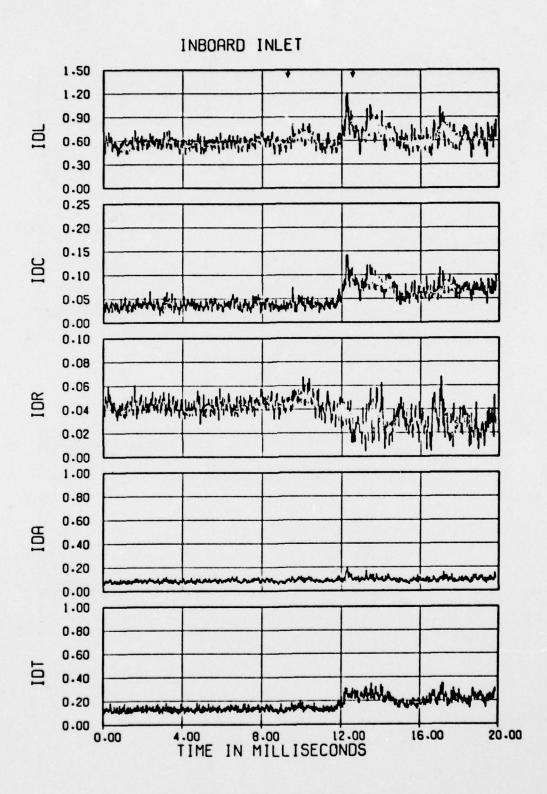


Figure 5.5. Continued.

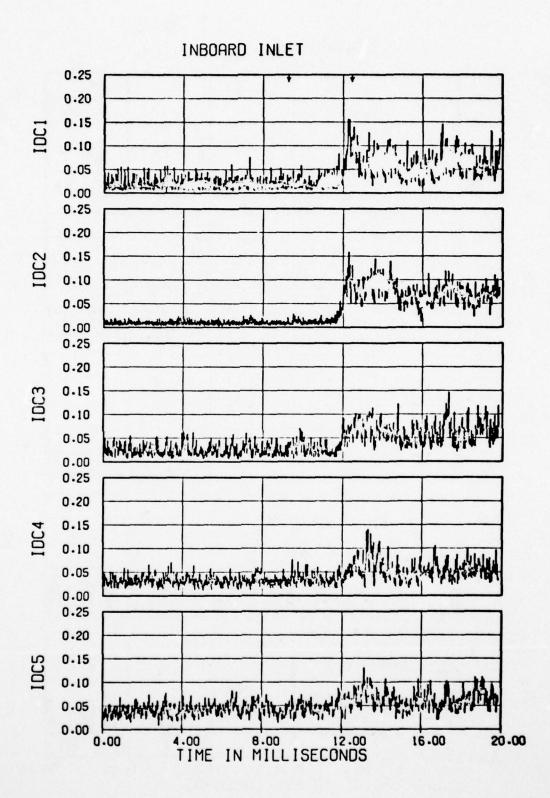


Figure 5.5. Continued.

the first to have the contract or their own

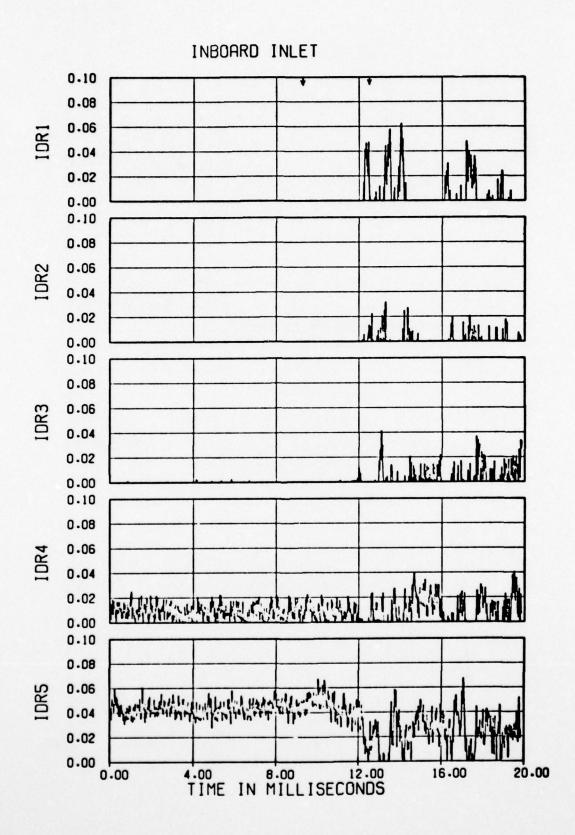


Figure 5.5. Concluded.

TABLE 5.1

EQUATIONS FOR CALCULATING DISTORTION PARAMETERS IDC, IDR, IDL, IDA AND IDT

Circumferential Distortion on Individual Rings

$$IDC_{i} = (p_{t2}_{avci} - p_{t2}_{min_{i}})/\overline{p}_{t2}$$

where

$$i = 1$$
 to 5 rings

Hub Distortion

$$IDC_{12} = (IDC_1 + IDC_2)/2$$

Tip Distortion

$$IDC_{45} = (IDC_4 + IDC_5)/2$$

Total Circumferential Distortion

IDC = Largest of
$$IDC_{12}$$
 or IDC_{45}

Radial Distortion on Individual Rings

ion on Individual Rings

$$IDR_{i} = Largest of (1.0 - \frac{P_{t2}}{\overline{P}_{t2}}, 0)$$

Total Radial Distortion

IDR = Largest of
$$IDR_1$$
, IDR_2 , IDR_4 , or IDR_5

Fan Stall Margin Ratio

$$IDL = b(KCIRC)IDC + (KRAD)IDR$$

where

$$b = \frac{IDR/IDC}{A+B(IDR/IDC)} + C$$

the state of the state of the state of

TABLE 5.1. CONCLUDED

масн	TUNNEL TOTAL			SUPER POSITION FACTOR b		
NUMBER	TEMPERATURE (°R)	KCIR	KRAD	A	В	С
0 < .15	A11	7.93	12.41	-0.536	-0.591	1.
.15 ≤ .35	A11	7.69	11.76	-0.520	-0.643	1.
.35 ≤ .65	A11	7.69	12.28	-0.520	-0.644	1.
.65 <u><</u> .75	A11	7.69	12.42	-0.520	-0.644	1.
.75 ≤ 1.5	Less Than/Equal To 560.	7.69	12.83	-0.520	-0.644	1.
.75 ≤ 1.5	Greater Than 560.	7.93	12.99	-0.553	-0.532	1.
1.5 < 2.3	A11	7.69	11.75	-0.560	-0.920	1.

Average Distortion:

IDA =
$$(\overline{p}_{t2} - p_{t_{min}})\overline{p}_{t2}$$

Total Distortion:

IDT =
$$(p_{t_{max}} - p_{t_{min}})/\overline{p}_{t2}$$

IDR and the speed altitude regime. An indication of the normally allowable range of these distortion parameters for subsonic flight of the B-l aircraft is given in Figure 5.6 (from Ref. 5.1). Generally, the inlet and engine can be considered to perform satisfactorily at values of IDL up to unity, which corresponds to values of IDC and IDR to the left of and below the solid line curve in Figure 5.6. For larger values of IDC, IDR or IDL the engine can stall, but will not necessarily do so.

5.3.1 Data Presentation

Typical time histories of distortion parameters for various overpressure levels are presented in Figures 5.7 through 5.17. Figure 5.7 presents IDL for the lower tested mass flow rate (\$\approx\$300 lb/sec) at Mach 0.70 for both inlets and Figures 5.8 and 5.9 present similar data for the higher tested mass flow rate (\$\approx\$350 lb/sec) for the blastward and leeward inlets, respectively. Figure 5.10 presents IDC, IDR and IDL for the lower mass flow rate (\$\approx\$300 lb/sec) at Mach 0.85 for the blastward inlet and Figure 5.11 presents IDL for the leeward inlet; Figure 5.12 presents IDC, IDR and IDL for the higher mass flow rate (\$\approx\$350 lb/sec). Mach number effects on IDC, IDR and IDL are indicated in Figures 5.13 and 5.14 for blastward and leeward inlets for firings from Tube 2 and, for IDL only, in Figures 5.15 and 5.16 for firings from Tube 1. IDL measurements made during the three yawed firings are presented in Figure 5.17.

5.3.2 Effects at Low Mass Flow Rates

Considering now the distortion effects at the lower tested mass flow rate of about 300 lb/sec (full scale), it can be seen from Figure 5.7 for Mach 0.70 and from Figure 5.10c and 5.11 for Mach 0.85 that the stall margin, IDL, is usually well below the normally safe limit of unity, usually being near to or below 0.5, for the time range where the test data are definitely representative of a blast wave (between the two arrows in the figures). Corresponding values of IDC and IDR, shown in Figure 5.10 for Mach 0.85 are similarly rather low, being generally below 0.10 for IDC and below 0.05 for IDR.

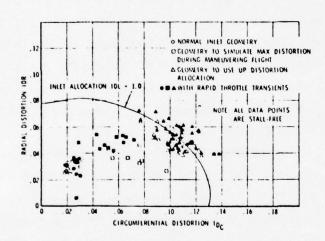
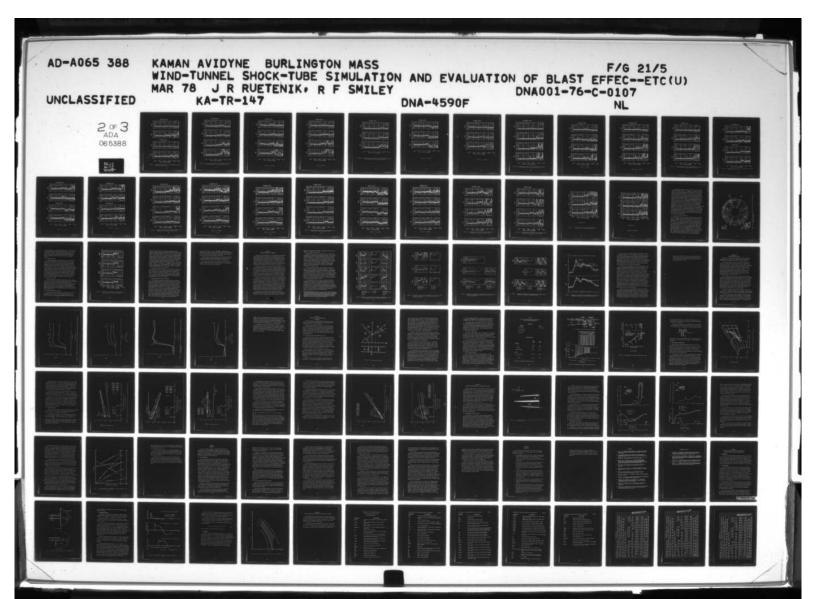


Figure 5.6. Range of distortion indices for B-1 inlet at subsonic cruise.



OUTBOARD INLET 1.50 $\phi = 106^{\circ}$ $\Delta p = 2.6$ RUN 7 1.20 0.90 0.60 0.30 PART 600 0.00 1.50 $\phi = 98^{\circ}$ $\Delta p = 5.0$ RUN 8 1.20 0.90 10 0.60 0.30 PART 573 0.00 INBOARD INLET 1.50 $\phi = 106^{\circ}$ $\Delta p = 2.6$ RUN 7 1.20 0.90 디 0.60 0.30 PART 600 0.00 1.50 $\phi = 98^{\circ}$ $\Delta p = 5.0$ RUN 8 1.20 0.90 0.60 0.30 0.00 0.00 TIME IN MILLISECONDS 16.00

Figure 5.7. Distortion time histories for two overpressures at Mach 0.70, flow rate ≈ 300 lb/sec, tube 2.

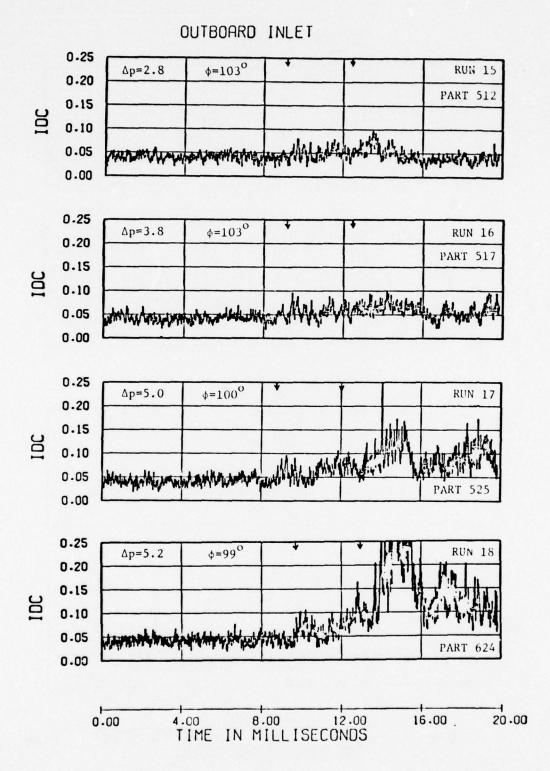


Figure 5.8. Distortion time histories for four overpressures at Mach 0.70 for the blastward inlet, flow rate ≈ 350 lb/sec, tube 2.

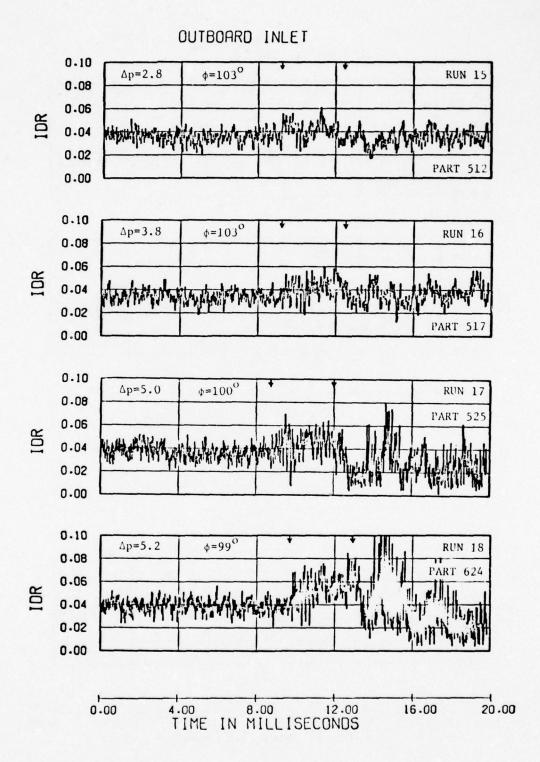


Figure 5.8. Continued.

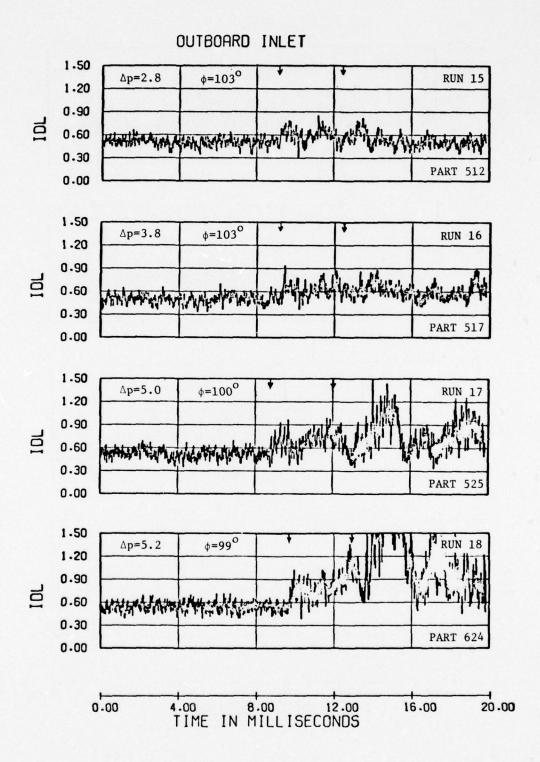


Figure 5.8. Concluded.

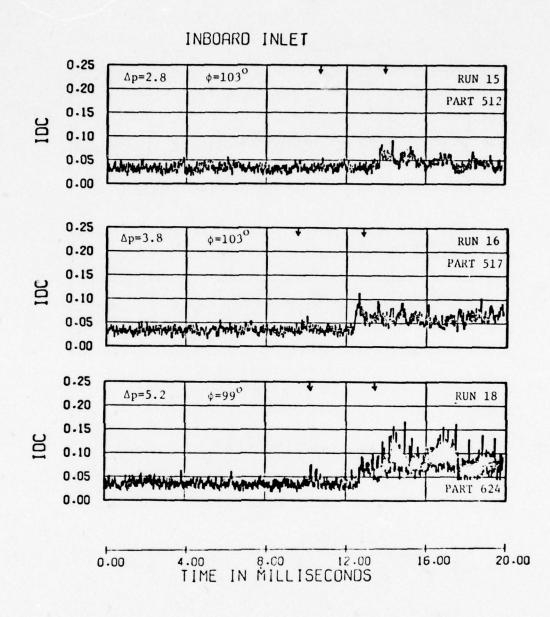
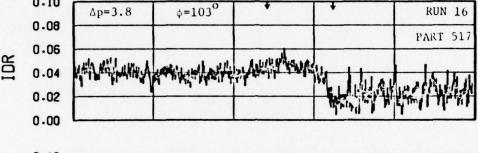
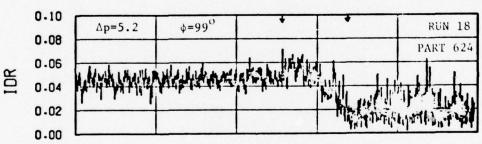


Figure 5.9. Distortion time histories for three overpressures at Mach 0.70 for the leeward inlet, flow rate $\approx 350\,$ lb/sec, tube 2.

The second of th

1 NBOARD INLET 0.10 0.08 0.06 0.04 0.02 0.00 PART 512





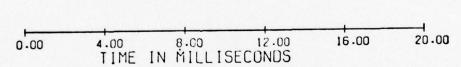


Figure 5.9. Continued.

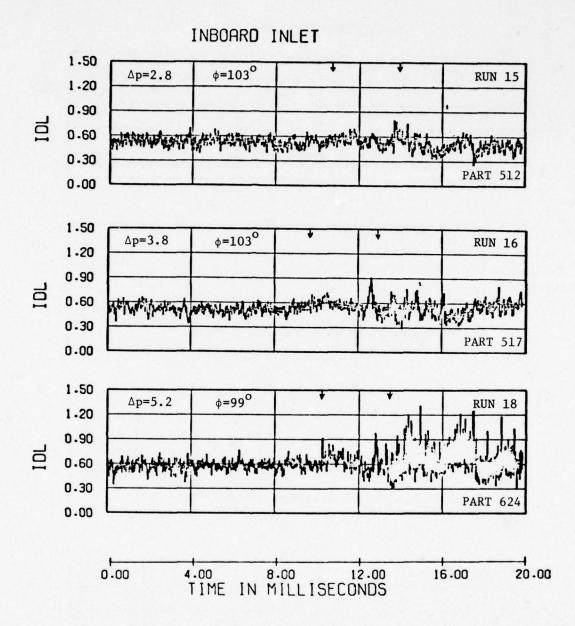


Figure 5.9. Concluded.

OUTBOARD INLET 0.25 φ=89⁰ RUN 26 $\Delta p=2.2$ 0.20 PART 559 0.15 100 0.10 0.05 0.00 0.25 $\Delta p=3.0$ φ=85° RUN 27 0.20 **PART 598** 0.15 3 0.10 0.05 0.00 0.25 $\phi = 82^{0}$ RUN $\Delta p = 4.4$ 0.20 0.15 0.10 0.05 PART 608 0.00 0.25 φ=82⁰ RUN 28 $\Delta p=5.0$ 0.20 0.15 0.10 0.05 PART 584 0.00 20.00 0.00 4.00 12.00 16.00 8.00 TIME IN MILLISECONDS

Figure 5.10. Distortion time histories for four overpressures at Mach 0.85 for the blastward inlet, flow rate ≈ 300 lb/sec, tube 1.

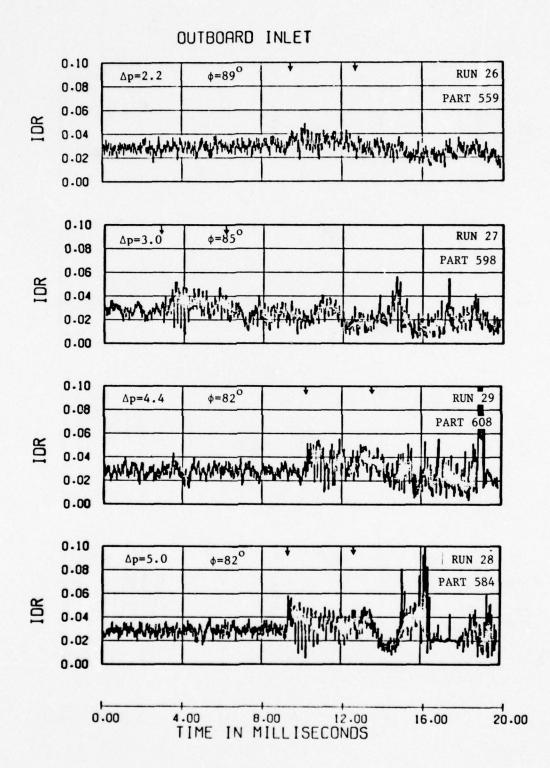


Figure 5.10. Continued.

OUTBOARD INLET

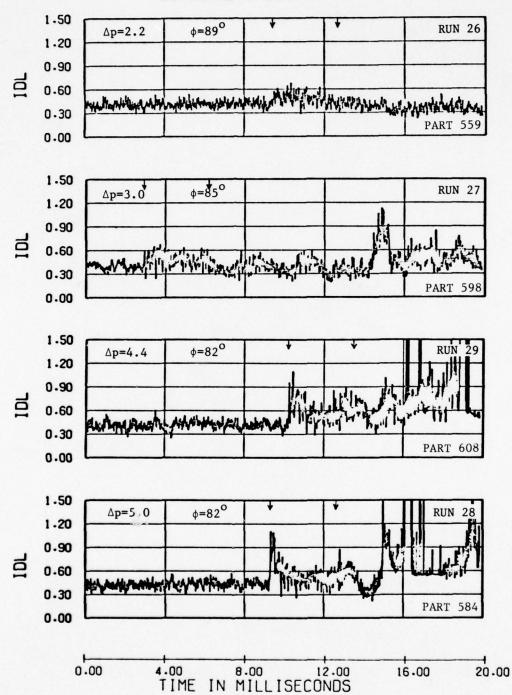


Figure 5.10. Concluded.

INBOARD INLET 1.50 $\phi = 89^{\circ}$ $\Delta p = 2.2$ RUN 26 1.20 0.90 IP. 0.60 0.30 PART 559 0.00 1.50 $\Delta p = 3.0$ $\phi = 85^{\circ}$ RUN₂₇ 1.20 0.90 디디 0.60 0.30 PART 598 0.00 1.50 $\phi = 82^{\circ}$ $\Delta p = 4.4$ RUN 29 1.20 0.90 디 0.60 0.30 0.00 1.50 RUN 28 $\phi = 82^{\circ}$ $\Delta p = 5.0$ 1.20 0.90 걸 0.60 0.30 PART 584 0.00 0.00 20.00 4.00 8.00 12.00 16.00 TIME IN MILLISECONDS

Figure 5.11. Distortion time histories for four overpressures at Mach 0.85 for the leeward inlet, flow rate ≈ 300 lb/sec, tube 1.

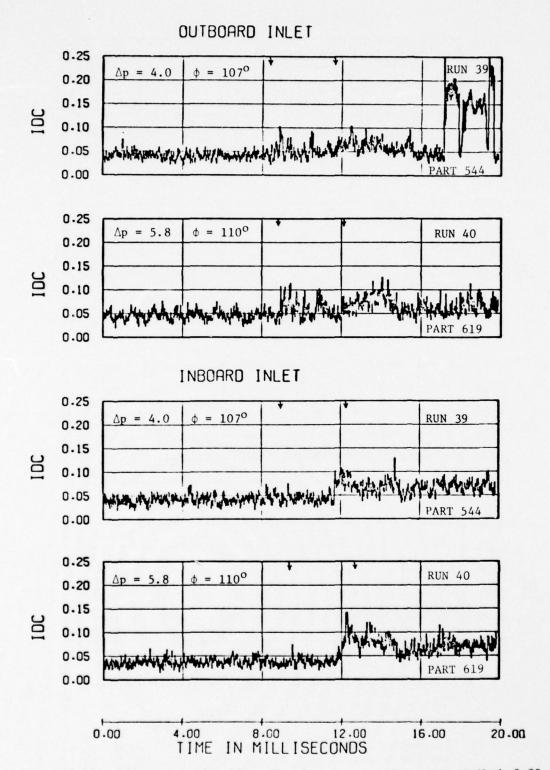


Figure 5.12. Distortion time histories for two overpressures at Mach 0.85, flow rate ≈ 350 lb/sec, tube 2.

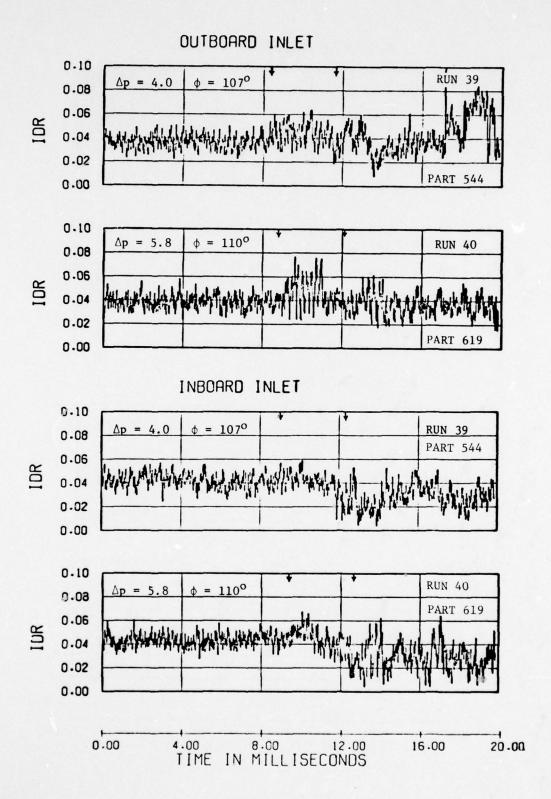


Figure 5.12. Continued.

OUTBOARD INLET 1.50 $\phi = 107^{0}$ $\Delta p = 4.0$ 1.20 0-90 0.60 0.30 PART 544 0.00 1.50 $\phi = 110^{\circ}$ $\Delta p = 5.8$ RUN 40 1.20 0.90 0.60 0.30 PART 619 0.00 INBOARD INLET 1.50 $\phi = 107^{\circ}$ **RUN 39** $\Delta p = 4.0$ 1.20 0.90 0.60 0.30 PART 544 0.00 1.50 $\phi = 110^{\circ}$ $\Delta p = 5.8$ 1.20 0.90 0.60 0.30 PART 619 0.00 0.00 8.00 16.00 20.00 TIME IN MILLISECONDS

Figure 5.12. Concluded.

OUTBOARD INLET 0.25 φ=97° RUN 4 M=0.55 $\Delta p = 3.8$ 0.20 0.15 0.10 0.05 **PART 589** 0.00 0.25 $\phi = 103^{\circ}$ $\Delta p=3.8$ M=0.70**RUN 16** 0.20 PART 517 9.15 0.10 0.05 0.00 0.25 φ=107⁰ M=0.85 $\Delta p = 4.0$ 0.20 0.15 301 0.10 0.05 0.00 0.25 $\phi = 107^{\circ}$ M=0.90 $\Delta p = 4.0$ RUN 44 0.20 PART 550 0.15 2 0.10 0.05 0.00

Figure 5.13. Distortion time histories for four Mach numbers for the blastward inlet, flow rate $\approx 350\,$ lb/sec, tube 2.

8.00

TIME IN MILLISECONDS

0.00

4.00

12.00

20.00

16.00

OUTBOARD INLET

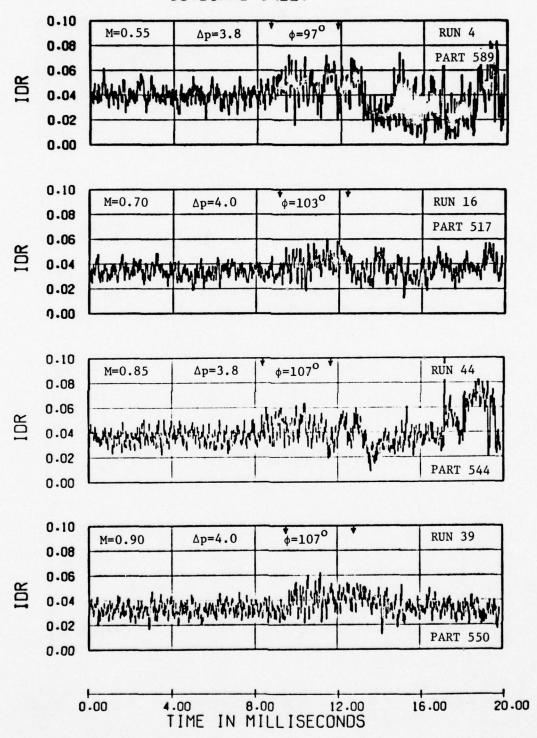


Figure 5.13. Continued.

OUTBOARD INLET 1.50 φ=97° $\Delta p=3.8$ M=0.551.20 0.90 0.60 Run 4 0.30 Part 589 0.00 1.50 M=0.70 $\Delta p=3.8$ φ=103° Run 16 1.20 Part 517 0.90 0.60 0.30 0.00 1.50 φ=107⁰ M=0.85Run 39 $\Delta p = 4.0$ 1.20 0.90 AND THE PROPERTY OF THE PROPER 0.60 0.30 Part 544 0.00 1.50 φ=107° M=0.90 $\Delta p = 4.0$ Run 44 1.20 0.90 0.60 0.30 Part 550 0.00 0.00 4.00 8.00 16.00 20.00 TIME IN MILLISECONDS

Figure 5.13. Concluded.

INBOARD INLET 0.25 φ=97° M=0.55 $\Delta p=3.8$ RUN 4 0.20 **PART 589** 0.15 0-10 0.05 0.00 0.25 φ=103° M=0.70 $\Delta p=3.8$ RUN 16 0.20 PART 517 0.15 0.10 0.05 0.00 0.25 φ=107° M=0.85 $\Delta p=4.0$ **RUN 39** 0.20 PART 544 0.15 20 0.10 0.05 0.00 0.25 φ=107⁰ M=0.90 $\Delta p = 4.0$ RUN 44 0.20 PART 550 0.15 0.10 0.05 0.00 0.00 20.00 4.00 8.00 12.00 16.00

Figure 5.14. Distortion time histories for four Mach numbers for the leeward inlet, flow rate ≈ 350 lb/sec, tube 2.

TIME IN MILLISECONDS

INBOARD INLET 0.10 φ=97° M=0.55 $\Delta p=3.8$ Run 4 0.08 Part 589 0.06 IDR 0.04 0.02 0.00 0.10 φ=103° M=0.70 $\Delta p=3.8$ Run 16 0.08 Part 517 0.06 IDR 0.04 0.02 0.00 0.10 φ=107° M=0.85 $\Delta p=4.0$ Run 39 0.08 Part 544 0.06 0.04 0.02 0.00 0.10 $\phi = 107^{\circ}$ M=0.90 $\Delta p = 4.0$ Run 44 0.08 Part 550 0.06 0.04 0.02 0.00 0.00 12.00 4.00 8.00 16.00 TIME IN MILLISECONDS

Figure 5.14. Continued.

INBOARD INLET 1.50 φ=97° M=0.55 $\Delta p=3.8$ RUN 4 1.20 0.90 0.60 0.30 **PART 589** 0.00 1.50 φ=103° M=0.70 $\Delta p=3.8$ RUN 16 1.20 PART 517 0.90 0.60 0.30 0.00 1.50 φ=107⁰ **RUN 39** $\Delta p=4.0$ M=0.851.20 PART 544 0.90 길 0.60 0.30 0.00 1.50 φ=107° M=0.90 $\Delta p = 4.0$ RUN 44 1.20 0.90 딜 0.60 0.30 PART 550 0.00 0.00 20.00 16.00 12.00 8.00 4.00

Figure 5.14. Concluded.

TIME IN MILLISECONDS

OUTBOARD INLET 1.50 $\phi = 76^{\circ}$ $\Delta p = 3.7$ M = 0.55RUN 3 1.20 0.90 0.60 0.30 PART 591 0.00 1.50 $\phi = 88^{\circ}$ $\Delta p = 3.8$ RUN 12 M = 0.701-20 0.90 0.60 0.30 **PART 519** 0.00 1.50 M = 0.85 $\Delta p = 3.6$ 1.20 0.90 0.60 0.30 PART 546 0.00 1.50 M = 0.90 $\Delta p = 3.0$ $= 86^{\circ}$ 1.20 0.90 급 0.60 0.30 PART 553 0.00 0.00 16.00 20.00 4.00 8.00 12.00 TIME IN MILLISECONDS

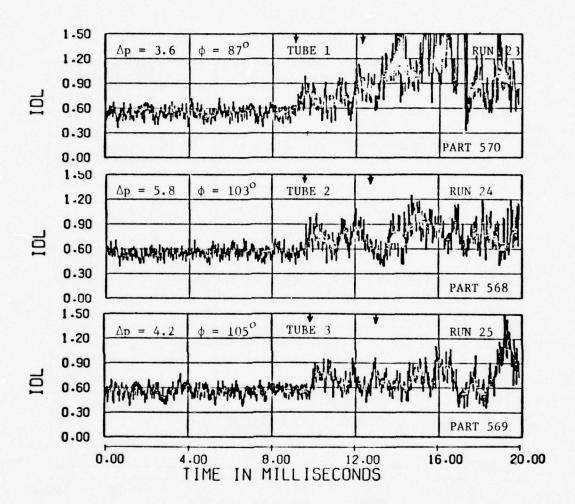
Figure 5.15. Distortion time histories for four Mach numbers for the blastward inlet, flow rate ≈ 350 lb/sec, tube 1.

De the water the said

INBOARD INLET 1.50 M = 0.55 $\Delta p = 3.7$ RUN 3 1.20 0.90 101 0.60 0.30 PART 591 0.00 1.50 M = 0.70 $\Delta p = 3.8$ 1.20 0.90 디 0.60 0.30 PART 519 0.00 1.50 M = 0.85 $\Delta p = 3.6$ 1.20 0.90 디 0.60 0.30 PART 546 0.00 1.50 M = 0.90 $\Delta p = 3.0$ **RUN 43** 1.20 0.90 0.60 0.30 PART 553 0.00 0.00 16.00 20.00 4.00 8.00 12.00

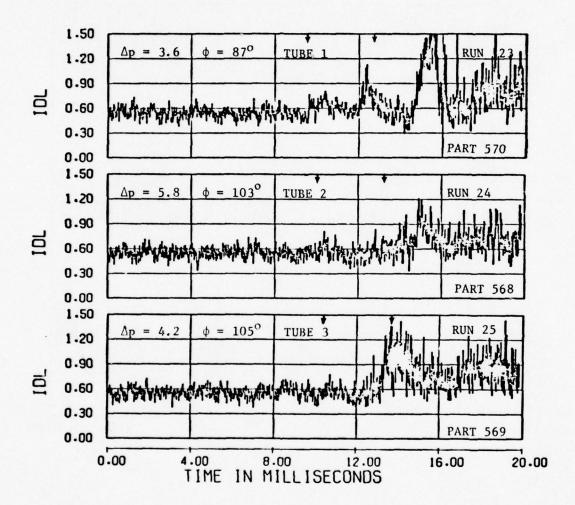
Figure 5.16. Distortion time histories for four Mach numbers for the leeward inlet, flow rate ≈ 350 1b/sec, tube 1.

TIME IN MILLISECONDS



(a) Blastward Inlet

Figure 5.17. Distortion time histories for three yawed runs at Mach 0.70, yaw = 5°, flow rate≈350 lb/sec.



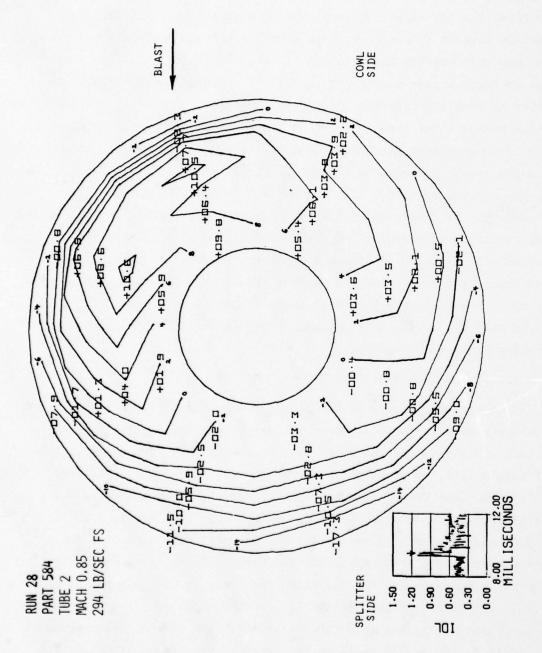
(b) Leeward Inlet

Figure 5.17. Concluded.

In a few cases, values of IDL, IDC and IDR in excess of normally allowable limits were observed. For example, for Run 28 (Part 584) in Figure 5.10, large distortion values were experienced in the blastward inlet shortly after blast intercept, but the duration of this large distortion appears to have been less than 0.1 msec (1 msec full-scale). It is uncertain whether the duration of this distortion pulse was long enough to imply a significant adverse effect on engine performance. As a matter of possible interest, Figure 5.18 presents engine-face totalpressure contours for this run, indicating the total-pressure variation across the engine face at a time close to the time of peak distortion (indicated by the arrow in the inset IDL plot). The corresponding instantaneous values of IDL, IDC and IDR are 1.05, 0.103 and 0.061, respectively. The numerical values in this figure represent the difference between the face-average total-pressure and the local total-pressure, expressed as a fraction of face-average total-pressure. Test data points (or interpolations thereof for a few bad data points) are represented as large numbers and contour levels by small handwritten numbers. It may be noted that the lowest total-pressure drop is about 17 percent below the face-average total-pressure.

5.3.3 Effects at High Mass Flow Rates

The distortion effects at the higher tested mass flow rate of 350 lb/sec are generally at least somewhat larger than for the lower mass flow rate. However, for the lower overpressures, up to about 4 psi, the stall margin, IDL, is generally observed to be well below the limit of unity in the blast range (between the two arrows), being generally near to or below 0.9 (see Figures 5.8 and 5.9 for Mach 0.70, Figure 5.12 for Mach 0.85 and Figures 5.13 and 5.14 for a range of Mach numbers). For higher overpressures than 4 psi, IDL sometimes appears to exceed unity in the blast range (e.g., for the blastward inlet at $\Delta p = 5.2$ psi at Mach 0.70 in Figure 5.8 and for the leeward inlet for $\Delta p = 5.8$ psi at Mach 0.85 in Figure 5.12), but only for a small fraction of a millisecond at most. Outside the blast range (to the right of the second arrows in the figures) IDL values appreciably larger than unity are observed



Outboard inlet total pressure contours for a large blast-induced distortion condition. Figure 5.18.

for some firings (e.g., for the blastward inlet at $\Delta p = 5.2$ psi at Mach 0.7 in Figure 5.8 and for blastward and leeward inlets at $\Delta p = 3.8$ psi at Mach 0.55 in Figure 5.13), but further study would be required to verify whether these late time data are relevant to the blast-inlet problem. Possible sources of late-time distortion are discussed in Section 9.

5.3.4 Mach Number Effects

No definite significant effects of Mach number on the distortion indices IDL, IDC and IDR were observed in the blast range (e.g., see Figures 5.13 and 5.14). This lack of observed effect is attributed primarily to the choking action of the vane system downstream of the simulated engine face, which tends to maintain the internal inlet flow at any location in the inlet at a constant Mach number condition, regardless of the state of the external flow conditions. Further more definite evidence indicating this apparent lack of Mach number effects on inlet pressures is given in Figure 5.19, which compares inlet ramp pressures for transducer 1980 (located about half-way down the inlet, see Figure 5.4) for four Mach number conditions. It may be noted that most fine details of the pressure histories in Figure 5.19 are almost identical for the different Mach numbers, especially for Mach 0.55 and 0.85.

5.3.5 Effects of Yaw Angle

No definite effects of yaw angle on distortion are readily evident from the results of the three yawed test firings (Figure 5.17). Appreciable increases in IDL occurred for both inlets in each firing, but the increases did not generally appear much greater than for similar unyawed firings (see Figs. 5.8 and 5.9). However, it should be noted that a significantly high level of distortion appears to have developed in the leeward inlet toward the end of the nominal blast event (at second arrow) of Run 25 (Fig. 5.17b).

5.3.6 Long Duration Distortion Effects

If the rate of decay of a blast wave is extremely small, as for a large nuclear burst, then the struck inlet-engine system will tend at late times to come to a quasi-steady equilibrium condition where the

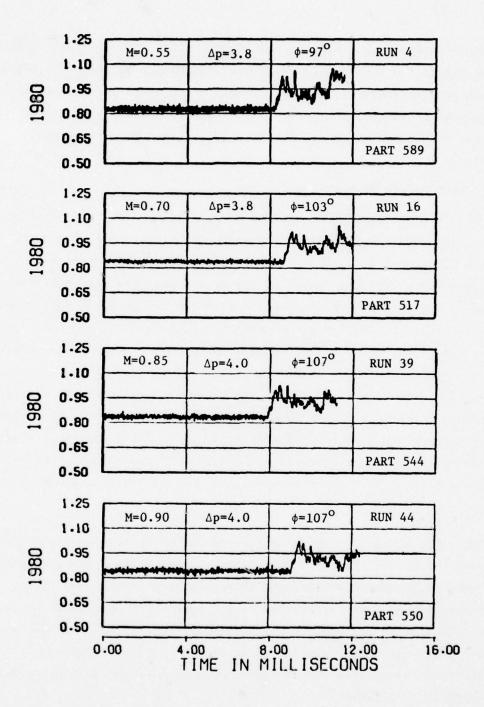


Figure 5.19. Comparison of ramp pressure time histories for four Mach numbers, tube 2, flow rate≈350 lb/sec.

effect of the blast wave will be essentially the same as would be produced by steady yawed flight at the side-slip angle and total pressure caused by the blast (as given by Figures 5.1 and 5.2. In regard to this point, it may be noted that our test results for steady yawed conditions generally indicate 10% or less increase, or decrease, in the distortion parameter IDL as the sideslip angle varies from the zero angle condition to angles anywhere in the range from -10° to +10°. Hence, it might be expected that late-time blast distortions would be small for blast overpressures producing blast-induced sideslip angles up to at least 10°, as given by Figure 5.1 in Section 5. For example, for Mach 0.85 flight, Figure 5.1 indicates that blast overpressures up to about 3.3 psi would not produce sideslip angles over 10° and, hence, would not be expected to produce large late-time distortion effects.

The value of the above observations is, of course, of limited value since we cannot at this time specify what we mean by "late time" in a very definite manner. However, judging from BID code calculations for times up to about 6 milliseconds, presented later in Section 7 (Figure 7.2), it appears that quasi-steady equilibrium would not be reached for the test model until times considerably greater than 6 milliseconds (or 60 milliseconds for a full scale B-1 inlet).

5.3.7 Concluding Remarks on Distortion Effects

In concluding this discussion of distortion effects, it should be noted that while generally very few large distortion values were obtained during the early-time definitely blast-type flow periods of the present tests, the distortion criteria used above (IDC, IDR and IDL) are not necessarily completely reliable indices of whether an engine would stall under transient blast conditions. Other distortion criteria should also be considered (e.g., Ref. 5.2 and 5.3) and attention should also be directed to the actual contours of pressure distortion which are obtained under blast intercept conditions, such as is illustrated in Figure 5.18 for one run at a time shortly after blast intercept (see arrow in inset IDL plot) when appreciable distortion was experienced in the outboard inlet. Also attention should be directed to the durations of any large observed distortion levels, comparing them with duration results

and the second second

from other tests (e.g., Ref. 5.4). Furthermore, attention should be directed also to effects of blast-induced longitudinal pressure variations (Sec. 9) and blast-fan interactions (Sec. 8) to assess more completely the possible stall inducing potential of blast waves.

These same types of questions should also be considered with respect to the large distortion values sometimes observed at times after the fairly definite blast type flow duration time of 3.3 milliseconds.

Most of the above topics are not explored in the present report because the reduced test data were not made available in a suitable form in time to permit such studies to be performed.

SECTION VI COMPARISON OF THEORY AND EXPERIMENT

Concurrent with the performance of this experimental investigation, Kaman AviDyne developed a theoretical two-dimensional computer code, designated BID (blast-induced-distortion), for predicting the transient flow field produced in a inlet by a blast wave striking the inlet at an arbitrary angle of incidence (Reference 6.1). Calculations of inlet pressure time histories were made with this code for four conditions similar to those of the 16T experimental tests and the results of these calculations are compared with the test results in this section.

The specific conditions for which BID calculations were made are: constant shock overpressure of 5 psi at one atmosphere ambient pressure, inlet mass flow rate (full-scale) 350 lb/sec, tunnel Mach number of 0.70 for a blast intercept angle of $\phi=90^{\circ}$ and tunnel Mach number of 0.85 for intercept angles of $\phi=90^{\circ}$, 105° and 135° . Calculated BID pressure time histories for various locations in the inlets are presented in Figures 6.1 to 6.5 together with experimental data for those test runs corresponding most closely to the conditions of the theoretical calculations.

The reader is reminded here that in looking at the experimental data in Figures 6.1 to 6.3, attention should be directed on times between the two arrows above each curve; the data at later times are not considered necessarily representative of a blast type flow (See Sec. 4). Also it should be recognized that the theoretical calculations shown in Figures 6.1 to 6.4 are for a constant-strength (step) blast wave (5 psi overpressure), whereas the test data correspond to a time-varying blast wave characterized by an initial shock value (shown below each figure), and possible subsequent increases in pressure, followed by a tendency to decrease to zero in 4-6 milliseconds after initial shock arrival.

The reader is also advised to make comparisons of theory and experiment primarily on the basis of wave shape rather than on amplitude comparisons, since the calibration factors used for some of the shown

ramp and cowl data are either nominal or questionable values and a few appear to be significantly in error * .

Considering first the Mach 0.7 condition, it can be seen from the presentation of ramp and cowl time histories in Figure 6.1 that there is a great difference in the pressure waveforms for different locations in the inlet (see Figure 5.4 to identify the locations indicated in the figure), and that in almost every case the theoretical results follow well most of the details observed in the experimental data. For example, for location 1970, the BID calculation clearly delineates the first three shock arrivals and, at late time, delineates a large pressure increase resulting from reflection of the blast from the simulated engine throat of the inlet model.

A similar comparison is made for ramp pressures for Mach 0.85 in Figures 6.2 and 6.3 and for cowl pressures in Figure 6.4. Again the theoretical and experimental wave shapes are generally in good agreement. A few noticible differences do appear to exist, such as the more rapid late time decays (say near the second arrow) of the experimental pressures for locations 1950 and 1970 in Figure 6.3 and for the cowl locations in Figure 6.4. These differences may be attributed in part to differences between the constant strength blast assumed for the calculations and the actual variable strength blast of the test.

A final comparison is made in Figure 6.5 between calculated and experimental total pressures at the simulated engine face location for a location near the ramp in the blastward (outboard) inlet. The two transducers shown are located vertically above one another in the inlet (see Figure 4.3) so that the theoretical (two-dimensional) BID prediction is the same for both transducers. Differences between the two experimental results are hence indicative of the importance of three-dimensional effects not covered by the theory in its present form.

^{*}These calibration factor problems arose as a result of pre-test mechanical and electrical malfunctions of the transducers which could not be resolved in the very limited time available for the 16T tunnel tests. Preliminary examinations of the test data indicated that more reliable estimates for some of these factors can be obtained by considering some redundant features of the data, but this has not yet been done.

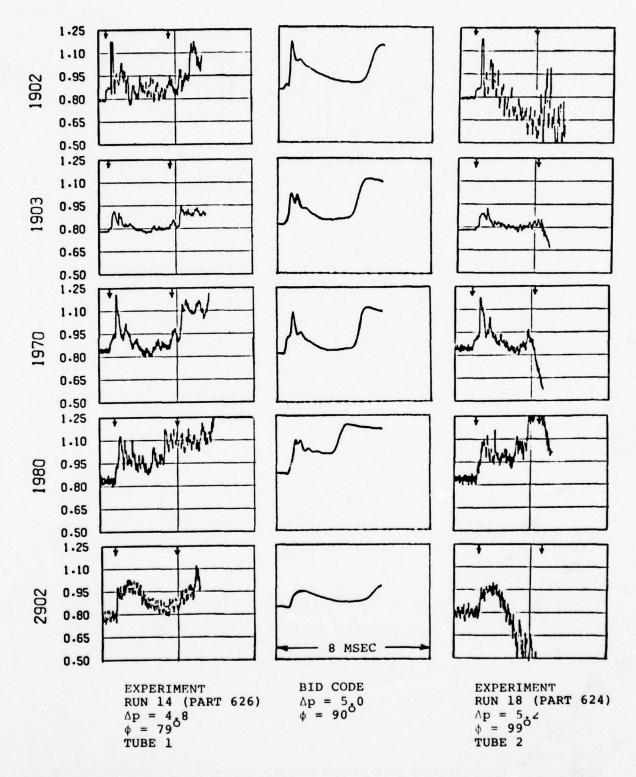


Figure 6.1. Comparison of theoretical and experimental time histories of ramp and cowl pressures at Mach 0.70, flow rate ≈ 350 lb/sec.

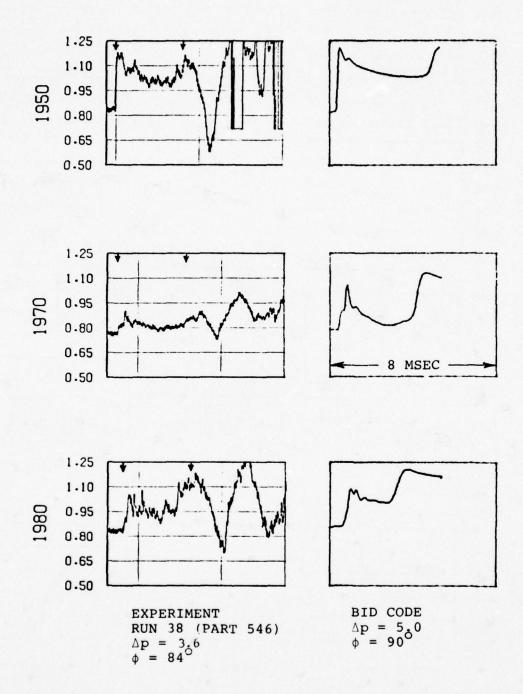


Figure 6.2. Comparison of theoretical and experimental time histories of ramp pressures in the blastward inlet at Mach 0.85, tube 1 data, flow rate ≈ 350 lb/sec.

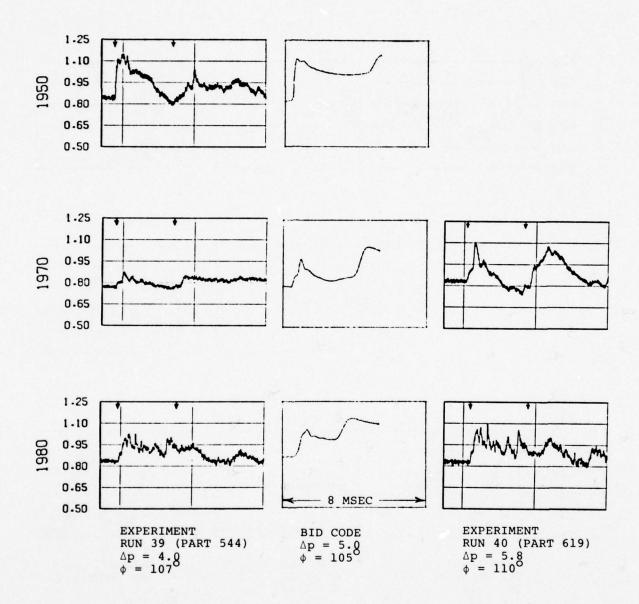


Figure 6.3. Comparison of theoretical and experimental time histories of ramp pressures in the blastward inlet at Mach 0.85, tube 2 data, flow rate ≈ 350 lb/sec.

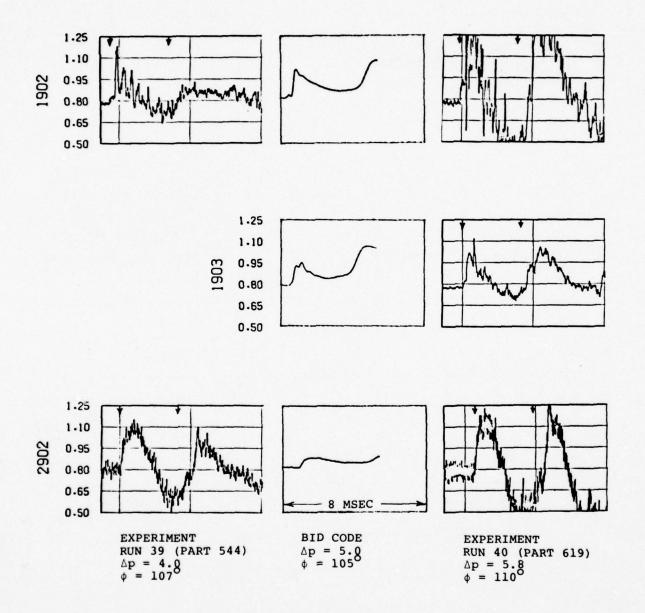


Figure 6.4. Comparison of theoretical and experimental time histories of cowl pressures at Mach 0.85, flow rate ≈ 350 lb/sec.

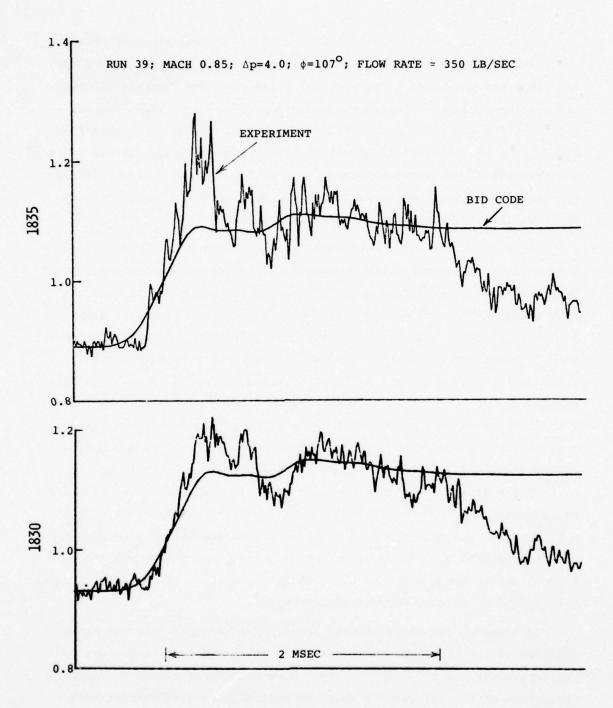


Figure 6.5. Comparison of theoretical and experimental total pressure time histories at the engine face for the blastward inlet.

In order to permit a reasonable quantitative comparison of theory and experiment in Figure 6.5, it was necessary to take into account the fact that the pre-blast (steady-state) pressures were slightly different and the input blast overpressures and orientations were significantly different for the two cases. This difference was taken into account by multiplying the theoretical BID code curve by the ratio of the experimental and theoretical values of the shock jump in input total pressure and by vertically shifting the theoretical curve so that the pre-blast steady-state values were the same for theory and experiment.

The theoretical and experimental total pressures in Figure 6.5 are seen to be in reasonably good agreement in the following respects. Both indicate a reasonably similar (slow) rate of rise of the pressure to a peak value in about 0.3-0.4 millisecond and both have about the same mean peak level of pressure for about 2 milliseconds. Also the third peak in the theoretical curve (at about 1 msec after blast arrival), which represents the return of the blast wave reflected from the simulated engine throat, is in agreement with the corresponding experimental time. There are, of course, some noticable differences, in that the experimental peak values are appreciably greater than the theoretical values and, at later times, may be smaller. These differences may be attributed in part to the finite resolution of the numerical code, some attenuation of the shock for the code due to an effective "artificial viscosity", with a fixed-mesh cell system, to three-dimensional effects (as evidenced by differences between the two experimental traces) not covered by the theory, and to the use in the theoretical calculation of the approximation that the blast wave is of constant strength.

In summary, the above limited comparisons indicate that the major features of the transient pressures observed in the inlet tests are well represented by the BID code results. However, a more extensive comparative study of the 16T results would be desirable to more definitively establish the limitations of the code predictions. Such a correlation would require incorporation into the BID code of the actual time history of the blast wave incident on the inlet (instead of the constant over-

pressure value used here). This, in turn, requires evaluation of the input blast time history from the test data, which is a nontrivial task because of possible significant fuselage inlet and claw probe interference effects.

SECTION VII SHOCK ORIENTATION EFFECTS

This section considers briefly some gross effects of the blast intercept angle, ϕ , on engine face total pressures for the test model as calculated from the BID code for Mach 0.85 flight conditions.

It was noted in Section 5 that for a blast wave of constant overpressure, the increase in blast total pressure in free space (before intercepting the inlet) is largest for zero intercept angle and decreases with increasing intercept angle, according to the curves of Figure 5.2. As might be expected, the same type of variation is obtained for the total pressure at the engine face, as is shown in Figure 7.1. This figure presents total-pressure time histories near the center of the blastward and leeward inlets as calculated with the BID code for a constant-strength 5-psi overpressure blast wave striking the inlets at intercept angles of 90°, 105° and 135°.

It may be noted in Figure 7.1 that, in addition to a decrease of face total pressure with increasing intercept angle, there is a noticeable reduction in the complexity of the pressure signature for the blastward inlet as the intercept angle increases from 90° to 135° . For the nearly side-on intercept angles of 90° and 105° there are two distinct peaks, the first representing the initial blast wave striking the face and the second representing the reflected shock from the choked section of the simulated engine. For the larger 135° intercept angle, where the blast wave overtakes the inlet from the rear, the distinction between the incident and reflected blast wave is hardly detectable.

It can also be observed in Figure 7.1 that the rate of increase of face pressure to its maximum value decreases considerably as the intercept angle increases from 90° to 135° , both for the blastward and leeward inlets.

In order to better relate the face pressures to the incident blast conditions, the total-pressure curves from Figure 7.1 are also presented in Figure 7.2 in the form of the ratio of the change in total pressure (due to the blast) to the change in total pressure across the blast front before it encounters the inlet (from Figure 5.2). It is evident from

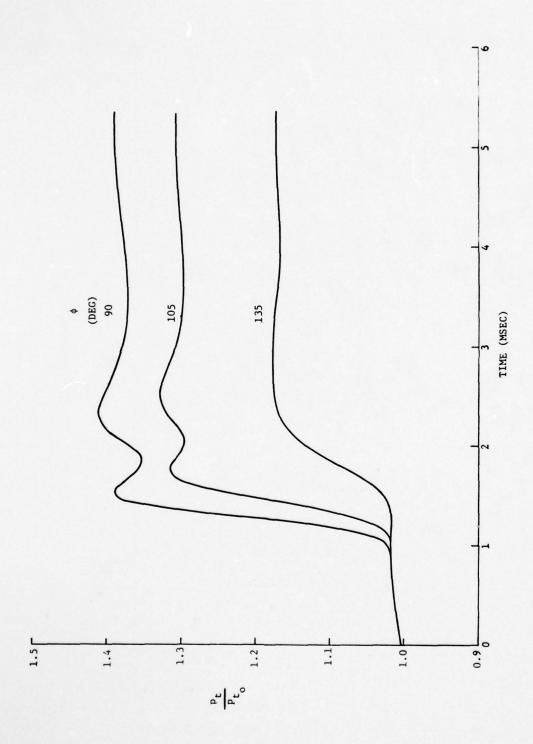


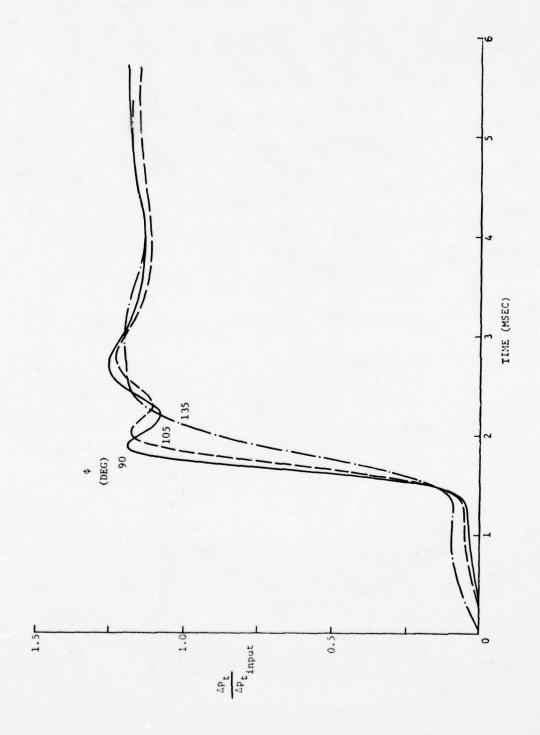
Figure 7.1. Comparison of engine face total pressure time histories for three blast intercept angles.

(a) Blastward inlet.

The spirit was made



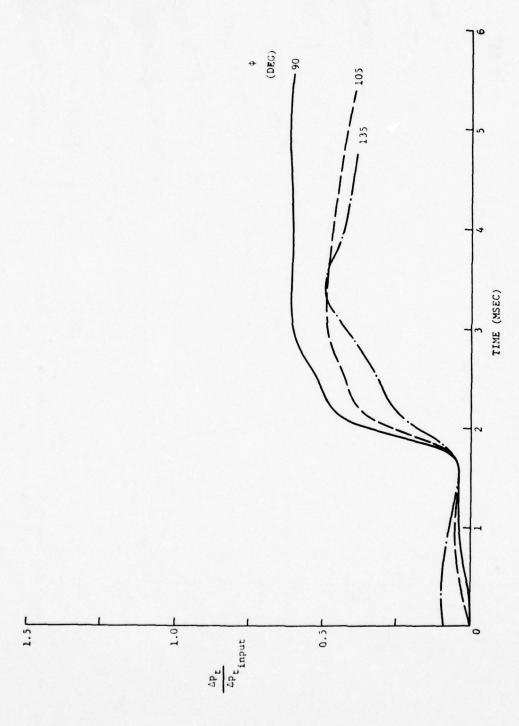
(b) Leeward inlet.
Figure 7.1. Concluded.



Comparison of engine face total pressure ratio time histories for three blast intercept angles. Figure 7.2.

(a) Blastward inlet.

The state of the state of the state of the



(b) Leeward inlet.

Figure 7.2. Concluded.

Figure 7.2 that, for the blastward inlet, the average total-pressure change at the simulated engine face has about the same ratio to the incident total-pressure change for all three intercept angles, the ratio being about 1.17 for the time range shown. For the leeward inlet, this ratio is smaller and varies somewhat with the intercept angle.

The significance of the above observations with respect to engine performance has not yet been explored in detail. However, both the decreasing intensity and the decreasing rate of change of total pressure observed for increasing intercept angle in Figure 7.1 may imply a decrease in inlet distortion with increasing intercept angle, at least in the 90° to 135° range.

SECTION VIII INTERACTION OF BLAST SHOCK WITH THE ENGINE FAN

The principal question regarding blast wave interaction with the engine inlet, of course, is what effect this interaction would have upon the operation of the engine downstream.

The effect would depend upon the nature of the transient events that take place when the blast shock and blast-induced flow reach the engine. At present there is no means for analyzing this sequence of events nor are there test data available for its assessment. As an admittedly limited first step in understanding the problem, the interaction at the fan stage of a turbofan engine will be examined here on a quasi-steady basis.

8.1 QUASI-STEADY BLAST SHOCK INTERACTION WITH A FAN

The quasi-steady interaction of a blast shock leaving the inlet and entering a fan will be analyzed by making the assumption that the interaction reaches an equilibrium rapidly enough that a new steady-state fan point is reached essentially immediately after shock arrival. Of course, the transient interactions of the blast shock with the rotor and stator blades are expected to be important, but, until the means are available for analysis of these interactions, the analysis of a quasi-steady interaction will have to suffice for providing an assessment of some of the features of shock interaction with a fan.

The time sequence of events associated with the interaction of a shock wave with a fan is shown in Figure 8.1. Here the flow going into and out of the fan is treated on a one-dimensional basis. Region 2 contains the preblast flow entering the fan and region 3 contains the preblast flow leaving it. The fan is located at the origin of the coordinates.

The blast shock at the fan is assumed for this analysis to be a step-blast, i.e. to have uniform properties in region 2' behind the

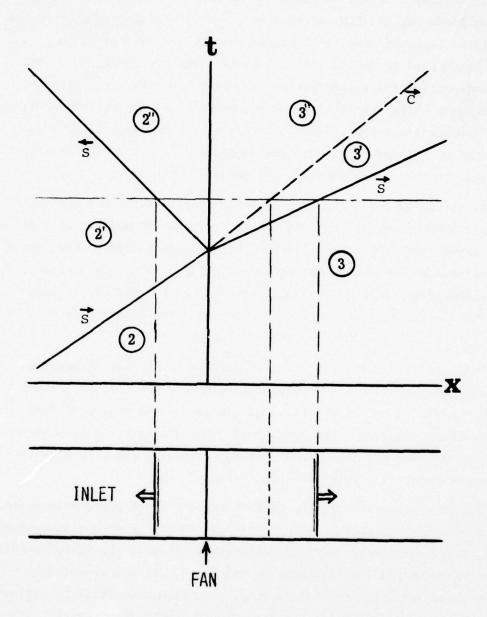


Figure 8.1. Shock interaction with fan.

shock. The shock wave is partially reflected upstream producing the flow in regions 2" ahead of the fan. It also is transmitted through the fan producing the flow in regions 3' and 3" downstream of the fan. The air in region 3' has first passed through the fan and is then shock compressed by the transmitted shock. The air in region 3" has been twice shock compressed before passing through the fan, first by the incident shock (separating zones 2 and 2') and then by the reflected shock (separating zones 2' and 2"). The air in regions 3' and 3" is separated by a contact surface; the pressures and particle velocities are equal in the two regions but the densities differ.

It should be noted that the shock interaction with a fan might possibly produce expansion waves in place of the transmitted or reflected shock waves. For the particular fan interactions analyzed here, which are believed to be typical for modern axial-flow turbo-fan engines, only shock waves would be possible, so only shock waves are assumed here for the transmitted and reflected waves. The addition of expansion waves to the analysis would be straightforward.

Prior to the arrival of the incident shock, the fan compresses region-2 flow upstream into region-3 flow downstream. After arrival of the incident shock at the fan, the fan compresses region-2" flow upstream into region-3" flow downstream. The fan therefore goes from a pre-interaction operating point between regions 2 and 3 to a post-interaction operating point between regions 2" and 3".

The flow properties in the initial regions 2 and 3 are determined by a match between the fan characteristics and the inlet and downstream engine characteristics. For typical current aircraft the flows entering and leaving the fan are subsonic, so the inlet, fan and downstream engine characteristics are interacting. The flow properties in region 2' are determined by knowing the strength of the incident shock. The properties in regions 2", 3' and 3" are determined by a match between the strengths of the transmitted and reflected shock waves and the characteristics of the fan. Results for a typical fan will be shown.

This quasi-steady interaction of the shock with a fan has been programmed into a FORTRAN IV code called QBIF (Quasi-steady Blast Interaction with a Fan). The fan characteristics are a code input.

The important questions stemming from the QBIF calculation are

(a) what operating point the fan would arrive at, (b) what effect the reflected shock would have upon upstream flow within the inlet and

(c) what effect the transmitted shock wave might have on the flow downstream at the compressor inlet or through the bypass duct to the afterburner and the turbine outlet.

8.2 BLAST SHOCK AT ENGINE FACE

In view of the large number of tests and variables in the 0.1-scale B-1 inlet tests at AEDC, calculations with the QBIF code have been concentrated in this study on the test conditions of a selected run in the test series at AEDC, Run 40 (Part 619). The pre-blast flow and blast conditions for this run are tabulated in Table 8.1.

The wind-tunnel Mach number for Run 40 (Part 619) was 0.85 and the mass flow at the engine faces was 351.9 and 351.0 lb/sec full-scale for the outboard and inboard inlets, respectively. The blast shock strength scaled to standard sea level conditions was 5.8 psi. The jump in average total pressure at the two engine faces when the blast shock arrived was 0.435 and 0.150 of the pre-blast free-stream total pressure, respectively, for the two inlets. The corresponding ratios of the static pressure behind the shock to the value ahead is 1.280 and 1.101 at the engine face for the respective inlets.

8.3 ENGINE FAN CHARACTERISTICS

For two-stage fan characteristics representative of current technology, the data of Reference 8.1 have been employed. A sketch of this fan and a tabulation of its passage dimensions are reproduced from Reference 8.1 in Figure 8.2. The fan was designed for a tip speed of 1450 ft/sec, an overall pressure ratio of 2.8 and a corrected mass flow of 184.2 lbm/sec. The efficiency at this design operating point was found to be 85.7 percent from tests (Reference 8.1). The overall performance maps for the fan are presented in Figure 8.3. An enlarged

TABLE 8.1

INLET DATA OF RUN 40 (PART 619) PERTINENT TO BLAST SHOCK-FAN INTERACTION

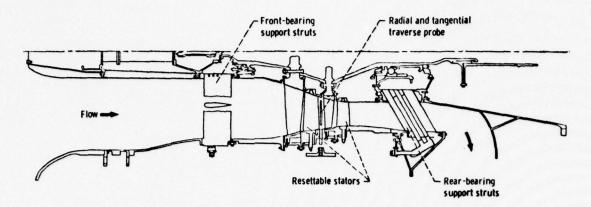
TUNNEL DATA

PREBLAST	BLAST	
$M_{o} = 0.850$	$\Delta p = 5.8 \text{ psi}^*$	
p _t = 11.801 psia		
p _o = 7.358 psia		
$T_{t_0} = 569^{\circ} F$		

ENGINE-FACE DATA

	OB INLET	IB INLET
PREBLAST		
$^{\mathrm{M}}_{2}$	0.519	0.511
p _{tav} /p _{to}	0.979	0.980
W2R-FS(1b/sec)	351.9	351.0
BLAST		
Ptavs -Ptav)/Pto	0.435	0.150
P _s /p	1.280	1.101

^{*}Scaled to one atmosphere ambient pressure.



(b) Schematic of two-stage fan test arrangement.

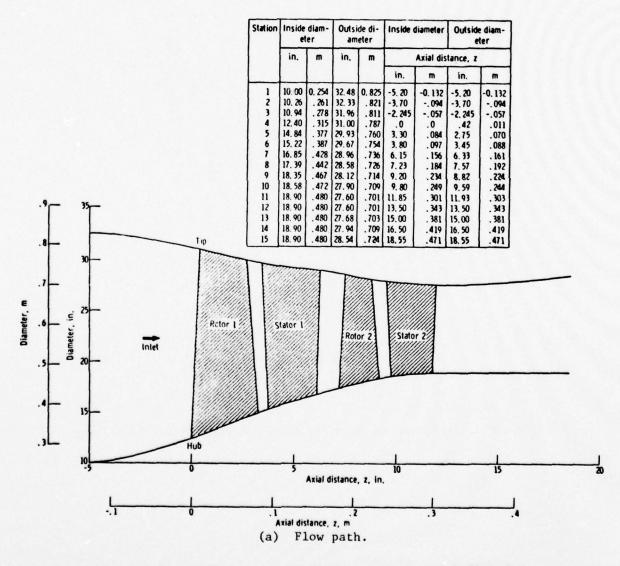
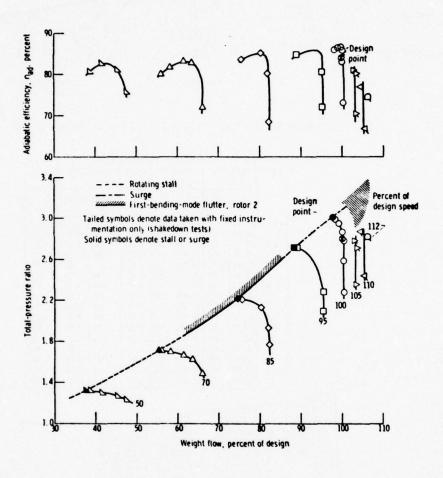


Figure 8.2. Configuration of NASA two-stage axial-flow fan.



Two-stage-fan overall performance

Figure 8.3. Performance maps for NASA two-stage axial-flow fan.

map is presented in Figure 8.4 for the fan total-pressure ratio. Four operational lines have been added to this map for fan exit Mach numbers of 0.45, 0.51, 0.64 and 1.00.

Six preblast operating points were calculated for the two engineface Mach numbers of Table 8.1 and for three values of the stall margin — 8, 15 and 24 percent. The definition of stall margin, SM, used here is

$$SM = \frac{\left(\frac{p_{t_3}}{p_{t_2}}\right) - \left(\frac{p_{t_3}}{p_{t_2}}\right)}{\left(\frac{p_{t_3}}{p_{t_2}}\right) \times 100, \text{ percent}}$$

$$X 100, \text{ percent}$$

where p_{t_3}/p_{t_2} is the fan total-pressure ratio at the operating point and (p_{t_3}/p_{t_2}) stall is the value at stall or surge for the same equivalent mass flow.

8.4 Blast Effect on Fan Operation

Calculations with the QBIF code were carried out for the fan of Reference 8.1 for three initial conditions of the two inlets. The fan operating points that would result are presented in Figure 8.4 for the three initial stall margins for the two inlets. The shock pressure ratio at the engine face, p_2^*/p_2 , is the parameter for the curves. The results show that increasing this shock strength reduces both the equivalent mass flow and the total pressure ratio.

The incident shock pressure ratio at the engine face for the inboard inlet in Part 619 was 1.101. The operating points resulting from this interaction with the fan for the three initial stall margins are joined in Figure 8.4 by the curve for $p_2'/p_2=1.10$. The points for double and half that shock overpressure, i.e. p_2'/p_2 equal 1.20 and 1.05, are joined similarly. These resulting operating points are all well within the area of the performance map where acceptable operation would be expected. Therefore the blast should produce no problem for the inboard fan according to the QBIF code calculations.

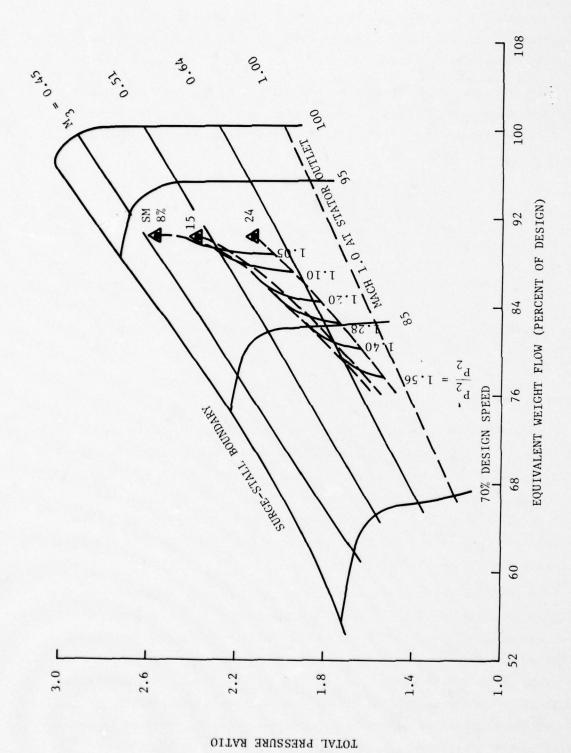


Figure 8.4. Two-stage-fan overall performance map.

The pressure ratio of the shock at the engine face in the outboard inlet in Run 40 was 1.28. The resulting three operating points for the three stall margins wind up much closer to the $\rm M_3$ =1.0 operating line. The flow in stator no. 2 of the fan would be expected to choke at about midway between the $\rm M_3$ =0.64 line and the $\rm M_3$ =1.00 line. Therefore the blast would be expected to choke the fan in the outboard inlet for this shock strength and an initial stall margin of 24 percent.

The resulting operating points are also shown for about a 42 and 100 percent increase in shock overpressure, i.e. $p_2'/p_2 = 1.40$ and 1.56, and one-half the overpressure, $p_2'/p_2 = 1.14$. The higher overpressures would be expected to choke the fan for the initial 24 percent stall margin.

Choking of a fan for the short durations that would be experienced during penetration of a blast wave is not expected to be harmful to its operation on this quasi-steady basis. The problem for the fan would arise if it be driven to the surge-stall boundary. The effect of this initial shock from the blast wave for the cases run, however, is to increase the downstream Mach number, thereby driving the fan away from the surge-stall boundary. What the effect would be for other initial fan points remains to be explored.

8.5 FAN REFLECTED SHOCK

The properties of the shock reflected upstream from the fan, following the interaction of the incident shock with the fan, are presented in Figure 8.5 from the calculations with the QBIF code.

In Figure 8.5(a) the pressure of the reflected shock in excess of the initial pressure is presented as a ratio to the overpressure of the incident shock, $\frac{p_2''-p_2}{p_2'-p_2}$. This excess pressure ratio is plotted as a

function of the pressure ratio of the incident shock, p_2'/p_2 . A value of the ordinate of unity corresponds to no reflected shock and a value of two indicates an overpressure of the reflected shock equal to the overpressure of the incident shock.

The second secon

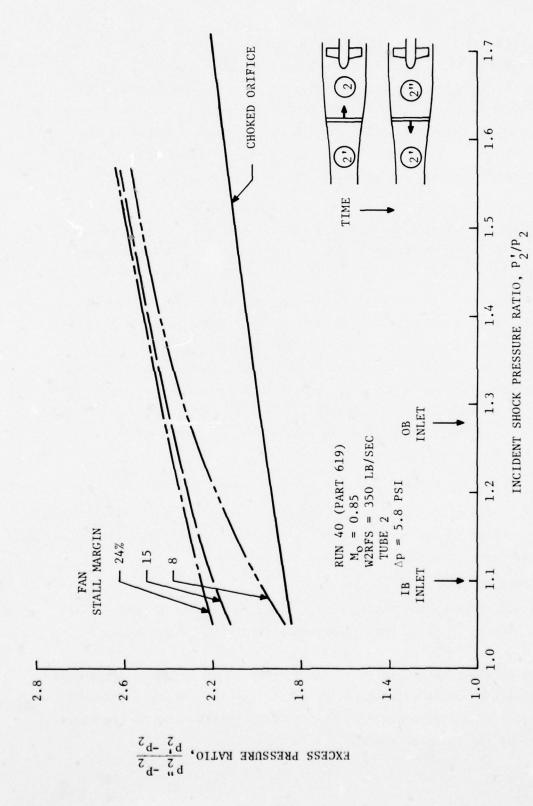
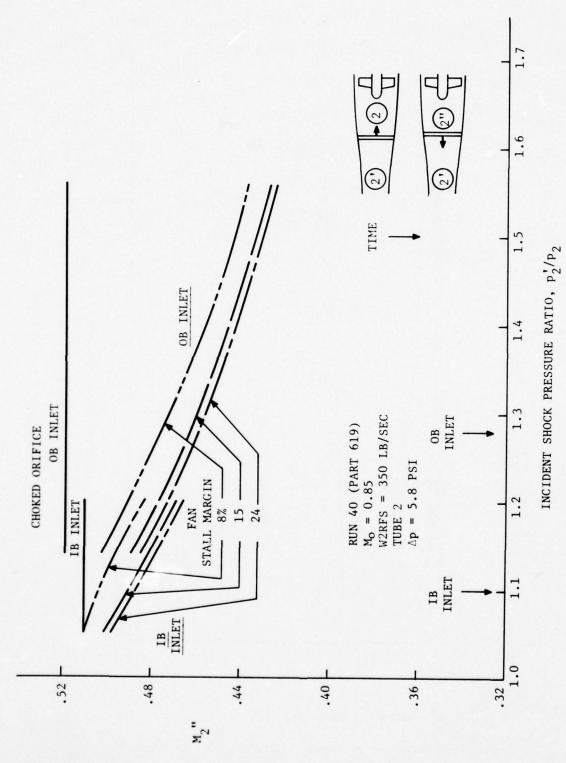
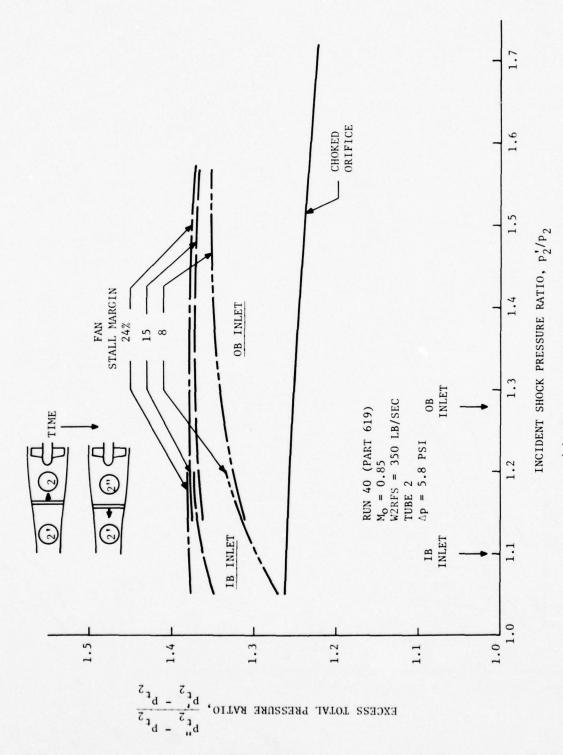


Figure 8.5. Variation of fan reflected shock properties with incident shock pressure ratio.

(a) Excess pressure ratio.



(b) Particle Mach number.
Figure 8.5. Continued.



(c) Excess total-pressure ratio.

A common method for simulating an engine in inlet testing is to choke the flow leaving the inlet at about the downstream location for the engine. This is done by using a fixed choked orifice or nozzle or adjustable vanes. The latter were employed with the 0.1-scale B-1 inlet and were located near the fan station.

The properties of shocks reflected upstream from a choked orifice (or nozzle or vanes) and fan are compared in Figure 8.5(a). The values of the incident shock pressure ratio at the engine face for Run 40 are indicated on the abscissa. The increment in excess pressure ratio of the reflected shock for the fan is markedly greater than for the choked orifice. Under the shock conditions of the outboard inlet in Run 40 it is 33 to 45 percent greater. This means that the strength of the shock reflected upstream from the fan would be that much greater with a turbofan engine than was experienced in the tests in the 0.1-scale B-1 inlet.

The partial Mach number, M_2'' , of the flow behind (downstream) the reflected shock and entering the fan or a choked orifice is shown in Figure 8.5(b). The inflow Mach number for a choked fan would be constant. The decrease for the fan is due primarily to the increase in temperature and speed of sound by the double shocking of the air, and only partially to the reduction, generally, in particle velocity.

Analyses of aircraft turbine engines are generally concerned with the total pressure. The excess total-pressure ratio,

$$\frac{p_{t_2}^{"}-p_{t_2}^{"}}{p_{t_2}^{"}-p_{t}}$$
, is presented in Figure 8.5 (c). It is not as large for

either the choked orifice or fan as was the excess static pressure. In other words, this means that the total pressure does not get incremented as much by the reflected shock relative to the increment by the incident shock as does the static pressure. However, the total pressure increment due to the reflected shock is markedly greater for the fan than for a choked orifice. For the outboard inlet and the shock conditions of Run 40 (Part 619), the increment would be 34 to 50 percent greater for the fan than for the choked orifice.

The variation of the properties of the shock transmitted downstream by the fan as a function of the incident shock strength are presented in Figure 8.6. The pressure ratio for the transmitted shock wave is shown in Figure 8.6(a). The ratio is always less than for the incident shock, but it is relatively large. The effect upon the downstream engine operation might be significant.

The particle Mach number M_3'' downstream of the fan for the transmitted shock is plotted in Figure 8.6(b). It increases with the strength of the incident shock in all cases. It is reasonable to expect that the second stator of the fan would choke at a downstream Mach number somewhere near 0.8, so the downstream Mach number would not increase beyond that point. In the absence of data on the choke Mach number, the curves have been continued as if there were no choking.

This condition for a choked second stator would be nearly reached for the fan operating at a stall margin of 24 percent and incident shock pressure ratios approaching 1.6. For lower initial stall margins the pressure ratio of the incident shock would need to be considerably greater for choking. In summary, the result of this analysis with the QBIF code is to indicate that this fan operating at the initial conditions of the Run 40 test would not experience any operational problems on a quasi-steady basis for (step) shocks at the engine face of the magnitude expected of Run 40 for the incidence angle, ϕ , of 100 degrees and shock overpressure of 5.8 psi scaled to 1 atm. The upstream reflected shock would be notedly stronger, however, than for the choked control vanes used (as the simulated engine) in the tests.

The effect of the reflected shock on the flow within the inlet will be examined in Section 9. The strength of the transmitted wave is large, Its effect on engine operation downstream is not known.

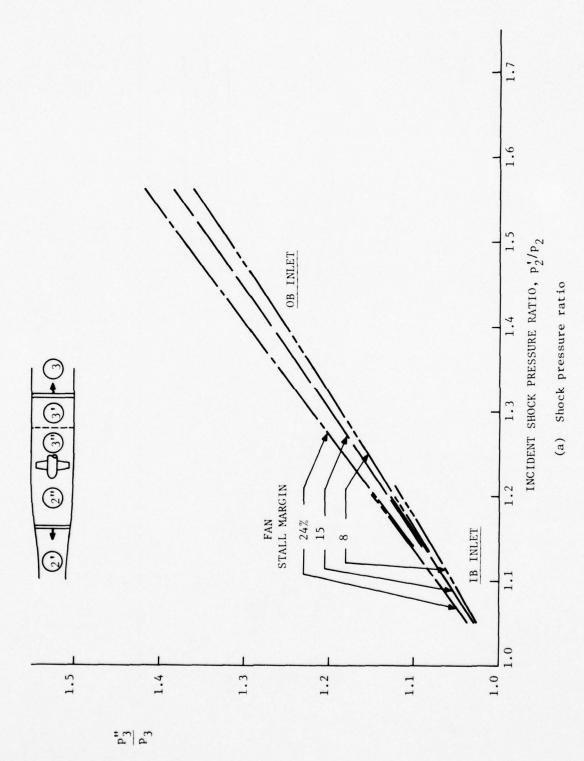


Figure 8.6. Variation of fan transmitted shock properties with incident shock pressure ratio.

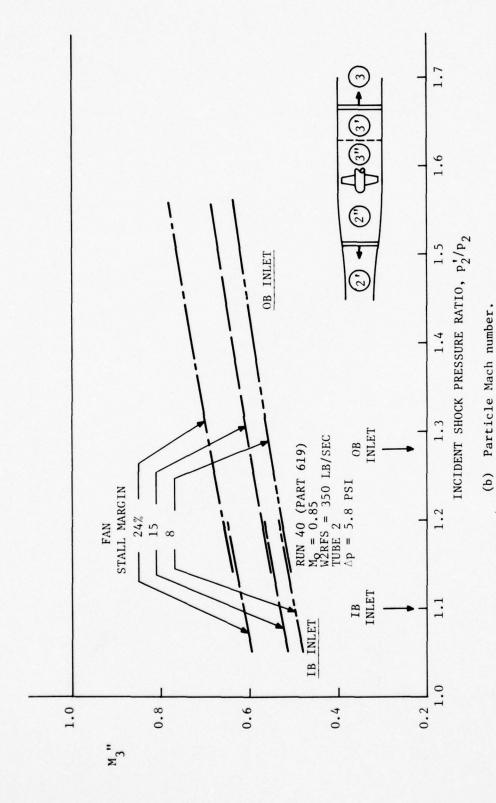


Figure 8.6. Concluded

154

SECTION IX

REFLECTED SHOCK-BOUNDARY LAYER INTERACTION WITHIN INLET

Another important feature of the inlet-blast interaction problem is the interaction inside the inlet between the blast shock waves and the inlet boundary layer. The sketch in Figure 9.1 depicts the features of shock-boundary layer interaction that might occur on the walls of the inlets of the B-1 type due to the reflected shock from the fan. The flow in the boundary layers would be forced to negotiate the adverse pressure gradients associated with these shock waves moving upstream from the engine forces. If sufficiently strong, the adverse pressure gradients could cause the boundary layers to separate on the inlet walls, depending upon the boundary layer characteristics. This possibility will be assessed in this section.

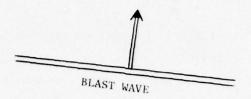
The interaction is complicated by the variation of the "free-stream" properties within the inlet both in the flow direction and time-wise. The total pressure and total temperature in particular both vary longitudinally and with time as the reflected shock moves upstream.

More data are required for this analysis than were measured in the tests with the 0.1-scale B-1 inlet, so calculations made of the flow with the BID code have been employed.

9.1 SHOCK-BOUNDARY LAYER CALCULATION

The development of the boundary layers was computed using the results of BID code calculations to provide the distributions of the free-stream properties of static pressure, total pressure and total temperature near each wall. The BID code models the fan as a choked orifice, in line with the 0.1-scale inlet model. The distributions for each wall of the inlets were selected corresponding to the time when the static pressure gradients appeared to be relatively steep within the blastward inlet. No systematic attempt was made to select the most adverse distributions for the boundary layers. These properties defined the conditions at the outer edge of each boundary layer.

and the heat the spirit of wait and the



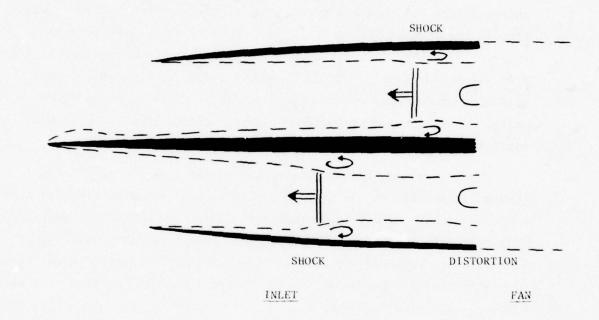


Figure 9.1. Boundary layer separation and distortion from fan reflected shock wave.

The growth and behavior of the boundary layers along the walls for these free-stream conditions were computed using the BLAYER code of NASA, presented in Reference 9.1. Since the Reynolds number of the boundary layers would be generally large relative to the transition value, the boundary layers were assumed to be turbulent from the leading edge of each surface.

The BLAYER code assumes a constant total pressure and total temperature outside of the boundary layer. Because they both generally vary significantly for the calculations made, the calculations were carried out piecewise taking the total pressure and total temperature as constant over each segment. This procedure was found to be significant to the values computed, but it is not believed to alter the general conclusions reached from the calculations.

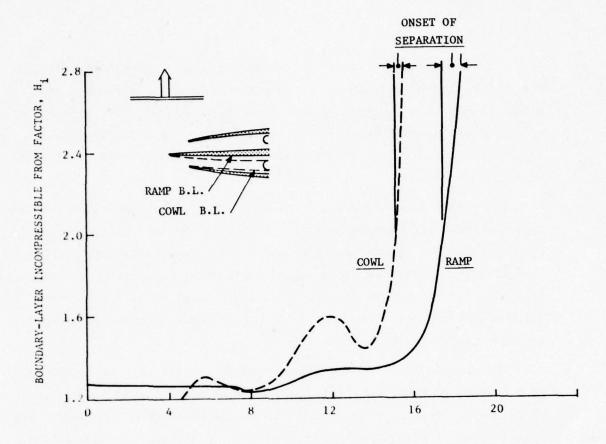
The distributions of the free-stream properties that were selected were assumed to be frozen. That is they were taken as non-varying in time, whereas they do change as the reflected shock moves upstream. The significance of this assumption is not readily assessable. The BLAYER code applies only for the frozen pressure distribution, so the question must be resolved at a later time.

The BLAYER calculations were performed for the full-scale B-l inlets, as scaled up from the 0.1-scale model. The blast wave in the BID calculation is assumed to arrive from the side of the aircraft, that is $\phi = 90^{\circ}$ (0° is a head-on intercept), with a shock overpressure of 5.0 psi. The flight Mach number was taken to be 0.85 and the mass flow rate in the inlets to be 350 lb/sec.

9.2 SHOCK-BOUNDARY LAYER RESULTS

The pressure distributions for the boundary layer calculations with the BLAYER code are presented in Figure 9.2 along with the boundary-layer incompressible form factor $\mathbf{H_i}$ that resulted from these calculations.

The boundary-layer factor $\mathbf{H}_{\mathbf{i}}$ is a parameter essentially representing the velocity distribution across the boundary layer (normal to the wall).



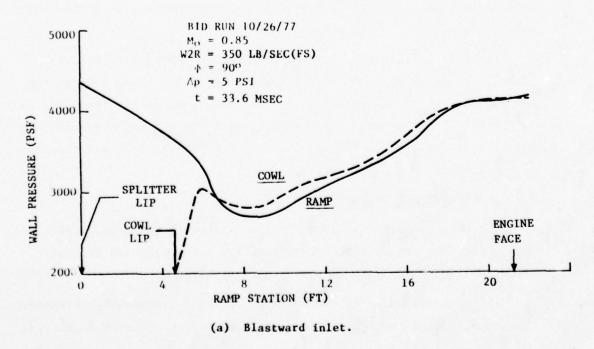
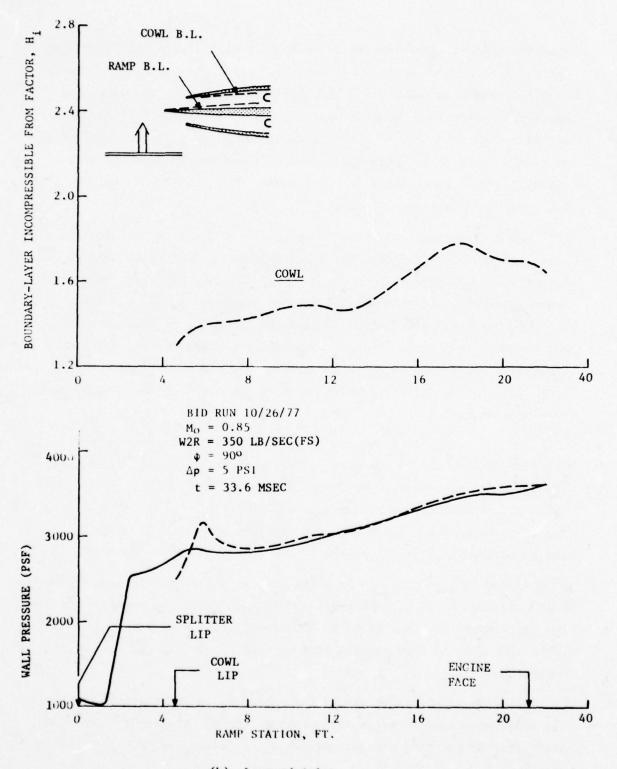


Figure 9.2. Effect of fan reflected shock on boundary layers of inlets.



(b) Leeward inlet.Figure 9.2. Concluded

When the velocity distribution is more uniform, the parameter approaches unity. A value of 1.2 to 1.4 is typical for a turbulent boundary layer on a flat plate in the absence of a pressure gradient. In an adverse pressure gradient (increasing pressure in the direction of flow) the velocities decrease toward the wall so $\rm H_i$ increases. When the velocity gradient normal to the wall goes to zero, the flow can separate from the wall. Experience shows that separation may occur for $\rm H_i$ values as low as 2.0 and definitely by 2.8.

The H_i distributions along the walls for the blastward inlet are presented in Figure 9.2(a). The results indicate that the boundary layers would separate on both the cowl and the ramp surfaces. The cowl boundary layer would separate upstream of the ramp, so it is quite probable that the stream would actually be deflected to the ramp side and that the ramp boundary layer would not separate. In any event, separation would take place on one side of the blastward inlet which would produce significant distortion at the engine face when the separated flow arrives there.

The $\rm H^{}_{i}$ distribution for the leeward inlet is shown in Figure 9.2(b). The distribution for the ramp is not presented because the longitudinal variation in total pressure outside of the boundary layer is so large as to make conclusions from the results undependable. The $\rm H^{}_{i}$ distribution for the cowl boundary layer reaches a maximum of only 1.8, which is below the threshold of separation.

In the BID code the fan is modeled as a choked orifice as mentioned (for matching to the 0.1-scale B-1 inlet model data), so pressure gradients for the leeward cowl may be 15 to 40 percent greater with a fan. This might be enough to separate the cowl boundary layer but the question is unresolved.

There is an effective antificial viscosity in the BID code because the cells are fixed in space (also called "shock capturing"). This has the effect of reducing pressure gradients, resulting in lower calculated values of $\rm H_{i}$.

The question then arises as to why larger values of the distortion parameters were not measured during the test periods with the 0.1-scale B-1 inlet. Some rough estimates of the time-distance relationships of events within an inlet are useful in examining this question. Several are depicted in Figure 9.3 for Mach 0.85 flight conditions. The initial shock would reach the engine face in about 0.9 milliseconds and the vanes is about 1.1 milliseconds. The reflected shock from the vanes moves upstream more slowly, as shown. Somewhere within the inlet the boundary layer would separate. To estimate when the separated flow might reach the engine face, some other velocities must be considered.

The particle velocity within the duct is about one-third of the initial (incident) shock velocity. Vorticity shed from the leading edge of the cowl or splitter lips would first travel at about one half of the particle speed and slowly speed up as it moves out into the free stream. Assuming a step speed-up half way down the duct, the vortex would reach the engine face at 4.2 milliseconds.

The blast-type flow period produced by the shock tube exit flow at the inlet is terminated by the arrival of the shock-tube cold gas or the backward-facing shock or compression wave, observed as a sudden increase in the rate of pressure change at the inlet. In the case shown in Figure 9.3 this event would occur at the inlet entrance at about 3.3 milliseconds, and could arrive at the engine face by about 4.2 milliseconds.

The speed of the front of the separated boundary layer is not known, but it is reasonable to expect it to be significantly less than for the free-stream particles. For estimation purposes, if the reflected shock would separate the boundary layer midway down the inlet and the front of the separated flow travels at one-half of the particle velocity, the separation zone would reach the engine face at somewhat more than a millisecond after the termination of the test period.

Figure 5.8 shows that the distortion parameter IDC increased considerably for the blastward inlet for $\Delta p = 5.0$ and 5.2 psi beginning at about one millisecond after termination of the 3.3-millisecond nominal test period, indicated in the figure by the arrows. IDR increased at

The second second second

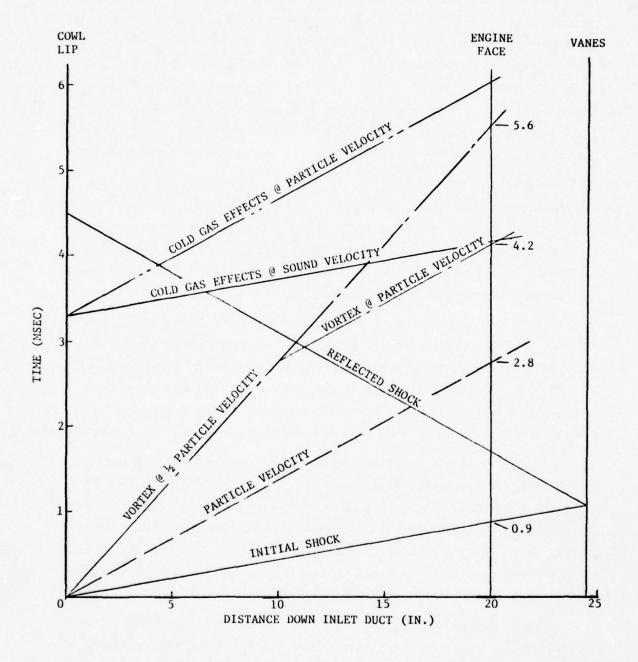


Figure 9.3. Inlet time-distance relationships for a flight Mach number of 0.85 and a mass flow rate of 350 lb/sec.

about the same time but not in as great a proportion, in comparison with the values during the test period. IDL increased apparently well beyond the full-scale value of 1.50.

For the leeward inlet, Figure 5.9, the distortion indicated is not as large. IDC and IDL appear to have increased beginning at about the end of the nominal test period, particularly for the 5.2 psi shock. IDR, on the other hand, decreased. IDL experiences only brief bursts above a value of about 1.1.

Because these large increases in distortion occurred after the expected arrival of the backward facing shock or compression wave, a question does arise as to what degree the high level of distortion may have been due to the character of the blast wave during the later period. This question should be examined to the extent possible for the present data.

SECTION X DISCUSSION

This section presents a summary and discussion of some of the important aspects of the development and testing program, most of which are described in detail in previous sections, and indicates some recommendations for future developments. Topics discussed are the blast generator development, the 16T wind tunnel blast tests, the BID code for predicting inlet blast flows and blast-fan interactions.

10.1 BLAST GENERATORS

The blast generation development program began with theoretical REFLECT2/S2D code calculations for the firing of a shock tube into still air, followed by firings of two-in.-dia shock tubes into the AEDC 1T (one-foot-square) wind tunnel at Mach numbers from 0.6 to 0.9 (Sec. 2). Results of these tests, for the case of the shock tube firing perpendicular to the tunnel axis, gave useful blast type flows in this Mach number range for the overpressure range 2 - 5 psi (referred to sea-level ambient pressure) for distances from the tube exit of about 4.5 diameters, for polar angles from the tube axis from -15° to +30° downstream of the tube. Durations of nearly constant blast pressure (to 30% decay) were obtained for these conditions in the range of about 0.5 to 2 milliseconds per foot of tube diameter, with best results being obtained at a polar angle of 15°. At downstream polar angles from the tubes of 45° or more, the blast wave durations were generally much shorter and were not of interest. Also, it was found from the 1T tests that if the shock tube driver pressure was too low compared to the ambient pressure a nonconstant pressure type of blast wave profile was produced, characterized by an extremely rapid decay.

Results of the above calculations and small shock tubes were found to be essential in selecting the shock-tube dimensions, locations and driver pressures for the subsequent development of large shock tubes for the AEDC 16T (16 foot square) wind tunnel tests.

The three large shock tube installation designed and constructed for the 16T wind tunnel tests had the following characteristics. Distances from the shock tube exits to the inlet were 3.8 to 4.3 tube

diameters, at polar angles from 11.2° to 28.3°. Shock tube driver pressures of 55 to 186 psia were used, usually at a tunnel ambient pressure of one-half atmosphere.

Definition of the properties of the blast waves produced at the inlet location in the 16T tests was made using both measured data from the tests as well as the test results from the 1T tests. The strength of the blast shock was well defined at probe locations by the 16T measurements, but interference from the inlet model degraded the definition of the flow following the shock somewhat. Firings in the 16T tunnel without a model would be useful for defining these blast properties, but they were precluded by limitations on tunnel time; as an alternative, an analysis of model interference on the blast measurements is recommended. The incidence angle of the blast shock was defined from comparative arrival times at several pressure transducers; shadowgraphs would be a useful alternative for this measurement in future tests for greater accuracy.

Shock-tube dimensions of a 22.6 in-ID and a 17-ft length were selected to provide the best combination of blast wave characteristics within space constraints of the wind tunnel for the three shock tubes. Commercial pre-scored, pre-stressed diaphrapms (rupture discs) in a double-diaphragm arrangement provided fast, clean-opening diaphragm bursts free of any petal debris. By using three shock tubes the number of firings during the test period was essentially doubled over using a single tube.

10.2 THE 16T WIND TUNNEL TESTS AND ANALYSIS

The 0.1-scale B-1 inlet model used in the 16T tests had been mated previously to the tunnel sting support, so only some strengthening of the model and the 16T tunnel walls for loading by the shock-tube driver gas was required for testing.

Blast tests were performed at Mach 0.55, 0.70, 0.85 and 0.90 with inlet mass flow rates ranging from 235 to 350 lb/sec (full scale), shock overpressures from about 2 to 6 psi (referred to sea level) and model yaw angles of 0 and 5 degrees (nose away from shock tube).

Typically, blast type flows lasting about 3.3 milliseconds were achieved at the inlet, with corresponding nearly constant pressure durations (to 30% decay) of between 1 and 4 msec. This met test requirements amply. However, for future tests vortex and boundary-layer separation phenomena effects that are now believed to be important at later times make it desirable to double the test durations.

The test durations might be increased about 50 percent by moving the model about four feet off the centerline of tunnel, increasing the distance from the shock tubes and thereby the blast duration, but the shock-tube dimensions would need to be reexamined. Any additional increase in duration would require using a smaller-scale model (gaining thereby in scaled duration).

The blast interaction with the inlet as observed in the tests can be divided into three characteristic phases in terms of events at the engine face. During the first phase the blast shock travels down both inelts and reflects from the choked vanes (or fan for the full-scale engine), then returning to the engine face. In the second phase any vortex shed from the leading edge of the splitter, for example, would reach the engine face, and shock wave-boundary layer interaction within the inlet would take place and also reach the engine face. After these two stages, events are believed to happen relatively slowly, that is on a quasi-steady basis, so steady-state test results and analyses would be applicable — this is called the third stage. Attention here is focused primarily on the first two stages.

In the blastward inlet during the first period the multiple reflections of the shock result in a "staircase" of shocks arriving at the engine face over about a 0.3-msec period followed by some decay preceding the arrival of the reflected shock in about another millisecond. In the leeward inlet the shock diffracts around the splitter and enters the inlet more normal to the model centerline. It reaches the engine face as essentially a single shock, much weaker than for the blastward inlet.

When the shock in the blastward inlet reaches the engine face, distortion IDL values near unity are observed which might be of some concern during maneuvering or other stressful flight conditions. The distortion patterns examined have had high total pressures on the cowl side of the face. The distortions in the leeward inlet during this period were generally lower.

Calculations were made of the blast shock interaction with a fan typical of current technology for turbofan engines. Shock strengths measured at the engine face in the 16T tests were used. The interaction was assumed for simplification purposes to be quasi-steady with a step shock (no ramp or decay). For the blastward inlet the results indicate the fan would choke at the second stator for the lateral ($\phi^{\approx}90^{\circ}$) blast intercept. This presumably presents no operational problem, but the results are not believed to be general. The interaction should be studied for the range of conditions expected. Of clear concern to engine operation are effects produced downstream by the transmitted shock wave upon the afterburner and turbine rear stages and upstream by the reflected shock upon flow within the inlet.

Concerning the latter, boundary-layer calculations indicate that the reflected shock would definitely separate the upstream boundary layers within the blastward inlet for a 5-psi blast shock. This is expected to result in serious distortion at the engine face.

In the tests IDL values over 1.25 were observed at the engine face at about 4 milliseconds after shock arrival there. This is about one millisecond after the end of the validated duration of blast type flow, therefore it is possible the distortion at that late time was due to variations in the blast wave. In view of the significance of this effect to engine operation, it is recommended that the blast data be analyzed further to verify that the late-time distortions are relevant to the blast-inlet problem.

Interaction of the reflected shock with the boundary layers in the leeward inlet could only be analyzed to a limited extent, because of restrictions in the methods of analysis available. Separation on the cowl side might occur if calculations were refined, but not as carried out. Estimation of separation on the ramp side requires an assessment

of separation effects in BID calculations for the leading edge of the ramp and the improvement in the boundary-layer method, needed also for the blastward inlet.

Vortex formation at the splitter is another possible source of distortion for the leeward inlet. Distortion values in the leeward inlet did reach large values in the tests for times after the 3.3-msec blast flow period but whether the shedding of vortices is also a blast inlet problem depends on resolution of the late-time blast-wave data.

During the about 3.3-msec period of blast type flow the maximum IDL values were affected by the inlet mass flow rate. But there were no definite significant effects of either Mach number or inlet yaw angle on IDL.

The whole question of blast distortion relative to its effect upon engine operation is an open question at this point. The particular distortion indices used in work with the B-l inlet (IDC, IDR, IDL and IDT) have been employed here, basically as parameters that have met with success for distortions of the type obtained in typical flight situations (maneuvering flight, throttle transients, etc.). There are many other distortion parameters in use. Also, there are factors involved in a blast interaction that are not reflected in these parameters, such as the rapidity of the changes due to the shocks, and features of the spatial distortions that are significantly different, etc. The effects of these differences on engine operation must be answered before the question can be resolved.

The BID code provides good predictions of the observed pressure histories in the inlet duct and at the engine face, particularly in reproducing the principal events, such as shock reflections. The pressures predicted at the engine face tend to be slightly low but the trends are generally good, so that a simple factor (accounting for numerical viscosity effects) would be expected to bring them into good agreement. The BID code at present does not include blast decay; this addition to the code would provide an improvement at late times. A second improvement that is recommended is to extend the code to three

dimensions; this would allow for modelling the hub and would account for differences in the vertical direction. Work is recommended to further correlate distortion predictions of the BID code with the test data.

BID code calculations have been made for intercept angles from 90 to 135 degrees from head on. The 90-deg intercept results in much larger total-pressure increment at the engine face with greater pressure-time variations than for the more rearward intercepts. Further studies extending the blast intercept angles are recommended.

Regarding the effects of the observed inlet pressures on an engine fan stage, the calculation of the quasi-steady interaction of the blast shock with a fan and with a choked flow for a 90-deg intercept indicates the reflected shock would be considerably stronger for a fan then for a choked-flow condition, as used in these tests, by as much as 43 percent for a typical case. Control of flow by means of a choked nozzle or vanes is a standard technique used in inlet testing. Consideration should be given to this problem of weaker reflected shocks in planning and analyzing results of similar blast-inlet testing.

SECTION XI CONCLUSIONS

From the analyses and wind-tunnel tests carried out to simulate nuclear blast interaction on a B-1 type engine inlet, the following conclusions are reached.

- Blast simulations capability has been developed and demonstrated in the AEDC 16T wind tunnel for blast strengths of 2 to 6 psi, scaled to sea-level conditions, and nearly constant blast pressures (with less than + 30-percent decay) lasting from 1 to 4 milliseconds.
- 2. A data bank of blast interaction data has been developed with the 0.1-scale B-1 inlet for lateral intercepts, varying wind-tunnel Mach number from 0.55 to 0.90, inlet mass flow rate from 235 to 350 lb/sec. (full scale), shock overpressures from 2 to 6 psi (sea level) and model yaw angles from 0 to 5 degrees.
- 3. The BID code predicts satisfactorily the principal features of the pressure time history within the inlet duct and at the engine face. Additional work is recommended for prediction of distortion at the engine face. Recommended additions to the code include accounting for blast decay and extending the code to three dimensions.
- 4. Four potentially adverse effects to engine operation from blast interaction were identified: blast-induced distortion, fan choking, afterburner blow out and shock-boundary layer induced distortion.
- 5. Blast-induced distortions during the time of definite blast-type flow in the inlet were usually smaller than but did sometimes reach normal inlet allocation levels for the B-l airplane.

 Distortions at later times greatly exceeded the allocation.

 Boundary-layer separation in the inlet by simulated fan (vane) reflection of the blast shock is suspect for the latter distortion levels.

6. Distortion studies made here are severely limited by the unavailability of a parameter for judging the effect of transient distortions on gas-turbine engine operation. Blast tests with an inlet-engine combination are strongly recommended for meeting this need.

REFERENCES

- 1.1 Pierce, D., <u>Simulation of Blast Waves in a Supersonic Wind Tunnel</u>, British Royal Aircraft Establishment, Tech. Note No. Aero. 2665, January 1960.
- 1.2 Test Facilities Handbook (Tenth Edition), Arnold Engineering

 Development Center, Arnold Air Force Station, Tennessee, May 1974.
- 2.1 AEDC Reports, Data tabulations, Plots and Tapes on the Inlet Blast Effects Test, AEDC Project P41A-07A, Test TM 332, 1975.
- 4.1 Mitchell, C.E., and Powers, J.L. Jr., <u>Pretest Information for</u>
 the 0.10 Scale B-1 Inlet Development Model II Nuclear Blast
 <u>Effects Test in the AEDC 16-Foot Transonic Propulsion Wind Tunnel</u>,
 Rockwell International Report NA-76-593, August 1976.
- 4.2 AEDC Reports, Data Tabulations, Plots and Tapes on the DNA B-1 Blast Effects Test, AEDC Project P41T-D2A, Test TF-419, 1976-1977.
- 5.1 Haagenson, W.R., and Randall, L.M. <u>Inlet Development for the B-1 Strategic Bomber</u>, Rockwell International, AIAA Paper No. 74-1064, 1974.
- 5.2 Hercock, R.G., and Williams, D.D., Aerodynamic Response, in Distortion Induced Engine Instability, AGARD-LS-72, 1974.
- 5.3 Koch, K.E., and Rees, R.L., <u>Analysis of Pressure Distortion Testing</u>, NASA CR-2766, 1976.
- 5.4 Brimelow, B., <u>Techniques for Establishing Propulsion System Stability</u>, Technical Memorandum APTA-TM-69-12, April 1969.
- 6.1 Thompson, J.H., Tomayko M.A. and Ruetenik, J.R. <u>BID Code for Computing Aircraft Engine-Inlet Response to Blast Disturbances</u>, Kaman AviDyne TR-130. (In preparation).
- 8.1 Ruggeri, R.S., and Benser, W.A., Performance of a Highly Loaded Two-Stage Axial-Flow Fan, NASA Technical Memorandum X-3076, August 1974.
- 9.1 McNally, W.D., FORTRAN Program for Calculating Compressible Laminar and Turbulent Boundary Layers in Arbitrary Pressure Gradients, NASA Technical Note D-5681, May 1970.

REFERENCES (CONT'D)

- A.1 Ruetenik, J.R., Analysis of Godunov Method with Fixed Mesh for Hydrodynamic Calculations, Sponsored by Kaman AviDyne Internal Research and Development Program, Proprietary, 1973.
- A.2 Lee, W.N., Smiley, R., Ruetenik, J.R. and Hobbs, N.P., <u>Evaluation</u> of Back-Blast Pressures Produced by a Wing-Mounted 105-MM Recoilless <u>Rifle</u>, Kaman AviDyne Report TR-97, Watervliet Arsenal Technical Report WVT-CR-74023, 1974.
- A.3 Thompson, J.H., <u>REFLECT2 Computer Code for Ground-Reflected Blast</u> Waves and Shock <u>Tube Jet Simulation</u>, Kaman AviDyne TM-98, 1976.
- A.4 Thompson, J.H. <u>REFLECT Computer Code for Ground-Reflected Blast Waves</u>, Vol. II, Computer Program Description, Kaman AviDyne Report TR-96, Defense Nuclear Agency Report 3470F-2, 1975.

APPENDIX A

THEORETICAL STUDIES OF THE FLOW FIELD PRODUCED BY FIRING A SHOCK TUBE INTO A STATIONARY FLUID

A.1 INTRODUCTION

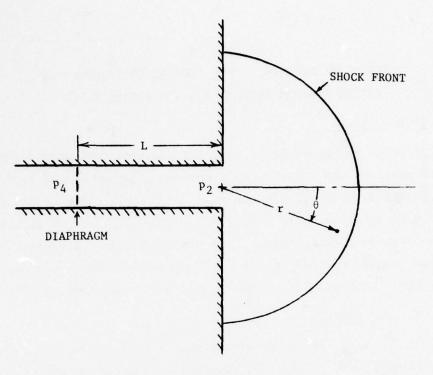
In order to obtain background and planning information for the wind tunnel tests of this report, KA performed a series of theoretical studies for the axi-symmetrical problem where a prescribed flow exits from a shock tube into initially stationary air ($\gamma = 1.4$) at an ambient pressure of one atmosphere (14.7 psia). The external transient pressure disturbance or blast field produced in the fluid was calculated by two KA computer codes for a wide range of shock tube firing conditions, as described below.

A.2 S2D CODE STUDIES

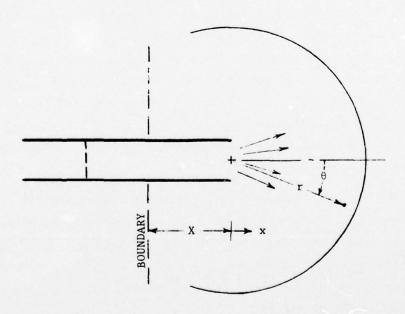
Initial calculations were made with the KA S2D Eulerian computer code (References A.1 and A.2), with several different representations of the geometry of the exit end of the tube. In one representation, shown in Figure A.1a, the shock tube was assumed to be fired into a half-space bounded by a rigid wall. In a second representation, the shock tube was assumed to protrude into the flow from a boundary by various distances, X, as shown in Figure A.1b, with a non-reflecting boundary condition being assumed to apply at this "boundary" distance behind the end of the shock tube. More specifically, the flow field for x < -X in Figure A.1b was assumed to have properties independent of x, with X being varied from about 0.3 to 1.5 tube diameters.

These particular S2D solutions were used to determine the sensitivity of the external flow field to the boundary conditions as described above. In general, it was found that, for the range of exit pressures considered, from 37 to 103 psia, the pressures at all distances two or more tube diameters downstream of the tube exit were essentially independent of the assumed boundary conditions.

Since our interest was primarily in large downstream distances, the above observations indicated that we could more profitably study this shock-tube fluid flow problem by making use of the REFLECT2 computer code described below, which permits better resolution of pressure transients,



(a) Wall boundary.



(b) No wall boundary.

Figure A.1. Problem of a shock tube firing into a stationary fluid.

but is presently less capable than the S2D code for handling complex boundary conditions.

A.3 REFLECT2 CODE STUDIES

Calculations were made with the KA REFLECT2 Lagrangian computer code (References A.3 and A.4) for the shock tube exit flow conditions of Figure A.1a for a range of exit pressures (p_2) from 24 to 103 psia.

Geometrical properties of the shock tube were taken as: inside diameter of 2 inches, driver length (LR) of 4.5 inches and driven length (LN) of 9 inches.

The shock tube exit flow conditions of pressure, density and velocity were taken to be the same as for a perfect one-dimensional shock tube flow with a specific heat ratio of $\gamma=1.4$. In some solutions the exit flow conditions were assumed to be constant corresponding to the initial blast field behind the shock front. In other solutions, account was taken of the change in density produced when the contact surface originally at the tube diaphram position reached the exit end of the shock tube. Consideration of this contact surface change appeared to have little effect on the initial blast phenomena discussed below and is not discussed herein.

Figure A.2 presents sample time histories of pressure time histories at several positions along the axis of symmetry (r = radial distance from tube exit, d = diameter) for several firing pressures ($p_{41} = p_4/p_0$, $p_{21} = p_2/p_0$, p_4 = driver pressure, p_2 = shock (exit) pressure, p_0 = ambient pressure).

The following important features may be seen in Figure A.2. For the lowest shown driver pressure ratio, $p_{41}=2.8$, the blast overpressure decays very rapidly after shock arrival reaching zero in less than 0.2 msec for the two inch-diameter shock tube. This waveform has a too rapid decay to be of interest for the present program. For the intermediate pressure ratio, $p_{41}=10.4$, a much longer positive overpressure duation is obtained, about 0.4 msec and the overpressure is much more nearly constant during the positive phase than for $p_{41}=2.8$. Finally, for the largest pressure ratio, $p_{41}=15.3$, the positive phase duration is again about 0.4 msec, and the overpressure remains nearly constant for over 0.3 msec.

E. S. Shart March & Sant Sant

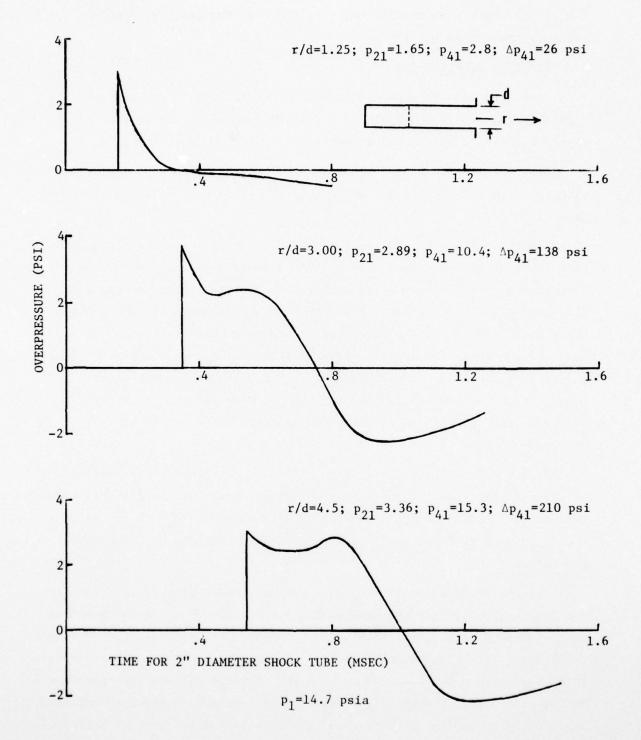


Figure A.2. Theoretical blast pressures outside of a shock tube.

Figure A.3 presents the calculated initial peak or transient blast overpressure, Δp , in the fluid along the axis of the shock tube, as a function of driver pressure ratio p_{41} , and exit pressure ratio, p_{21} and radial distance in tube diameters from the tube exit, r/d.

The initial blast pressure is observed to increase nonlinearly with increasing pressure ratio and to vary roughly inversely with distance from the tube exit in the range of interest (0.1 < $\Delta p/p_0$ < 0.4).

These theoretical results can be represented fairly well by the empirical equation:

$$\Delta p/p_0 = 1.5 (6.39(r/d)p_{21}^{-1.75} + 0.4)^{-1.5}$$
 (A.1)

for the range 0.1 $<\Delta p/p_0<1.0$ where 1<r/d<10 and 2<p₂₁<7.

A.4 CONCLUSIONS

The above results of these studies indicated that for reasonable shock tube driving pressure (under 600 psia) external shock overpressures in the desired range of 2 - 5 psi could be obtained at distances from the tube exit in the range of 3 - 10 diameters. Also the calculated durations of the shock overpressure appeared to be long enough to be useful for simulating a nuclear blast on a small inlet model. For example, at a driver pressure of 225 psia, at 4.5 diameters from the shock tube along the tube axis, the shock overpressure along the axis of the tube was calculated to be about 3.0 psi and the duration of nearly constant overpressure to be about 2.5 milliseconds per foot of tube diameter.

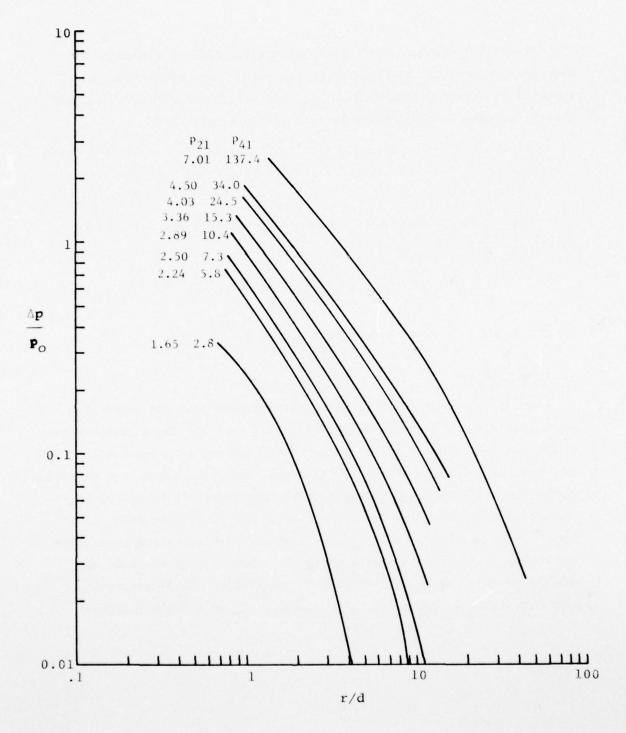


Figure A.3. Variation of overpressure with distance from shock tube.

APPENDIX B

STEADY-STATE PRE-BLAST TEST CONDITIONS IN THE AEDC 16T TUNNEL

This appendix presents AEDC tabulations of the steady-state wind tunnel and inlet operating conditions and inlet pressures and distortions existing immediately before the firing of each shock tube. The data are presented in the chronological order of the firings, by Part number, and are preceded by a table of nomenclature.

In these tables the following parameters are in error: IDCO, IDCI, IDLO and IDLI for data set 2 and PDO, PDI, PDPO and PDPI for both data sets 1 and 2. Corrected values of these parameters are available, but are not included here since they are not essential for the present study.

Steady-State Printout Nomenclature

DNA B-1 Blast Effects Test

P41T-D2A (TF-419)

Parameter	Description
AB1¢-I	Outboard and inboard total bleed zone I areas in. ²
AB2¢-I	Outboard and inboard total bleed zone II areas, in. ²
ALPHA	Model angle of attack defined positive nose up, deg
BETA(SIC)	The angle of yaw defined positive pilot's right, deg
B5-1	Fuselage configuration
С	Structural mode control fin's angle relative to the model axis
С3	Structural mode control fin configuration
CPISS	Claw probe one static pressure ratioed to free-stream total pressure
CP2SS	Claw probe two static pressure ratioed to free-stream total pressure
CP3SS	Claw probe three static pressure ratioed to free-stream total pressure
Date	The date the data were taken
Day	The day the data were taken, deg
ERCODE	Tunnel error code
E10	Boundary layer control system configuration
G34-2	Wing gutter configuration
ни	Inboard lip height, in.
ньф	Outboard lip height, in.
н16-1	Wind hood configuration
HR	The hour the data were taken, hr

Steady-State Printout Nomenclature (Continued) Page 2

Parameter	Description
IDA	Average engine-face distortion index
IDC	Engine-face total circumferential distortion index
IDL	Fan stall margin ratio
IDR	Engine-face total radial distortion index
IDT	Engine-face overall total pressure distortion
140	Inlet configuration
IDC12	Engine-face total circumferential distortion index at the hub
IDC45	Engine-face total circumferential distortion index at the tip
J27	Porous bleed hole configuration
L7	Cowl configuration
М	Free-stream Mach number
MA	First ramp Mach number
МВ	Mach number constants box
MIN	The minute the data were taken, min.
MFR2	Engine-face mass flow ratio
MFR100	Engine-face mass flow ratio corrected to 100% recovery
MODE	Mode code
M2	Engine-face Mach number based on engine-face static to total pressure ratio
M2S	Engine-face Mach number based on weight flow
м6	Flow meter configuration
NCN	Nozzle contour number
NSP	Normal shock parameter
N30-1	Nacelle configuration

Parameter	Description
P	Tunnel static pressure, psfa
Part	Part number
PCA-1	Primary plenum pressure, psfa
PCB-2	Back-up plenum pressure, psfa
PD	Back-up prediction of peak instantaneous fan stall margin ratio
PDP	Primary prediction of peak instantaneous fan stall margin ratio
PLX	Model measured pressure ratioed to free-stream total pressure where L refers to outboard (L=1) and inboard (L=2) and X refers to the pressure designation (X=020, 030, 035, etc.)
PMIN	The minimum engine-face total pressure ratioed to free-stream total pressure
PMAX	The maximum engine-face total pressure ratioed to free-stream total pressure
PTI	Tunnel compressor inlet total pressure, psfa
PTA-1	Primary tunnel total pressure, psfa
PTB-2	Back-up tunnel total pressure, psfa
PSTCE1	Exit control pressure for shock tube number one, psia
PSTCE2	Exit control pressure for shock tube number two, psia
PSTCE3	Exit control pressure for shock tube number three, psia
PSTCD1	Driver control pressure for shock tube number one, psia
PSTCD2	Driver control pressure for shock tube number two, psia
PSTCD3	Driver control pressure for shock tube number three, psia
PSTC11	Interstage control pressure for shock tube number one, psia

Parameter	Description
PSTCI2	Interstage control pressure for shock tube number two, psia
PSTCI3	Interstage control pressure for shock tube number three, psia
PSTRD1	Driver pressure for shock tube one, psia
PSTRD2	Driver pressure for shock tube two, psia
PSTRD3	Driver pressure for shock tube three, psia
PSTRI1	Interstage pressure for shock tube one, psia
PSTRI2	Interstage pressure for shock tube two, psia
PSTRI3	Interstage pressure for shock tube three, psia
P1700	MA total pressure ratioed to free-stream total pressure
P1701	MA static pressure ratioed to free-stream total pressure
Q	Free-stream dynamic pressure
R2	Engine-face total pressure recovery
RBφ-I	Outboard and inboard second ramp angle, deg
RCφ−I	Outboard and inboard third ramp angle, deg
REX10 ⁻⁶	Free-stream unit Reynolds number times ten to the minus six, ft^{-1}
SCHED	Tunnel parameter
Sec	The second the data were taken, sec
SHOCK TUBE SELECT	Shock tube select code with the last two digits referring to the volumetric size, cu.ft.
S19	Sideplate configuration
TAVG	Engine-face tip average static pressure ratioed to free-stream total pressure
Test	Test number
TI2	Average engine-face turbulence factor

The second secon

Steady-State Printout Nomenclature (concluded)

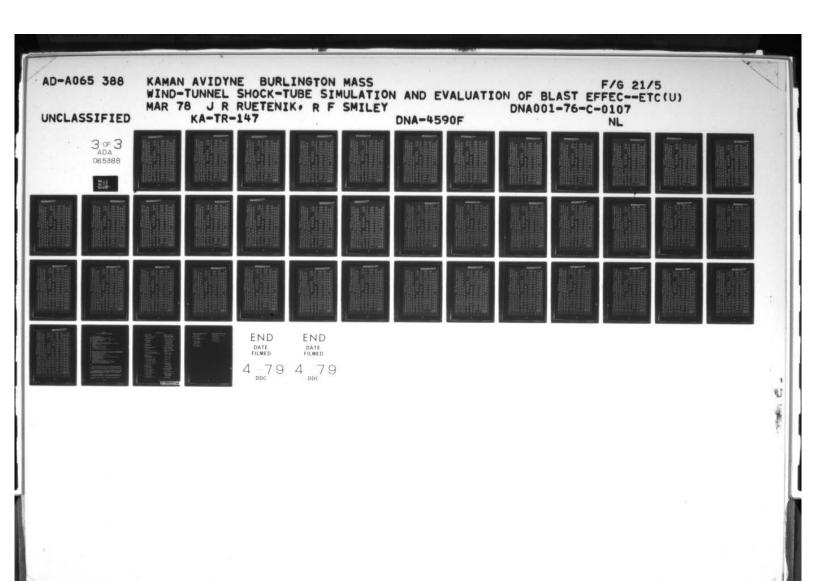
Page 5

Parameter	Description
TPR	Tunnel pressure ratio
TT	Free-stream total temperature, °R
TTA-1	Primary tunnel total temperature, °R
TTB-2	Back-up tunnel total temperature, °R
U	Bypass door position
U1	Bypass configuration
VANEI	Inboard flow throttling vane angle, deg
VANE¢	Outboard flow throttling vane angle, deg
WAE	East wall angle, deg
WAW	West wall angle, deg
WA/WT	Mass flow ratio of tunnel make-up air
W8-1	Wing configuration
Wind-off	Part and point number of current wind-off
W2	Engine-face weight flow, lb/sec
W2R	Engine-face weight flow corrected to standard conditions, lb/sec
W2R-FS	Full scale engine-face weight flow corrected to standard conditions, lb/sec

### FILDATE #IND-OFF AEDC PROPULSION WIND TUNNE IIB 1166.6	ERCODE HOBE SETIDATE HIND-OFF AEDC PROPUSION WIND TUNN LIGHT 1 100-1 1 110-1 1	The color of the	11 391 59								TH	IS:	COP	EIS	irn	ist Ish	ED	10 I	DC	1	TICABL	
TIB-0 PTI NCN HAE TIB-0 PTI NCN HAE TIB-1 1166.6 0-0.00 THE 5.4825-180.1 H16 THE 5.4825-1803.1 H16 THE 5.4825-1803.1 H16 THE 5.4825-1803.1 H16 THE 5.4825-1803.1 H16 THE	ERCODE MODE SETIDATE WIND-OFF 1066.1 1066.4 110 116 1166.6 0-0.00 1106.1 1066.4 110 116 1166.6 0-0.00 1112 107 1069 0.0353 0.033 0.503 1057 0.0980 0.0353 0.033 0.503 1057 0.0980 0.0353 0.033 0.503 1057 0.0980 0.0353 0.033 0.503 1057 0.0980 0.0353 0.033 0.503 1057 0.0980 0.0353 0.033 0.503 1057 0.0980 0.0353 0.033 0.628 1058 0.786 0.737 1058 0.786 0.787 1059 0.788 0.785 0.8153 0.6613 10611 0.7915 0.8153 0.6613 10611 0.7915 0.8153 0.978 10611 0.7915 0.8153 0.978 10611 0.001 1.000 1.001 1.001 1070 0.922 0.999 0.999 0.994 1.001 1070 0.922 0.999 0.999 0.994 1.001 1070 0.923 0.923 0.913 0.942 0.906 1070 0.003 0.003 0.003 0.003 0.0045 1077 1.000 1.2013 0.9789 0.0045 1077 1.000 1.2013 0.9782 0.0045 1005 1.0001 1.2013 0.9782 0.0045 1.005 1.0001 1.2013 0.9782 0.0045 1.005 1.0001 1.2013 0.9782 0.0045 1.005 1.0001 1.2013 0.9782 0.0045	Tary Harman Sec	The part Test Date Dat He His SEC ERCODE HODE SETIDATE HIND-OFF	DC PROPULSION WIND TUNN TRANSONIC 16T	1.256 0.0098 0.700	C3 726.C	PDP 104 07 1.2611 0.074 01 1.2613 0.066		C PLENUM .	0,775 0.8 0,775 0.8 0,7753 0.8	PL704 P1700 P17	0.7761 1.0010 0.787	TD	.5 247,5 292,5 337	001 1.000 1.000 1.0	000 0.987 0.969 C.9	953 0,963 0,927 0,9		2.5 247.5 292.5 33	001 0.006 0.014 0.004	45 PHIN PHAX 331 0.9057 1.001 238 0.9129 1.001	385 0.9129 1.0
	PCA-1 PCB-2 T1A-1 1066.1 1066.4 110 11066.1 1066.4 110 1112 1007 0.0980 0.03 10555 0.0980 0.09 10555 0.0980 0.09 10555 0.0980 0.09 10555 0.0980 0.09 10555 0.0980 0.09 10556 0.98 10556 0.98 10556 0.98 10557 0.098 1057 0.098 1057 0.098 1057 0.098 1057 0.098 1057 0.098 1057 0.098 1057 0.098 1057 0.098 1057 0.098 1057 0.098 1057 0.098 1058 0.098 1058 0.098 1059 0.0	TI PIA-1 PIB-2 PCA-1 PCB-2 TIA-1 TIA-1 PCB-2 TIA-1 T	HOJECT TEST DATE DAY HR MIN SEC ERCODE MODE 3 117-224 FE419 9/22/76 2691.1.391 SEC ERCODE MODE 3 115-224 FE419 9/22/76 2691.1.391 SEC ERCODE MODE 3 115-24 FE419 9/22/76 2691.1.391 SEC ERCODE MODE 3 115-24 FE410	0/27/76 502/ -1	8-0 PTI NCN WAE 18 1166.6 0-0.00 0	11 M6 G34-2 W8-1 H16	3 0.0331 0.5079 1. 0 0.0238 0.5203 1.	735	N. PRESSURES	91035 P1045 0,8153 0,6613 5 0,8330 0,9728	PL702 PL703	0,9860 0,798	*** INBOARD PT2	7,5 112,5 157,5	000 1.001 1.004 1	979 0.954 1.001 1	913 0.941 0.946 0	INBOARD AM	003 0.000 -1.000	011 0.000 0.001 0	R2 1DC12 1D 0.9789 0.0022 0.	0.9782 0.0967 0

TEST DAY DO MIN SEE ERPORT MANE CETTOLIC DIADARE AFOR DESCRIPTION OF THE CETTOLIC DAY
11-02A 1619 9/25/74 269: 1: 59: 15 0 0 3:10/27/74 502/
AT 1 1060.5 363.8 2.490 569 1471.1 1471.6 1070.1 1070.4 109 118 1171.9 0.0.00 0.00 1.255 0.0062 0.700 1
36:1 VANEO VANEI SHOCK TUBE SELECT 140 SI9 L7 J27 EIG UI H6 G34-2 H8-1 H16-1 N30-1 B5-1 C3 40,000 18,00 15,58 5017 RBD-1E7,8CD-1e2,1,AB10-1e,5,AB20-1e0,HL0e2,733,HL1e2,726,Ce0,Ums
92 - FR2 HFR100 HZR HZR-FS T12 1DT 1DR 1DC 1DL PD PDP 1DA 0.787 0.7897 0.7897 0.7897 0.7897 0.7898 0.7898 3.438 343.82 0.0055 0.0901 0.0430 0.0236 0.5204 1.0001 1.2615 0.0657
0.456 0.511 0.596 0.8102 0.6189 2.280 0.736 0.768 0.737 0.474 0.487 0.000 0.8349 0.8310 2.232
*** 9AMP PRESSURES ***
35 P_450 PL470 PL480 PL490 PL020 PL030 PL030 PL035 PL045 PL045
0,5098 0,8403 0,7096 0,8552 0,8566 0,8102 0,7908 0,833 0,8729 0,7751 0,8256
*** FLDWYETER PRESSURE ***
690 PI.681 PL682 PL683 PL690 PL691 PL692 PL693 PL702 PL703 PL704 P170
643 0,4619 0,4586 0,4643 0,9854 0,7983 0,7759 1,0008 0,7 656 0,4625 0,4634 0,4664 0,9640 0,8048 0,7908
••• GUTBCARD P12/P13 •••
67.5 112.5 157.5 202.5 247.5 292.5 337.5 22.5 67.5 112.5 157.5 212.5 247.5 292.5 337.
1.000 1.001 1.001 1.001 1.001 1.001 1.001 1.000 1.000 1.000 1.001 1.001 1.001 1.000 1.000 0.000 0.000 1.000
969 0,975 0,992 0,999 0,979 0,994 1,000 1,000 0,987 0
0.929 0.948 0.971 0.944 0.936 0.906 0.923 0.913 0.941 0.946 0.952 0.962 0.928 0.928 0.929
*** CUTBGARD RMS2 ***
5.50 6 67.5 112.5 157.5 202.5 247.5 292.5 337.5 22.5 67.5 112.5 157.5 202.5 247.5 292.5 337.5 5.00 6.00 6.00 6.00 6.00 6.00 6.00 6.
0.0973 0.0744 0.0330 0.0390 0.5045 0.0076 1.0006 1.2613 0.9787 0.0022 0.0330 0.9058 1.0010 0.0301 0.0050 0.0030 0.5045 0.0078 1.0001 1.2613 0.9787 0.0047 0.0236 0.9129 1.0010
0.3901 0.0667 0.0887 0.0430 0.5188 1.0110 1.2428 0.9781 0.0887 0.0384 0.9129 1.0010
PSTGE2 PSTGE3 PSTGD2 PSTGD2 PSTGD3 PSTG12 PSTG13 PSTRD1 PSTRD2 PSTRD3 PSTR11 PSTR12 PSTR13

10 1 1 1 1 1 1 1 1 1 1 1 1 1 1 1 1 1 1
0 1467.4 1058.4 362.5 2,484 569 1467.4 1467,8 1067,9 1068.2 109 116 1170:1 0-0.00 0.00 1.254 0.0022
ALPHA BETA VANEO VANEI SHOCK TURE SELECT 140 S19 L7 J27 E10 U1 H6 G34-2 H8-1 H16-1 N30-1 B5-1 C3 3.0 0.001 19.01 15.55 5015 880-1e7.RC0-1e2.1.AB10-1e.5.AB20-1e0.HL0e2.733.HL1e2.726.Ce0.ues
607HBARD 0.9792 3.7449 0.7608 3.487 348.72 0.0076 0.0953 0.0382 0.0323 0.4939 1.0002 1.2820 0.0729 1.882ARD 0.9738 0.7337 0.7503 3.439 343.93 0.0070 0.0905 0.0432 0.0240 0.5229 1.0010 1.2604 0.0672
1125 H2S H2 HA NSP TAVG H2 CPISS CP3SS CP3
*** SAMP PRESSURES *** BLC PLENUM ***
78849 0.815 P.450 PL470 PL490 PL490 PL020 PL030 PL035 PL045 P
LICETICAL DISTRICT CONTROL BY STREET OF THE CONTROL PARAMETERS OF THE
PL693 PL690 PL691 PL692 PL693 PL702 PL703 P
JARD 0:5589 5:5595 0:5592 6:5592 0:4313 0:4313 0:4325 0:4345 0:9642 6:8041 0:789
3 67.5 112.5 157.5 202.5 247.5 292.5 337.5 22.5 67.5 112.5 157.5 202.5 247.5 292.5 337.5
1.000 1.001 1.000 1.001 1.001 1.000 1.001 1.000
0.975 0.393 0.999 1.000 0.969 0.976 0.992 0.999 0.979 0.994 1.001 1.000 0.986 0.986 0.994
6.958 0.932 0.950 0.969 0.945 0.937 0.908 0.924 0.923 0.912 0.946 0.946 0.951 0.962 0.927 0.923
*** CUTBOARD RMS2 ***
1.3 22.5555 67.5 112.5 157.5 202.5 247.5 292.5 337.5 22.5 67.5 112.5 157.5 202.5 247.5 292.5 337.5
0.001 0.000 0.015 0.000
107 104 10C 10R 10L T12 PD R2 10C12 10C45 PYIN PYAK
0.0953 0.0729 0.0323 0.0382 0.4939 0.0076 1.0002 1.2620 0.9792 0.0017 0.0323 0
DATA SET 2 AUCTRED 0.0953 0.0729 0.0893 0.0832 0.8236 1.0120 1.2418 0.9778 0.0893 0.0388 0.9121 1.0006 1.8748 0.0909 0.0672 0.0893 0.0432 0.8236 1.0120 1.2418 0.9778 0.0893 0.0388 0.9121 1.0006



PTA-1 PTB-2 PCA-1 PCB-2 TTA-1 TIB-0 PTI NCN 1468.1 1468.5 1067.9 1068.2 110 117 1167.7 0 1468.1 1468.5 1067.9 1068.2 110 117 1167.7 0 1068.1 1468.5 1067.9 1068.2 110 117 1167.7 0 1068.1 1468.5 1067.9 1068.2 110 117 1167.7 0 1068.1 1468.5 1067.9 1068.2 110 117 1167.7 0 1068.1 1468.5 1067.9 1068.2 110 117 1167.7 0 1473 347.83 0.0067 0.0964 0.0432 0.0238 0.55 1 1242.2 2.22 0.736 0.768 0.787 0.8185 0.8 1 1242.2 2.22 0.736 0.768 0.787 0.8185 0.8 1 1242.2 2.22 0.736 0.788 0.787 0.8185 0.8 1 1242.2 2.22 0.787 0.787 0.8185 0.8 1 1242.2 2.22 0.787 0.787 0.8835 0.8 1 1242.2 2.22 0.787 0.787 0.893 0.893 0.893 0.893 0.893 0.893 0.893 0.893 0.993
1 1 1 1 1 1 1 1 1 1 1 1 1 1 1 1 1 1 1

HIN SEC
1 4 40 1 4 7 1 0 1 0 1

1DC 1DL PD PDP 1DA 1.5.AB2D=1BD.HLD=2.733.HL] R2.726.CEG.UES 1.0320 0.4994 1.0004 1.2617 0.0731 1.0239 0.5242 1.0010 1.2604 0.0673 1.0239 0.5242 1.0010 1.2604 0.0673 1.025 PL045 1.025 PL045 1.026 0.6037 0.772 0.8080 1.025 0.8030 0.7805 0.9997 0.7877 1.026 0.8030 0.7805 0.9997 0.7877 1.027 0.990 0.8030 0.7805 0.9997 0.7877 1.028 0.8042 0.7805 0.9997 0.7877 1.029 1.000 0.8042 0.989 0.989 0.984 1.029 1.000 0.997 0.997 0.994 1.029 0.997 0.997 0.997 1.021 0.994 0.995 0.995 0.995 0.994 1.021 0.994 0.995 0.995 0.995 0.993 1.020 0.900 0.903 0.903 0.903 0.909 1.020 0.900 0.903 0.903 0.903 0.909 1.020 0.900 0.903 0.903 0.905 0.909
SURES CONIRGL 1.2604 0.0672 SURES CONIRGL PARAMETERS CONIRGL PARAMETERS CONIRGL PARAMETERS INBOARD PTZ/PTG CONIRGL PARAMETERS INBOARD PTZ/PTG CONIRGL PARAMETERS INBOARD PTZ/PTG CONIRGL PARAMETERS INBOARD PTZ/PTG CONIRGL PARAMETERS INBOARD RMSZ CONIRGL CONIRGL PATAMETERS CONIRGL PATA
ELTOZ PLZAS CONTROL PARAHETERS C
PL045 PL045 0.8537 0.7772 0.8772 0.8772 0.8772 0.7772 0.8772 0.9700 0.8030 0.9040 0.8030 0.7805 0.9970 0.9040 0.9070
PL045 6 0.8637 6 0.8637 8 0.8727 8 0.8727 8 0.8727 8 0.8030 8 0.8030 8 0.8042 8 0.8042 8 0.8042 8 0.8042 8 0.8042 8 0.8042 8 0.8042 8 0.8042 8 0.8042 8 0.8043
CONIRGL PARAMETERS CONIRGL PARAMETERS 0.9900
PL702 PL703 PL704 P1700 0,9900 0,8030 0,7805 0,9997 0,9646 0,8042 0,7805 0,9997 - INBOARD PT2/PTC
- INBOARD PT2/PTG 2.5 157.5 202.5 247.5 292.5 33 2.15 157.5 202.5 247.5 292.5 33 2.15 1500 1.001 1.00
2.5 157.5 202.5 247.2 292.5 33 001 1.000 1.001
187.5 202.5 247.5 292.5 33 0.000 0.001 0.003 0.003 0.003 0.015 0.015 0.015
0.000 0.003 0.003 0.015 0.00 0.001 0.003 0.003 0.015 0.00

PAGT POINT PROJECT TEST DATE DAY HR MIN SEC ERCODE MODE SETIDATE MIND-OFF AEDC PROPULSION WIND TUNNEL 527 2 PAIT-D2A IE419 9/23/76 2681 7: 14: 34 0 0 3:10/27/76 524/ -: TRANSONIC 16T
. 21 14551 1756.7 362.0 2,480 559 1465.1 1465.9 1066.2 1066.4 109 114 1167.6 0-0.00 0.00 1.255 0.0078 0.700 1
ALPHA BETA VANED VANET SHOCK TUBE SELECT 140 S19 L7 J27 E10 U1 MG G34-2 MB-1 M16-1 N30-1 B5-1 C3 3.0 3.0 3.0 3.0 3.0 3.0 3.0 3.0 3.0 3.
2 0701 5 7444 6 7447 1 448 448 55 0 0778 0 0050 0 0324 0 032 0 4040 0 000 1 2440
2,7341 0,7508 3,442 34414 0,0068 0,0907 0,0432 0,0239 0,5231 1,0009 1,2605 0,
PUTGRA93 0.452 0.502 0.593 0.8112 0.2240 2.255 0.737 0.768 0.737
ALTERNATION OF THE PROPERTY OF
2453 PL476 PL486 PL496 PL696 PL626 PL136 PL036 PL036 PL036 PL636 PL547 PL5
7847 0.8178 0.8632 0.7773 7897 0.8321 0.8730 0.7754
*** FLOWFETER PRESSURE ***
PL640 PL641 PL662 PL663 PL693 PL699 PL691 PL692 PL693 PL702 PL702 PL703 PL704 P1704
*** 6UTBOARD PT2/PTG ***
RIVG 22.5050 67.5 112.5 125.5 202.5 237.5 22.5 67.5 112.5 202.5 247.5 202.5 337.5 1 0.01 1.000
*** BUTBOARD RMS2 ***
81.5 22.50E5 67.5 112.5 157.5 202.5 247.5 292.5 337.5 22.5 67.5 112.5 157.5 202.5 247.5 292.5 337.5 1 0.00 0.00 0.00 0.00 0.00 0.00 0.00
107 104 106 106 106 108 106 108 106 112 PD PDP 1.205 0.075 1.0002 1.205 0.0507 0.0675 1.0002 1.205 0.0507 0.0507 0.0508 1.206
PSTOEL PSTOE2 PSTOEJ PSTOD2 PSTOD3 PSTOLL PSTOLZ PSTOLJ PSTROL PSTROJ PSTRIL PSTRIZ PSTRIJ

SETIDATE WIND-OFF AEDC PRCPULSION WI 3.1272726.522 -2 -2 -2 -2 -2 -2 -2 -2 -2 -2 -2 -2 -	*** STEADY STATE *** *** STATE ** *** STATE *** *** STATE *** *** STATE *** *** STATE *** ** STATE *** *** STATE *	ERCODE HODE SETIDATE HIND-OFF AEDC PROPULSION WIND TUNN AE ALL TRANSMILL 161 2. PCA-1 PCG-2 IJA-1 IIGO PIL NCN MAE NAW TER MAYIT HE SCH 140 S19 10 1261 0.057 0.0375 0.5121 1.0010 1.2614 0.0773 0.0573 0.0560 0.1033 0.0376 0.0572 0.0572 0.0572 0.0372 0.0373 0.0572 0.0572 0.0572 0.0373 0.0572 0.0572 0.0572 0.0373 0.0572 0.0572 0.0572 0.0373 0.0572 0.0572 0.0572 0.0373 0.0572 0.0572 0.0572 0.0373 0.0572 0.0572 0.0572 0.0572 0.0572 0.0373 0.0572 0.05					COPY FURNI	ST QUALITY I	
SETIDATE WIND-OFF A SIGNITION WARE LIDO 1343,1 0-000 0 0 0 0 0 0 0 0 0 0 0 0 0 0 0 0	ERCODE HODE SETIDATE WIND-OFF AS 110/22/74 542/ -27 1-2 PCA-1 PCB-2 ITA-1 ITB-0 PTI NGN WAE 140 150 150 150 150 150 150 150 150 150 15	SALOR STATE SALOR STATE SALOR SETIDATE WIND-OFF AND OFF SALOR SALO	PRCPULSION WIND TUNN TRANSONIC 161 TPR HA/HT MB SCH 1.261 0.0261 0.850 0-1 85-1 C3	1.2614 0.074	0.7448 C. PLENUM 0.7433 C. 0.7348 C.	PLZ04 PLZ00 PLZ 0,7714 0,9996 0,7 0,7764 0,9996 0,7	25 247;5 292;5 337 01 1:001 1:001 1:0 01 1:001 1:001 1:0 01 1:001 0:986 0:9 97 0:996 0:957 0:9	247,5 292,5 33 1 0.001 0.001 0.004 0.003 0.004 0.004	0.9039 1.0 0.9039 1.0 0.9039 1.0
	8-8 STEADY STATE 1-2 PCA-1 PCB-2 JJA- 1-4 1072.5 1072.7 110 1-10 S19 L7 J27 E10 1-10 S19 L92 L92 1-10 S19 L92 L93 1-10 S19 L92 L93 1-10 S19 L	SATE DAY HR HIN SEC ERCODE HODE	SETIDATE WIND-OFF 1 3110/22/76 542/ -2 1 TIB-0 PTI NCN MAE 110 1343,1 0-000 0 01 M6 G34-2 W8-1 H16-1	DR 10C 10L 377 0.0375 0.5121 1. 436 0.0313 0.5420 0. 8355	ERNAL PRESSURES	93 PL702 PL703 969 0,9983 0,7951 021 0,9914 0,7949	07.5 112.5 157.5 2 001 1.001 1.001 1 001 1.001 1.001 1 .97 0.995 1.001 1 .937 0.957 0.986 0	67.5 112.5 157.5 20 0.001 0.001 0.001 0.001 0.003 0.002 0.003 0.	607 0,9796 0,0030 0.614 0.9805 0,00948 0.

The state of the s

### ### ### #### #### ################	DATE DATE HIN SEC EFFONE HODE SETIDATE WIND-OFF AEDC PROPULSION WIND TUNN AS THE STATE STATES AND THE SELECT STATES AND THE STATES AND THE STATES AND THE SELECT STATES AND THE STATES AND											ROM		IS	NIS	ETO TEST		DD	PRACT	ICABL
REY10'6 TI PIA-1 PIB-2 PEA-1 PEB-2 TIA-1 TIB-2 PII NCN HAE HAE MAN MAR MAN M	EGT TEST DATE DAT HE HIN SEC ERGOGE HODE SETIDATE WIND-DFF AED DATE TALL PLANS PROPERTY 9.22726 271211 561 52 1	The state was a made of	TRANSONIC 161	.261 0.0262 0.850	85-1 C3	1.2606 0.		LC PLENUM	7426 0.7345 D.	PARAMETERS	P1700 P1701 0,9991 0.728		1.001 1.001 1.	1.001 0.988 1:	6.974 0.935 0.		0.001 0.001 0.	0.001 0.004 0.	0.9038 1.000 0.9075 1.000	0.9075 1.001
DATE DAT HR HIN SEC ERCODE HODE SETIDATE 9/27/76 271/21 561 52 3.10/27/2 3.1069 569 1693,7 1694,0 1072,7 1072,6 110 110 11 3.106 569 1693,7 1694,0 1072,7 1072,6 110 110 11 2.29 5620 2.20 5620 1693,7 1694,0 1072,7 1072,6 110 110 110 11 2.7081 3,476 347,81 0,072,1 0,0954 0,0378 0,00 2.7081 3,476 347,81 0,072,1 0,0954 0,0437 0,00 2.7081 3,473 3473 347,31 0,072,1 0,0954 0,699 0,00 2.7081 3,473 3,473 3,473 0,072,1 0,0954 0,699 0,00 2.7083 0,0974 0,917 2,603 0,699 0,699 0,699 0,097 2.7083 0,0945 0,2810 0,2810 0,7914 0,774 0,0814 0,097 2.7083 0,0945 0,2810 0,2810 0,7914 0,774 0,097 2.7083 0,0945 0,2772 0,2760 0,2760 0,2814 0,097 2.7083 0,0945 0,2772 0,2760 0,2760 0,2814 0,097 2.7083 0,0945 0,0944 0,097 0,094 0,097 0,097 3.7083 0,007 0,094 0,007 0,094 0,097 0,097 3.7083 0,007 0,094 0,007 0,004 0,001 0	EGT TEST DATE DAT HR HIN SEC ERCODE HODE SETIDATED TO A TITAL TIBED Set STATE STATES THAT THE SELECT TEST DATE DATE SELECT TEST DATE DATE DATE DATE DATE DATE DATE DAT		25	1 0-0.00 0	H16-1	10L PD 5131 1.001 5488 0.999		S	PL045 0,861 0,867	:	9967 0.7948 9967 0.7948	INBOARD PT2/PT	1,001	1.001	0.940 0.95	INBOARD RMS2	0.001	0.001	0030 0.0	0.0983
DATE DAY HR HIN SEC ERCODE HODE 9/27/26 2711511 561 562 8.160 2716 2711511 561 562 8.160 270 40 1693,7 1694,0 1072,7 1072,8 8.160 270 40 1693,7 1694,0 1072,7 1072,8 8.160 0 1070 40 172 2,602 0,0954 9.700 1 3,470 91,490 8172 2,602 9.700 0 1070 0 108172 2,602 0,0954 9.700 0 1070 0 108172 2,602 0,0954 9.700 0 1070 0 108172 2,602 0,0954 9.700 0 1070 0 108172 2,602 0,0954 9.700 0 1070 0 108172 2,602 0,0954 9.700 0 1070 0 108172 2,602 0,0954 9.700 0 1070 0 108172 2,602 0,0954 9.700 0 1070 0 108172 0,272 0,273 9.700 0 1070 0 1070 0 1070 0,0954 11.001 1.001 1.001 1.001 1.001 1.001 1.001 11.001 1.001 1.001 1.001 1.001 1.001 1.001 11.001 1.001 1.001 1.001 1.001 1.001 1.001 11.001 1.001 1.001 1.001 1.001 1.001 1.001 11.001 1.001 1.001 1.001 1.001 1.001 1.001 11.001 1.001 1.001 1.001 1.001 1.001 1.001 11.001 1.001 1.001 1.001 1.001 1.001 1.001 11.001 1.001 1.001 1.001 1.001 1.001 1.001 11.001 1.001 1.001 1.001 1.001 1.001 1.001 11.001 1.001 1.001 1.001 1.001 1.001 1.001 11.001 1.001 1.001 1.001 1.001 1.001 1.001 11.001 1.001 1.001 1.001 1.001 1.001 1.001 11.001 1.001 1.001 1.001 1.001 1.001 1.001 11.001 1.001 1.001 1.001 1.001 1.001 1.001 11.001 1.001 1.001 1.001 1.001 1.001 1.001 11.001 1.001 1.001 1.001 1.001 1.001 1.001 11.001 1.001 1.001 1.001 1.001 1.001 11.001 1.001 1.001 1.001 1.001 1.001 11.001 1.001 1.001 1.001 1.001 1.001 11.001 1.001 1.001 1.001 1.001 1.001 11.001 1.001 1.001 1.001 1.001 1.001 11.001 1.001 1.001 1.001 1.001 1.001 11.001 1.001 1.001 1.001 1.001 1.001 11.001 1.001 1.001 1.001 1.001 1.001 11.001 1.001 1.001 1.001 1.001 11.001 1.001 1.001 1.001 1.001 1.001 11.001 1.001 1.001 1.001 1.001 11.001 1.001 1.001 1.001 1.001 1.001 11.001 1.001 1.001 1.001 1.001 11.001 1.001 1.001 1.001 1.001 11.001 1.001 1.001 1.001 11.001 1.001 1.001 1.001 11.001 1.001 1.001 1.001 11.001 1.001 1.001 11.001 1.001 1.001 11.001 1.001 1.001 11.001 1.001 1.001 11.001 1.001 1.001 11.001 1.001 1.001 11.001 1.001 1.001 11.001 1.001 1.001 11.001 1.001 1.001 11.001 1.001 1.00	ECT TEST DATE DATE HANN SEC ERCODE HODGE D24 TF419 9/22/76 271/21 561 52 B	26.4.4.6	3110/27/74	118=9_PI	H6 G	108 0.037 0437 0.031	CP3	NTERNAL PRESS	7784 0.7748 0.		2766		1 1.001 1.	0.977 0.	0 0.001 0		0.001 0.	0.004	2606 0.979	90
PEXID-6 11 PIA-1 PIB-2 3.164 569 1693.7 1694.0 3.164 569 1693.7 1694.0 2.164 569 1693.7 1694.0 2.7041 3.473 47.31 0.7041 3.473 47.31 0.7041 3.473 47.31 0.7041 3.473 47.31 0.7041 3.473 6.9218 2.1070 0.6020 0.9218 2.1070 0.6020 0.9218 2.1070 0.6020 0.9218 2.1070 0.6020 0.9218 2.1070 0.6020 0.922 2.1070 0.993 2.1070 0.993	ECT TEST DATE DAY HR HIN SEC PEATO 9/2726 21121 501 55 18.49 14.29 14.29 1693.7 1694.0 18.49 14.29 14.29 1693.7 1694.0 18.49 14.29 14.29 16.20 16.37.31 35 0.5936 0.7001 3.478 347.31 35 0.5936 0.7001 3.478 347.31 35 0.5936 0.7001 3.478 347.31 35 0.5936 0.7001 3.478 347.31 35 0.5936 0.7001 0.9210 0.921	2000	acone non	PCA-1_PCB-2 072,7 1072,8	4r S19 L7 J27	712 0080 0.098 0021 0.095	CP1SS CP2S 3 0,650 0,6		7914		691 PL692 2810 0.272 2760 0.278		5 337,5 2 01 1,601 1,	33 0.946 0.	04 0.923 0.		0,004	0.013 -1	120000000	20
PEXIDE DATE DATE DATE DATE DATE DATE DATE DA	ECT TEST DATE DATE DATE DATE DATE DATE DATE DAT	2 77.7	201	-1 PTB-2	SELECT	28 W28-FS 478 347.81 0 473 347.31 0	TAYG H2 0.8172 2.6 0.9218 2.6		400	ER PRESSURE	PL690 P	:	1.001 1.	0.962	0.936 0.		0.004	0.015	1DL 0.5131 0	90
	24	24.45	9777776	PEXT	VANE 1	0.7081 3.		PRESSURES	0.7693	FLOWMET	PL682 0.4936 0.4927	GUTASARD, P	157.5	0.992	0,939	CHACBTU	0,003	0.000	0.0374 0	0.0983

							PRO								RAC	TICAL	
PART PSINT PROJECT TEST DATE DAY HR HIN SEC ERCODE MODE SETIDATE WIND-OFF AEDC PROPULSION WIND TUNNEL SEL : PALTEDZA TE419 9/27/76 271:231 221 32 0 0 3110/22/76 548/ -1 TRANSONIC 16T	0.90C 1787.4 1057.3 598.9 3.426 570 1787.4 1788.5 1071.8 1072.3 110 110 1445.7 0-0.00 0.00 1.236 0.0366 0.900 1 ALPM BET VANES VANES VANES SHOCK TUBE SELECT 140 519 HIGH BET HIGH NAD-1 85-1 63 17.30	92 "FR2 MFR190 W2R W2R-FS T12 1DT 1DR 1DC 1DL PD PDP 0.9968 0.0350 0.0370 0.4858 1.0000 1.2624 0.9921 0.6994 0.7121 3.542 354.16 0.0023 0.0927 0.0413 0.0334 0.5307 0.9991 1.2623	мутаркар 3.443 0.499 0.712 0.8044 0.8274 2.760 0.620 0.677 0.620 таракар 3.491 0.502 0.000 0.8005 0.8267 2.803	PAPP PRESSURES PL470 PL490 PL020 PL030 PL035 PL045 PL543 PL543 PL573 PL5	DAGE CONTROL CONTROL CONTROL CONTROL CONTROL CONTROL CONTROL PARAMETERS	### PLOS PL69; PL682 PL683 PL690 PL691 PL692 PL693 PL702 PL702 PL703 PL704 P1704 P17	*** GUTBSARD PTZ/PTG.*** INBOARD PTZ/PTG.	49 22.4350 67.5 1:2.5 157.5 202.5 247.5 292.5 337.5 22.5 67.5 112.5 157.5 202.5 247.5 292.5 33	1.001 1.001	964 0.965 0.987 0.997 0.976 0.995 1.001 1.001 1.001 0.992 1	5.977 0.957 5.973 6.948 5.943 5.939 6.908 6.926 6.921 6.910 6.942 6.940 5.961 6.986 6.948 6.	.50EG 67.5 112.5 157.5 202.5 247.5 292.5 337.5 22.5 67.5 112.5 157.5 202.5 247.5 292.5	0.004 0.004 0.010 0.005 0.015 0.014 0.004	- 17. 4.1. 4.1. 4.1. 4.1. 4.1. 4.1. 4.1.	1	2 2.2954 6.2741 2.2948 6.0352 0.8325 1.8326 1.0126 1.2418 0.9988 0.0948 0.0525 0.9088 1.0	PSTORE PATORS PSTODS PSTODS PSTOLE PSTOLE PSTOLE PSTROLE PSTROLE PSTROLE PSTROLE PSTROLE PSTRILE PSTRILE PSTRILE

	SCHED 900 1	Cepules			NUM	PL573 0.7985 0.8035		P1701 0.7109		337.5 1.001 1.000 1.000 0.936		337.5 0.001 0.001	5	91
TRANSONIC 16T	237 0.	11.2.726.	1.2619 0.0754 1.2632 0.0721		See BLC PLEN	PL543 0,7352 0,7264	PARAMETERS	704 P1700 7778 0,9991 7843		1,001 7,001 1,000 7,000 1,000 7,000 1,001 7,000 0,992 0,972 0,981 0,951		0.001 0.001 0.001 0.001 0.001 0.004	0.9962 1.001 0.918 1.000	0.9118 1.0008
	CN KAE	-JFD. HLD=2,233	101. 4949 1.0002 5198 0.9985		s	.8727 .8727	CONTROL	2 PL763 Pt 88 0.7997 0. 86 0.8030 0.	BOARD PT2/PT6	1.001 1.001	NBOARD RMS2	157.5 202.5 0.001 0.001 0.001 0.001	.0033 0.0377	0903 0.0473
3110/27/76 548/	110 1446,4	813=1x.5.AB20	357 0,0377 0 404 0,0328 0	355	RNAL PRESSURE	61 0.8174 0		47 0.99 65 0.99	NI	67.5 112.5 1.000 1.001 1.000 1.001 0.978 0.996 0.940 0.960 0.942 0.960	1	67.5 112.5 0.001 0.001 0.003 0.002 0.003	R2 0.9801 0	436 0.9826 0.
6 6	1072,9	Z.RCD-182.1	0.0973 0.03	155 CP255 CP ,619 0,676 0	COML. INTE	PLC20 PL03 0.7883 0.78 0.7892 0.78		PL692 PL69 0.5521 0.55 0.5543 0.55		1,001 1,001 1,000 1,000 0,945 0,947 0,947 0,925 0,925		137,5 22,5 ,003 0,001 ,013 -1,000	1.0002 1.261 0.9985 1.263	1.0101 1.24
61.35	PTB-2 PCA-1 1789,2 1072,5 ECT 140 S1	88.	49,93 0,0076 48,47 0,0019	2,766 0 2,761		.8408	SSURE	.5552 0.5546 .5544 0.5532		993 6.999 1999 1999 1999 1999 1999 1999 199		47.5 292.5 3 .003 0.003 0 .015 0.010 0	1DL 712 .4949 0.0076	8458
2711231 4	6 17 PTA-1 8 570 1786,5 SHOCK TUBE SE		3,499 3	0.8006 0.8235 0.8040 0.8298	RES	0.8381 0.8476	FLOHMETER PRE	9,6551 0	SARD PTZ/PTG.	7.5 207.5 2 001 1.000 1 000 1.002 0 958 0.984 0 958 0.984 0	DARD RHS2	57.5 202.5 24 ,003 0.003 0. ,010 0.005 0.	0.0357	57 0.0357 0.
15419 9127/76	599.3 3.42		5.6896 0.7036 5.6896 0.7036	0.505 0.714 0.497 0.000	RAMS PRESSURE	0,8335 0,7754 0,8335 0,7754	:	PL681 PL682 0.6552 0.653 0.6547 0.654	*** CUTBO	2100000	*** BUTB	0.003	3.0754 0.0377 3.0721 0.0328	0.0721 0.0953
2 P417-D2A	98.5 105	6 1727 18.	AD 0.9801	0,484	:	0.7803		71.687 80 0.6547 80 0.6546		22.50EG 67.5 1.001 1.001 1.000 0.994 0.996 0.980 0.977 6.986		22.50EG 57.5 2.203 0.203 2.203 0.203	0.0973	80 0.0973
553	1 10	-	1x87ARD	PUTBCARD 1193ARD		TESTARD		CUTSCARD 1:32ARD		0		- m m	1.35483	1.3748

ا	ED														o doc	+	2
TUNKE	SCH	Sall	- 9		NUM	P1573 0.8541 0.8605		0.7385	1 .		100	-	2	1000	70	70	PSTRI
NIX U	HT HB	C3 726,C=0	0.0547		C PLEN	7871	ERS	9966	6	000	000		92.	0.005	1,0001	90	STRIZ
CPULSION RANSONIC	32 0.0	-1	1.2694 1.2729		998 BL	400	ARAHET			00			.4	.001	FIN 9312	90	TRI1 P
DC PR	.00 1.2	N30-1 85-	9955 1 9928 1				TROL P	0.0		100	1000	2	2.5	001 0	285 0	362	PS
P AE	. 00 o	H16-1 N	00				CON	0.85	5 2	14.	126	0 0	10-	010	8 4	90	PSTRD3
41ND-0FF	3 0-0	1 -	0.3845 0.3596		RES	PL045 0.9041 0.9124	•	9985	INEOA		400	INBO	1	2	0.000	90	STR02
10ATE H	1377	634-2 W	10c 0285 0248		PRESSU	PL035 6.8717 0.8816	1	1 1	3	-	1000	•	112	00	R2 0.9852	989	TRD1 P
SET 10	1 118-	AB10=1	DR 281 0	0.645	ERNAL	525		93	-	000	4 6 6 6 6 6 6 6 6 6 6 6 6 6 6 6 6 6 6 6			0.008	129	543	3 PS
906	-2 TTA-1	J27 E10	00	2555	WL. 1ST	P.0 8.0 8.0 8.0		P. 0 0 0.3	1 .	000	0 0 0		22.5	0.00	955 1,2 928 1,2	7-	PSTCI
ACODE I	1071	9 L7	101	155 CP	8	PL020 0.852 0.861		PL692 0.348 0.351	37	000	986		37.5	0.011	666	~~	PSTC12
-	4 5	140 S1 RBC-18	0.0061	258 0,			:	PL691 0.3518 0.3498	2.5	000	968		2.5	9.00.0	112 0,0761 0,0923		1011
SEC 1.37	0.0	ECT	24-FS 99.53	51 2.		8855	SURE.		2.5	100	975 0		7.5	207	3845 3596	5709	CD3 PS
11 15	697.5	BE SEL	428 +29 1,995 29	0.882		24.0	R PRES	22.5		100		2	2 2	05 0.	271 0.		PST
DAY 6 2721	570	5015 5015	100	0.8707	s	90.0	OWNETE	0.47	2 6	-	400		100	9 0 0	00	90	PSTCD2
9/28/2	22	E1 SH	1F 8100	0.671	ESSURE	PL470 0.8441 0.8476	FL	171	•	1	000	10	-	0.00	0.0285	069	STCD1
EST F419	535.7	21.22	.6001 .5973	0.415	SAUP PR	6.8709 6.8777		7 -1		1.00	100		112.	0.004	10847 10516	0.0504	CE3 PS
3JECT T	57.8	25.67	9652 C		:	124	-	721	67.5	1.001	100		67.	900.0			PST
10 4	1607,5 10	PE74	19	23.00	-	7 5 5		4	20.00	60	2.97		5.5383	2.000	10.072	200	PSTOEZ
SS7 2	. 151 16	41.P#4	UTBEARD.	PUTACARD INBBARD		FUTBOARD INSOARD		UTBEARD INMOARD	0.1		n 4		10		14 SET	5474 SET 21782483 1783483	STCE1

TIB-0 PTI NCN HAE WAN TPR HAVIT MB SCHE 111 1375.6 0-0.00 0.00 1.233 0.0328 0.850 1 M 6 33-2 M5-1 H16-1 N3-1 B5-1 C3 10-18.5.4820-180.41682.733.41182.726.620.185 1 0 0.0281 0.3822 0.9954 1.2996 0.0543 1 0 0.0281 0.3822 0.9954 1.2996 0.0543 2 0.874 0.9040 0.9954 1.2732 0.0512 2 0.874 0.9040 0.9954 1.2732 0.0512 2 0.874 0.9040 0.7878 0.6543 2 0.874 0.9040 0.7878 0.6543 2 0.874 0.9040 0.7878 0.788 0.6543 2 0.874 0.9040 0.7878 0.788 0.6543 2 0.992 0.992 0.9644 0.8536 0.9922 0.7889 2 0.992 0.992 0.0644 0.8536 0.992 0.7889 2 0.992 0.000 1.000 1.001 1.001 1.001 0.993 0.993 3 0.992 0.995 0.996 1.000 1.001 0.993 0.993 3 0.993 0.995 0.996 1.000 1.001 0.993 0.993 3 0.995 0.995 0.996 1.000 1.001 0.993 0.993 3 0.985 0.002 0.002 0.003 0.002 0.002 3 0.985 0.002 0.002 0.003 1.0018 3 0.985 0.002 0.002 0.003 1.0018 3 0.985 0.002 0.002 0.003 1.0018 3 0.985 0.002 0.002 0.003 1.0018 3 0.985 0.002 0.002 0.003 1.0018 3 0.985 0.002 0.002 0.003 1.0018 3 0.985 0.002 0.002 0.0034 0.935 1.0008 3 0.985 0.002 0.0024 0.935 1.0008 3 0.985 0.0022 0.0034 0.935 1.0008 3 0.985 0.0022 0.0034 0.935 1.0008 3 0.985 0.0022 0.0034 0.935 1.0008 3 0.985 0.0022 0.0034 0.935 1.0008 3 0.985 0.0022 0.0034 0.935 1.0008	P.CS-2 TA-1 TIB-D PTI NCN WARE WAN TRP WAYNE WAND TUNNE LOTO, 7 110 111 1375.6 D-0.00 0.00 1,233 0.0328 0.050 LOTO, 7 110 111 1375.6 D-0.00 0.00 1,233 0.0328 0.050 LOTO, 7 110 111 1375.6 D-0.00 0.00 1,233 0.0328 0.050 LOTO, 7 LOTO, 7 LOTO LOTO	DAY HA MIN SEC ERCODE MODE SETIDATE NIND-OFF AEDC PROPULSION WIND TWNNE C 167 11 291 44	10 9/29/76 2721.1129141 SEC ERCODE MODE SETIONE WIND-OFF AEDC PRODUSION WIND TUNNER 18-20-21.129141 SEC 10 3 3100/27/76 595/ -1 TRANSDUSC 161	The project Figs Day He will sec										FROM	00	PY	IS I	US	HED	TO	DDO	PR	CTIC	B
TIDATE WIND-OFF AEDC 111 1375.6 0-0.00 0.00 111 1375.6 0-0.00 0.00 111 1375.6 0-0.00 0.00 10 0.0248 0.3628 0.9922 10 0.0248 0.3628 0.9922 10 0.0248 0.3628 0.9922 10 0.992 0.9639 10 0.992 0.9640 10 0.962 0.9640 10 0.962 0.0026 10 0.962 0.9640 10 0.962 0.0026 10 0.962 0.0026	CODE HODE SETIDATE WIND-OFF AEDC 1070,7 110 111 1375,6 0-0.00 0.00 0.00 0.00 0.00 0.00 0.00 0	26 2221 11 277 14 MIN SEC	19 9/28/78 2721 11 291 41 1 1 1 1 1 1 1 1 1 1 1 1 1 1 1 1 1	### 17.00 1.00	SION WIND TUNNE	7PP HA/HT MB SCHE	1 85-1 C3	1,2696 0.0 1,2732 0.0		LC PLENUM	543 PL573 7873 C.654 7798 C.860	L PARAMETERS .	18466 0,9992 0,738	247.5 292.5 337	1.001 1.001 1.0	1.001	0.987 0.973 0.9		0.001 0.001 0.0	0.001 0.002	NIN	0.9315 1.000	0.9315 1.000	
TTB-0 PT1 1375.6 PT 1 111 1375.6 PT 1	PCB-2 TTA-1 TTB-0 PT1 1070,7 110 11111375,6 PT1 1070,7 110 11111375,6 PT1 1070,7 110 11111375,6 PT1 1070,7 110 11111375,6 PT1 1070,7 110 110 110 110 110 110 110 110 110 11	26 272.1.1.291.41 56 72.1.1.291.41 56 9 1695.7 1686.2 1070.4 1070.7 110 56 9 1695.7 1686.2 1070.4 1070.7 110 11375.6 1150.0 1 10 10 10 10 10 10 10 10 10 10 10 10	19 9/29/26 2721.11 291.41 19 9/29/26 2721.11 291.41 10 3/177 569 1695.7 1696.2 1070.4 1070.7 110 111 1375.6 12.12 5620 10.6051 10.6051 10.6052 10.6051 10.6052 10.6052 10.6052 10.6053 10.60	### FEAT FEAT DATE DATE DATE DATE FROM ERCODE HODE SETIONTE HIS FALLS FRANCE FROM FRANCE FRANC	AEDC	CN HAE HAH	5-1 H16-1 N30	1DL PD 3822 0.99 3620 0.99		:	904	CONTR	2 PL703 P 86 0.8576 0 92 0.8649 0	DARD PT2/PT	000	1.000	.956 0.97	BOARD RMS2 .	57.5 202	001	C12 1DC4	0026 0.028	0692 0.03	
	CODE HODE 1 0.70 - 1 10 10 10 10 10 10 10 10 10 10 10 10 1	76 TY HR HIN SEC ERCODE HODE 3	1.0 9/28/76 DAY HR HIN SEC ERCODE HODE 3 1.0 9/28/76 2721.1 291.1 1 29	The Project Test	SETIDATE WI	TTB-0_ PTI_N 111 1375,6	U1 M6 G34-2 W	0.0281 0	355	RNAL PRESSURE	22 0.8714 0 47 0.8819 0		59 0.99	NI 1N	1,00	985 0.99	939 0.96	:	67.5 112	1.000	82	96 0.9850 0 32 0.9892 0	99 0.9892 0	1
SEC ER SE			24 2 2 2 2 2 2 2 2 2 2 2 2 2 2 2 2 2 2	PROJECT TEST DATE PROJECT TEST DATE 15.7 1.57.2 534.8 3.17) 2.977 0.485 0.699 0.603 2.375 0.699 0.603 2.495 0.485 0.603 2.495 0.485 0.603 2.495 0.485 0.603 2.495 0.485 0.603 2.495 0.485 0.603 2.495 0.485 0.485 2.495 0.485 0.485 2.495 0.485 0.485 2.495 0.485 0.485 2.495 0.485 0.485 2.495 0.485 0.485 2.495 0.485 0.485 2.495 0.485 0.485 2.495 0.485 0.485 2.495 0.485 0.485 2.495 0.485 0.485 2.495 0.485 0.485 2.495 0.485 0.485 2.495 0.485 0.485 2.495 0.485 0.685 2.497 0.994 0.999 2.498 0.994 0.999 2	DAY HR HI 6 2721 11 2	6 TT PTA 569 1695	HOCK TUBE SE	1 2,995 2 5 2,927 2	.4588 n.8	ES	PL480 9 0.8861 0	LOWKETER PRE	5 0.4693 0	D PT2/PTC	01 1:031 1.	00 1.000 0	74 0.955 6.	ARD RHS2 .	.5 202,5 2	0.0050	108	0.0280 0	0.0274 0	

	1				
SAR 2 PATTED2A T	TEST DATE	6 2721 51 431 40	ERCODE MODE SET	127/76 567/ -1	EDC PROPULSION WIND TUNNEL
.730 1459,0 1059,4	162.9 2,482	570 1449.0 1469	-2_PCA-1_PCB-2_JA-1_JTB	0 2167.7 0-0.00 0.	.00 1.258 0.0091 0.700 1
ALP44 BETA VANEC	S VANET SH	SOLS SELECT	14° 519 L7 J27 E10 U1 MG	M6 G34-2 MBF1 H16-1 Gele,5,4820-fe0.HLGe	N30-1 B
42	-	WZR HZR-F	T12 10F 1DR	100 100	P D P
1432430 0.9758 0.	7416_0,7640	3,502 350,19	0.0076 0.0913 0.0390	0.0420 0.5671 1.	.0004 1.2617 0.0651
225	2.505 0.508 C	NED TAYS	Z .		
93492 C1492	0.00	.9364_E.8	252		
	THE PRESSORE		CONT INTERNAL	PRESSURES	BLC PLENUM
PLC35 P	453	PL480 PL490	PL020 PL030	L035 PL045	L543 PL573
1483480 0.035 0.	.6256 0.7667	0.6364 0.64	0.7937 0.7826	0.8161 0.8609	0,7598 0.8053
	J FL	OWMETER PRESSURE	:	85	NTRCL PARAMETERS
0 + 9	P. P.	P1.693 P1.69	L691 PL692 PL6	L702 PL7	PL704 P170
1 VB3AR3 0.5463 3	0.5461 0.5455	0.5449 0.4063	0.4070 0.4	0.9324 0.791	5 0.7751 0.9991 0.8
	*** BUTBOAR	D PT2/PTG		INBOARD PT2	/PTG •••
13 22.50EG	112.5 157.	202.5	1 1.001 1.00	5 112	001.5 247.5 292.5
	9.978	1.001	.957 C.996 D.995 D.95	2 0.979 1.001	.001 0.950 0.983 0.
0.999	0.025	3 0.944 0.	912 0.927 0.93; 0.89	4 0.934 0.943	.980 0.944 0.934 0.
	ACETTES	RD RMS2		INBOARD RM	\$2 •••
A11.6 22.50% 67.5	0,004 0,00 0,011 0,00 0,014 0,00	5 202.5 247.5 3 0,003 0.003 3 0.005 0.007 2 0.011 0.009	292.5 337.5 22.5 67.5 0.003 0.009 0.009 0.009 0.000 0.000 -1.000 0.003 0.003 0.003	112.5 157.5 0.003 0.001 0.003 0.001	202.5 247.5 292.5 337.5 0.001 0.003 0.001 0.002 0.001 0.004 0.002 0.002 0.004 0.003
0.0013	104 10651 0.0316 10851 0.0420	0.0390 0.4990 0.0420 0.5671	0.0776 1.0004 1.2617 0.0030 1.0006 1.2596	R2 1DC12 1D 0.9758 0.0117 0.	0045 PHIN PPAX 00346 0.9124 1.0015 00420 0.6936 1.0012
0.1101	0.0831 0.1086	0.0390 0.7817	1,0107 1,2441	0.9749 0.1086 0.0	0398 0.9124 1.0015 0538 0.8938 1.0012
PSTCE1 PSTCE2 PSTCE3	95 B.00	PSTCD2 PSTCD3	PSTCII PSTCI2 PSTCI3 PST	TRD1 PSTRD2 PS	TRD3 PSTRI1 PSTRI2 PSTRI3

											1	ROM			TUR	NIS	HET			+	-
	TONNEL	SCHED	Sam				7914		P1701	•	:	966.0	. 8	95		337.5	9 0			10	74.65
	2 4	3 0,70	9 9	104		PLENUM	100		0			280		200			200	100	3	000	7.45
	E C	NA/HI 0.006	53	no		BIC	PL54	ETE	P170	•	:	100		00		2	66		1]	10	•
	A S	255	85-1 H 1s2	PDP 1.262		:		PARAH	704	754		0.993				5 6	800	700	0.8995	-	4
1	TR TR	AN 1.	N30-1	900				5	277		, ,	200	100	646	2	5.5	115	298	187	~ °	
11	YE.	H 0	H16-1	40	1 1	1		CONT	703	7 4	• •	9-1-	-	60	RIS	20	000	700	. 9	0.0	42.75
1	1	A O	18-1 H	101		:	6492	2 1	4	2 2		1.001			NBGARD	57	100	212	0935	~	7.55 1
	567.	TI_NC	4-2 HB	00		SURES	400		PL702	0 2		100	5	36		NO	200		4		
	127776 127776	-0 P	3 2	100.0298		PRES	PL035						0	00			00	200	.963		14.15
10	E	11	U1 46	364	751	TERNAL	7736		2	12		1.00	20	0 0		67.	000	623	1	2 0	•
		1101	37	0.0	2.5	LIVE	P.103		9	-		100	0	2 2		5.0	7.77			1.2	00.0
- 1	100	65.8	7 327	1050	CP25	5	7786		569	020	1	7		00			7		2	-4 10	
1	9	40	19 L	100	155	:	1.6		4	•	:	000	88	2 2		37.	000		1	1.	0
1	•	PCA-1	HBB-1	115	4.5				100	4		790	63	40		20	510	1 200		163	
1	10	18-2	-	288	100		200	RE .	9 6			200	1			~ 0	800	1 100		91	•
1	571	10.	SELEC	352	20		0.00	SSU	0 0	4		000		. 90	:	47	000	54.			00.0
1	֓֞֜֞֜֟֓֓֓֟֟֝֟֟֟֟֟֟ ֓֓֓֞֓֓֓֓֓֓֟֓֓֓֟֓֓֓֓֓֓֓֟֓֓֓֓֟	1468	UBE	513	500		232	9	2	4		000	00	9 4	25	200	900	800	364	5 °	
1	6 272	569	FOCK 7	ne	796	ES	4 8 8	1110	0					0.0	ARD RH	~ 0	40	- 00	9	0	000
- 10	972877	Ex10-6	0	7644		SSURE	7646	4	PL682	5451		100			BOTBOA		40000		0.0935	2	
1		.7 2	VANE	100	100	8	900					2000	526	699		2.5	90.0	100	9	• "	- 1
	15419	365	NEC 1	0.7361	0.503	Chya	0.8:49		PL681	0.545		1						436	6590 3	10.06	6.99
	-02A	155.7	18.62	9433		:	25.5	, '	0	+		140		•. •			0.016	1	5	- 1	
100	2 P417-D2A	6	5.623	0.0	128	i	47.6	. 1	• •	5	1 300	100	956	900		SDEG	000	733	3	. In	7.57
	2	1458	1 2	480	6.6		3480		1	5432	1	3-10	10	٠		2"		ARD.	SET 2	STARD TOES	
	549	0.703	34	OCA COLO	0.1994AD		1.87		10			3	m.	-		RING.	m er	FUTATARD	11	1:83	25.52

			TROM COPY		TO DDC	CABI
523 7 P31VT PRUJECT TEST DATE DAY HA HIN SEC ERCODE HODE SETIDATE HIND-OFF AEDC PROPULSION WIND TUNNEL 573 3 P41T-02A TF419 9/28/726 2721 71 191 28 0 3110/22/74 5727 -1 TRANSCRIC 161	APD 0.9965 0.6524 0.6613 3.034 3.03.42 0.0061 0.0701 0.0266 0.0268 0.3601 0.9946 1.2709 0. APD 0.9965 0.6524 0.6613 3.034 3.03.42 0.00619 0.0294 0.0234 0.3750 0.9937 1.2715 0. APD 0.9962 0.6657 0.6595 0.6747 1.986 0.734 0.769 0.735	RATP PRESSURES RATP D.6515 D.6516 D.6026 D.6026 D.6026 D.6026 D.6026 RATP D.6015 D.6012 D.	# 1.05 27.55 67.5 112.5 157.5 292.5 247.5 292.5 337.5 22.5 67.5 112.5 157.5 202.5 247.5 202.5 337.5 1 1.05	*** GUTBOARD RHS2 *** RING 22:50EG 67.5 112.5 157.5 202.5 247.5 292.5 337.5 22.5 67.5 112.5 157.5 202.5 247.5 292.5 337.5 1 0.003	SET 1 107 104 106 10645 1086 108 108 108 108 108 108 108 108 108 108	PSTCE1 PSTCE2 PSTCE3 PSTCD1 PSTCD2 PSTCD3 PSTC11 PSTC13 PSTRD1 PSTRD2 PSTRD3 PSTR11 PSTR12 PSTR13 PS

The state of the s

TTA-1 TTB-0 PTI NON MAE MAH TPR HAN 109 110 110 110 110 110 110 110 110 110	SEC ERCODE MODE SETIDATE MIND-OFF AEDC PROPULSION SEC ERCODE MODE 3110/27/76 572/ -1 TRANSON1	RK110-6 TT PIA-1 PIG-2 FRALE PIG-2 TAA1 TIB-0 PII NON MAE MA	LIND TUNNE	0063 0,700 1 C3 726,Ce0,UES	10A 0.0536 0.0510	ISHED	43 P1573 133 0.860 086 0.864	ERS - • • • 700 P1701 9993 0.7971		92.5 337.5 .001 1.001 .006 1.001 .966 1.001		.001 0.000 .003 0.001	PHAX 1.0012 1.0012 1.0012
TTA=1 TTB=0 PT1 NC 109 110 1171.7 109 110 1171.7 100 100 000 000 000 000 000 000 000 00	THE CODE HOPE SETIDATE WIND THE CODE HOPE SETIDATE WIND THE CODE HOPE TO THE	Paire Day HR HR SEC ERCODE HODE SETIDATE HIND	OFF AEDC PROPULSTO	1.00 0.00 1.253 0. H16-1 N30-1 85-1	591 0.9945 1.271		14 0 6	PL703 PL704 P1 0.8591 0.8476 0.	ARD PTZ/PTG	57,5 282,5 247,5 1001 1.001 1.001 1001 1.001 1.000 989 0.999 1.000 957 0.973 0.986	SARD RHS2	.001 0.001 0.001 .001 0.001 0.001	021 0.0268 0 031 0.0233 0
	198-2 1046-1 1068-2 1046-1 1068-2 1046-1 1068-2 1046-1 1068-2 1046-1 1068-2 106	REX10-6 TT PIA-1 PIB-2 1040.8 EC ERCODE 2.487 2221.7 PTA-1 PIB-2 1040.8 1001	DE SETIDATE WIND D 3110/27/76 572/	110 1171,7 U1 H6 G34-2 W8 B10-12,5,4820-	0.0265 0.0268 0.0233 0.	69 0.735	P.030 P.035 P.0 0.6517 0.8720 0.0.8533 0.8809 0.	PL693 PL702 0.4217 0.996 0.4244 0.999	e. INB	22.5 67.5 112.5 .001 1.001 1.001 .001 1.001 1.001 .000 0.986 0.998 .974 0.959 0.973 .943 0.939 0.973	2.	2.5 67.5 112.5 006 0.001 0.001 008 0.008 0.002 008 0.002 0.007	1.2710 0.9865 1.2710 0.9884 1.2710 0.9884

*

The state of the s

	-								FROM			1					-		
CANEL	300	4				573 5550	761		1.001	100.	966	1	17.5	140					10
101	1.95	Crost	200	11	ENIM	4 - 4	4 6		1	1-	1	1	2			.0010	2		9
2 4.		100	20.0		PLE	7906	2 400			000	973		5.5	200	,	1.001	1.00	1.002	STRIP
Sept of	.0770	354	1 1		of c	1:1	244CTESS		9.	1 6	• •		-	-			1.		PST
5 700	15	5.7	2401		1		1 .		1.001	100	0.007		2.7.5	n. n.		0.01		55	-
Thauda	1.24	30-1 05-1 33314 1-9.	1.1				ъ т.	4		1	1	:		1 1		1	1	-	PST
FTC	30.0	130	0.9057				2		1.061	1.0.0	. 677	. 68	202.5	1.01		0.0280		9.0.51	
	.00	20-1=0+4 0=p.	000			11	1 4 4	Though atoker	1	1	1	u,				6	F ?		STEP
100	10	1 6 1	3820		1	0.9764	1 1	1 4	1.0.1		0.956	OAPD	57.5	0.00		0.002	2	0623	•
NIND-0F	-	3 2	100		4	439		3000		1	1	INB	100	1 1			9 9	90	STP32
	1343.	614-2	028n		SKURE	8720	ا م د	}	412.5	20.	0.005	:	17.	0.00		9851		25	
T: DATE 0/24/74	1 _	9	0.0		28.0	6.0				1	1			1		0		0.9492	STeb
SFT;	===	9 10	122	355	REAL	1 1	474	+	1.001		. 93		47.	0.008		1	1	-	PST
7	110	610 U1	400	3	N.T.	510.10 0.8524 0.8554	FL603	4		1	1			!!!	•	1.2593		.259	1013
900	7.	· n	14	.701	7				1.001	66	. 9		22.			" "			PST
ODE #	073.	L7 J77	0.0704	30	1HC3-	0500	346	9		1	1		5	07	0	9057	2	1.000	1012
	1 -	90	1 1	155	•	900	9 3	1 1	337,	0.987	90		337	0.010		- 0	1	-	PSTC
"	1373.8	4n S1	115 0066 0028	CP4			1.3439	347	4.5	1	1					.0066	- 1		12
	1:	- 4	00	2.271				1	1.0	0			292	0.00		00	•		PSTC11
SEC.	1496	ECT	301.57 301.57 205.18	1 1		0.0462	PRESSURE PL690 0.3487	4	45	25	556		2.4	2.5		3829	250	5739	
5.4	+4	Sete	301	14VG 0. P749		400	PESS 0.3		247.5	-	00	:	247	0.011	1				STCD3
9 6	1605	u.F.	1014	#		9840	1 40	2/8:0	4.0	0	52	15		2000		.0232	6		•
272	170	× 6	1.0	150 1587	:	7. 884.0	3 P. 0	4 2	1.002	:	9 6	9HS2	200	- 4	200	00	2 4	0.027	STCD2
TE 8,75	1	5×0×8	155	SM C G	RES	15:	FLOUNETER 682 PLORA 4718 0.471	1 4	157.5	000	27.4	3049	5.2	9.00		90	1 1	453	0
DATE DISALL	3.169	-	1.5149	100	SERVES	P. 470	Pt 682	e de la	4.			DITT	13	-		0.0290	4	0.04	Tr.Ds
	4	VAV.		3 0		1 1		1 7	110.5	1.031	0.070	:	112.5		,	1			PST
1643	532.4	6	0.5049	119.	84 SY42 88	0.8764	2,621			-				1	5	0.9544	7	0.050.0	17063
		VANES		4.5	•				1.00.1	1.010	0.073		47.5	9.00.0					PSTCES
P#30501	1063.6	- 1	0.9831	9.674 0.674		0.811	Dicen.	1	1.	1	1		5		7	0.0704	0.0306		
4		4.035	60	1		9 = 4	90	1	25 e 1F 2	000	40.		22. E 3E G	0,018					PSTCE3
2C1.T PR3UE	4.69	:	9.5	154		25	2		3		1		2		1	000	5 7 3		- 1
+ 4	F.847 1605.5	1,244	CHITACA &	11364		CV73CA50	CUTACAE		4		5		2	P. W	1414 561	CUTSCARD	Cutacash	INACAFO	PetrE1
4 4	:		127	Ē		2.	3	1	9				-		3	3	2.4	;=	•

	TUNNEL	SCHEN :	8:0.0	64 54 5		200		9.7423		1	- 1	1.001	. 6		317.5	0.001				PSTP13
	STON KIND	0.0265 0	13 .726.0±0.0±8	6.6		0.7901	ETEOS	5000.0			1	060.0			,	500.0			1.0011	PSTP12
	PROPULSTON PROPULSTON	1.243 0	130-1 B5-1	1.2405			1819	2724.		+	1	-		:	,		4		0.0187	PETPI
	AEFC	.00.00	16-1 130	0.9054			t Nus	0 2454.0	•	1				B RVS7 .		100.0	T	0.034	0.0.52	PSTPDE
	1 Nn-0FF	0-0	G*4-2 HR-1 MJK-1	0.3424		0.9066		0 9060	+Con-i		1	1.301		INGUYA			5	9.6065	C.042	STPD2
	SETIDATE SETION S	11 1343.	H6 GT4-2	0.0290	0.447	no.		16	•	1	1	985 0.098		:		00.000	200	0.9492	0.9002	PSTPD4 P
		774-1-779 110 11	L7 J27 E10 U1 M6	0.0281	9 2	100		0.3585		1	001	929 0.	44 0.		-	000	9.00	1.2724	1.2594	STC13 P
	CODE HOD	1074.7	1 L7 J27	0.0704	648 0.701	0.9527		0.3567		1	001	040	943 0.			0.010 -1.000			1.000	STC12 PS
-	# H	1074.7	140 S19	0.0061 0.0025	273 n.		: 4	0.3565		*	400	0.060	931			0.000		0.0025		Cl ₁ PS
	#IN SEC	4 pre-2	SELECT	424-FS 301.78 208.91	19 2.	0.8466	SSUME.	9.3583			1	0.975 0				0.010	-	3426	0.5758	Se soo
-	H 94 Y 40	77 074-1 7n 1596.6	TUBE		8.0 8.4	0.9454	16 4 al	0.4757	12/210	4 :		1.000	. 955	RMS2	5.	0.005	108	1	0.0275	20 PS
	14TE	149	1 SH	6144	45 A.	.0700	1,60	4750	934RD-	25.5	1.900	0.000	0.074	11740AR	157.5	0.004	105 0280	82C0.	9240	D1 PS
	TEST	537.7 3	FO VANE	0.4152 n	0.41% 0.646 0.40% 0.000	0.4774 0		0.4737 0	- Out	***	- 1	1.001	- 1			7.034	194 0	1.0511	0.0411 n.	STEEN PST
-	PESUECT		BETS VANED	0.0057	7.404 p.	0.8116		6736				. 0003				10.004				0
-	61.13	2. 1241 A. A.A. 1641.5	AL D+ A B:	00	1 1 1	11		00		96.20		1,007	1.047		22.5056	-1.000	+	~	0	a
	1973	1.047	4 4	CUTACAED PA 9C4+D	Cutacaed	GUTACTUD GRACES		CUTSCAFS		*	-	-,	•		9710		CUTACARD	TATA SET	INDCAFO	PSTCES

	TUNNEL	SCHER 0 1	+				0.8547	1000	7411		nu1	100.	900			100	D DAD				STRIS
	KIND	5 0.45	1 2016-010-5	0.0545			120	:	0004 0.	1	100	060	0.073 0		5.5	0.005	Y.K	1.0011	4	1.0011	STR12 P
	POPULSTON	243 0.024	85-1 C3	1.2405		270	0.78	Pare 1				001	0.047		47.5			0.0412 0.9365	6120	0.93A5	STELL PS
	AETC PR	0.00 1.	130-1	0.9955				100	0.6	200 6 0	100.	1.003	920	Rrss				0.0280	13.0.	0.0154	TRD'S PC
	n-0FF	0-0-0	AP-1 H14-4 N30-1 B5-1	3839		-	0.9067 0.9124	1	06 n. 8583	TNEOARE-PT	1.001	1.00.1	0.956	MACABI		0.00	645	.0n31	- 1	0.0624	PD2 PS
	ATE WIND	144.9	674-2	0280		3	975 9716 8800	1	1.090	NT	1,001	1.00 E	n. 962			0.001		0.9892 0	9900	2646	STRD, PST
	SET:DATE	A-1 478-n 09 111	0 U1 M6 G14-2	104 0282 0275 0	0.647	RNAL	8521 0. 8540 0.	167	.3457	1.17	1,00	0.985	0.93			0.00	a d	2727	1	1.2554 0.	TCI3 PST
	E MUE	1074.9 11A	L7 J77 E10	0.0700	0.701	7.5	8525 0.8	1	3387 0.	200	*1	6 0.958	9 -		2	000		.0050	1	1.0004 1.	CI2 PSTC
	ERCOD	074.7 10	510	120053	0.648		0.85	1 1	3479 0.	101	1.0	0.090	0.0		33	000		0061 0.	-	-1	PST
	SEC	697.5 10	CT 140	7.87 0.0	2.171		853 97A	4	00	202	1.		955 0.93		2 0	011 0.008		3635 0.0	268	5780	3 PSTC11
	NI W AL	695.9 1	E SELE	478 247 456 245	0.8750 0.8813		9.0	A DR	71 0.346	10 000	1.0	90	96	2	20	ċ	1	200	6	0	PSTCD3
-	255	560	FOR TUB	1	1. P586 0. 8647	3	10 0.8454 11 0.5931	-	0.4571	3480-PT2/PT(999 1.000	1	DART PMS2		500.0		10 0.028		28 0.0275	PSTCD2
	PATE O	8 3.177	VANET S	3 0.5961	3.548	u	0.000		A 0.4579	143	-	1.001	90	*** OUT30		0.004	1	1 0.0240	A041.0. A	n.06	PSTCD1
	TEST TO	.5 -32.0	VENED	0.5773	0.415	•	9.8752	1 1	1				073	•	67.5 112.		1	7.0545	44546	0.0513	PSTCER
	SELLT PESUE	104	PCT.	0.000	9.3		1.9105	9	0.4870	0303	,	1	7.548 0.		25.Eneg 6	000	1 4	0.0770	90200	0.0434	DETLES
	5	r.P47 1464.0	41014	CUTACAKD HACAED	CUTSCAED		CUTSCAFO		**************************************	9116					PINE 25		1414.581.	- 1	CLTACASS	INSCARD	PSTCE1 6
	-			=			1		5	'					•		1	=	- 4		

and the second of the second

			11		18		E IS BEST	3 0 2	O D	DC _	T		1		1	1
3	## /# #E SCWED	C.8 -726.0=0.0±3	104 0.0465 0.0755	11	of California ass	4n16 n.7946		2 111 2	ORK 0.	347		1.4	0.004 0.005	1.0007	1.0007	51012
PROPULST	1.1.75 0.01	N30-1 B5-1	1.241			C. C C C C C C C	0.743 1.		987	200		247.5	1.00.	0.9047	9000	11072
»Erc	3.00 0.00	16-1 130	1.0010			66 N # 8 0	1 .	3 000	1	c e c	2	200	. 4	0.0295	0.0454	STODY P
MIND-DFF	-0	2 Mm-1 L1	0.5004		4	0.6512	0200	1			1 Bill	5 157.5		10612 0.0195	6.1016	100
SETIDATE		#6 G14-	0.0295	41 0.825	-	0.8434		76 49	- 1	960 n.08n 922 n.042 605 r.02P	:	= 9	•	0.9487	0.9480	STebs
NODE SE	1101	F10	0.0462	841 0.82	61939	0.7727	0.3191	22.5	000 1.	955 C.		.609 0.01	29	1.2611	1.2382	PSTC13 P
ERCODE NO	-1 PCB-6	519 L7 J27	100	0.625 0.843 0.625 0.843	1	0.7798	0.3142	337.5	- 1	.995		337.5		1.0017	1.0134	PSTC12 F
	4.0 1453	140	5 0.00	2.729			7 0.3206 3 0.3169	282.5	1.000	0.036		~ 4 0	2	0.00%		PSTC11
P 182 G	3.3 177	F SELECT	352.1	0.8103 0.8097	1		0.321	4774	1.00	000	:	247.5		0.5004	0.8995	PSTC03
DAY	560 177	SHOCK TURE	3.52	1.8290 0.8574 0.85	4	0.870 0.828	0.5045 8 0.5012	1		107 1.000 104 0.092 160 0.045	5	200.000		0.0407	0.0442	PSTCD2
74.	2.5	VANE I SI	0.00	0.487	6.4	9.7.4	7.592 0.592 0.500	7	0	999	40FT110	151	1	0.0394	0.1016	PSTrū1
CT TEST	1444.7 304.0	VANED	7 0.8541	0.519 0.487		1000	0.5619	1	-	0.978 0.944 0.974 p.934 0.911 p.915	:	67.5 112.5 0.012 0.008	1	0.0465	0.0755	PSTCES
AT PROJECT	1773.3 144	ae7.	11	2.4	4	9.4075	0.5034	d		0.050		4.000 57.5	1	0.1004	0.100	PSTres
EAST PCINT	6.546 17	AL Pre	CUT3CA5D	CUTRCA ⁶ D 449rA ⁶ D	Carage and	6.40641	CUTBCARD INDEASD	2 344				PING 23		CUTSCA50 0.300	1196450	PSTrE1

1.									PY		741;						2
UNNEL	SCUED	-			950	503	1	0 0	946	22		337.5	200				STAI
-	1 5	1020.023	-	1 5	5.5	0.950	1 7			1				1 1 2	100	3	•
UNIN	2 0.0	1	990.	HON-97a	3.5	9 9 9 9 9 9 9 9 9 9 9 9 9 9 9 9 9 9 9 9	1	986	0.0	018		2.5	900.0	NA C		65	STP12
NOL	N. 010	2	00	1 9	4.4		1					2	٠,			1-	PAT
ur	. 1	1:	2412	1 1 1	1 "	8 1.	1 1	087	0 2 4	025		2.	20.0		803	n. 8371	=
Thava	91.	1	1-1			0.7439		6	e e			787	c	7 6	•	-	1013
0	1 1-	130-1 PS-1	55	111		\$ 400	4	00	960	52	:	n. d	200	45	9	\$ 5	-
PE'		- 6	.0.0.	111		1,707 0.	0467-01940		-		REST	200	-	. 00	0.0.0	0.0446	130.
		-			1.1	0.77	9	000.	000	44	0	2.4	15		1	1	PST
-066	1 :	17	5007	111	200	1 1 1	9.0	1.0	000	0.0	80AP	157.5		Tucks	680	0.000	STRDS
ENTH	10:	3 6	00	1 3	900	0.969	440	00	200	30	-	2.4	4	1 7	, 9		PST
	6 45	3	200	S S S UNES	8036	1		4.0	n.082	n.03n	:	112	0.0		646	9491	
DATE	1 -	U1 M6 G74-2 ha-1 min-1	00	1 1 4	400					807		2					STRD
SET:D	41	5.	1 3 5	CRESS 0.825 TERNAL	125	1 200	1 3	1.00	90	9.9		47.5	0.0	!	00	4	0
	10	E13	198	40 1	0.773	0.319			1	-		1		0. 4	1.56	1.239	1013
30		37 E	00				300	00.1	9.99	. 6		22.5			. (1	PST
E HO	53.	25	1000	40 3	0.7805	0.374A			1	1		1		1 15	0	1.0128	1012
RCOD	-	519 17	00	0.125	100		1	1.09	1.005	.0.		337.5	0.0	9.	1	1-	PST
a a	53.4 53.4	5	112			3226		1	1	1				1 1	030		1
	9 -	- 4	000	25.00		40.0	1 6	1.00	1.001	9.90		292.	010.0	1	9		STC11
SEC	PTR-2	-	1.45	1~~	136	4 04		1	1	1		1		1 1-	79	8841	0
2		ELECT.		100	0.833	essua 8,590 0.322 9.331		1.900	9.950	9.0		247.5	0.01	7	0.537	9.0	TCD3
DAY HB FILL	113.1	l o		9.0	100	a			1	1	:			1 1	1	1	PS
1	77	SCK TUBE	41.4		828	0.504 0.4098	614/51	1.00.	1.001	40.0	B4S2	000	0.00	9 8	0435	0.0435	200
0	2 2 3	Ž Š	1	0.0288 6.8504 6.8504	400	5	19-0		1	1	6	1		1 1.	1	1	PST
PATE	1:	S.	\$51	1 9	900	5021 5021	8 C		0.990	.04	40F	157.	0.007		9.0.0	4 6	6
40	4 4.0	I ANE I	100	0.487 9.089	0.390	4 5 4	a a	1	1	1	Tuc	1		1 7	= 4	4=	STC
-	. 1:	13	223		424	1	• (0.090	0.045	2.01	:	112.	0.015		2	35	•
TEST	305	0	n.8522	7.511 7.511	7.8427 0.8244	0.501		1	1	1		1		1 4	0.026	0.0743	PSTCEX
	:	VANEO	1	1			1	1.048	A.050	1.026		47.5	0.0	4		1	10
PCINT PROJECT	6.9 6 173.7 1444.8 305.2	9676	0.049	1::	5. 8.02 9.8.03	0.5023			1	1			1	1 3	4000	0.106	E5
P P P	12	19 1	00	100	4 00	dee		00.	1000	r.650		25.5056			-	40	PSTCES
.13	17.3		00	25	00	24	1 8		1	-		12	1	1 4	1	90	1
-		4 1 P. 4	CUTACAED	CUTACA ^E D	CUTSCAFD PASCAFD	CUTSCAFD	1			1		olve.		£414_SE1_4	TAPEARD	CLTSCAPD INSCAFD	PETCES
PAGT			3	51	3	37	1	1	1"	1		•		1 4	= 72	\$-	•
1		11						1	1	1					1		1

								THIS	PAGE	IS B	LS	HE	010	DDC	-	-	-				
	TUNNEL	SC-ER	9				0.7959		8495		800	903	9 80		37.5	0.005					STRIS
	I.I.	4 c	44-1 Lik-1 N30-1 05-1 C3	10.0564		4	220		50		. 987	940	. 918			n. 104 n	1		1.000	1.0004	STP12 P
	POPUL STON	17 0.009	05-1 (1)	1.2413		J-18-44		111	14 0.00		800	0.955 0	613			0.005		0.0045	16091	0.8973	9 119
	6 0	771.1 00.	N.30-1	1.0008	1 1			Ħ,	3 0.7448 F 0.748	/610	000	960	. 055	58	2.5	0.00.0		100	1	0.0445 0	0 F D
	1	-0.00	1 Likes	4083 1. 5150 1.			6507		0.770	4		1	9.4	OAS RM		0.001		5	1		bd
	41.4P-	5.0 0.8		1 - 1		ans	0		0.0303	đ,	עם יו	280	934	INB		3.004	1 .			n 0.0994	PSTeD2
	SETIDATE	118-A P	M6 G14-2	0.000		9	0.813				100	962 0	307 0			0.005 ".	1 6	0.048	•	0.949	PSTPD1
-	25	109	50	0.0491	1 0.	INTERNAL	0.7727		0.3165		00	95	955 0.				6	1.2513	1.5011	1.2397	STC13
1	DE MOD	457.0	L7 J27 E10 BC0=1-2,1	0.9097	6.0	7-00	0.7800	6	0.3141	1	100		e e		1	10 7.00		1.0009	0000	1.0125	C12 P
	ENCO	456.9 1	140 S19	712 000d6 0038	3 0.8				3766		.100 1.0	+ 6	00		5 337.5		1	30.86	A5 40		11 PS
000	53	780.1 1	ECT 1	8.63 0. 5.34 0.	2.71		8335	ā	3224 0.	1 "		70	.929 n.9		5.5	15 1.009		983 0.		018	9.5
1	12 102 12 102	779.4 1	13S 3	84 348 53 345	0.8106		00	ad	2n 0.3		-	90	045 0.9	2	7.5 247	0	lei	01 0.4		0	PSTCD3
	255	568	40CK TUB	6.4	. 0201		0.829	UNE TE	0.50	579	-	† -	ç è	SHA CH	00	c	108	0.0	0.0	0.0434	PSTCD2
27.0	218510	7.562	VF1 SH	0.8714 0.8714	0.000	3 1	0.0000	J	A 4004	CUTROARD.		• •	200	AGETHO	5 157.5		100	0	0000	n.0994	STCD1
	1549	307.2	2	9.8442	0.511 0	E NP	0.9235	197	0.4576		9.08	0.0	0.01	:	112.	5.n1	101	0.0564	,,,,,,,,,,,,,,,,,,,,,,,,,,,,,,,,,,,,,,,	1.0741	STEE3 P
1000	841.000	1446.2	.1	90,0.0	0.4.0		0.9000		0.4697			1	1		6 47.5		Inl		2000		
	100	1779.4	* A BCT	100			0.6			66	000.0	r. 977	7.450		25. FDEG	1.00.			-		D.
	1 1 1	9.55	41 Pr A	CUTSCA-D 44-CA-S	CUTECAPO		CUTRCALO		CUTSCA ⁶ D IAGCA ⁶ D	9110	-		-		5114	٠. ١	135 414	rutar	EATA SET	INSCAFD	PSTCE

1177	### ##################################
### ### ### ### ### ### ### ### #### ####	115 0.0 574:1 3.177
117	### ##################################
F7100 HPR 118 118 118 118 118 118 118 118 118 11	### ##################################
	A A A A A A A A A A A A A A A A A A A

DJY HR MIN SEC FRODE MODE SF154TF HIND-DFF	1. TEST DATE DAY HE HIN SEC ERCDE MODE STIDITE HIND-OFF 1. SAR. O S. 1276	AETC PROPULSION WIND TUNNEL	0.00 1.270 0.056 0.850 1	-1 A30-1 P5-1 C3 0-27-743-41 1-27-726-C-0-U±S	0.0052 1.2607 0.0530 0.0050 1.2714 0.0515		0.243 PL573 0.7891 0.8546 1.7735 1.45992	00 PERSON	1010	1.001 1.001 1.	000.0	0.987 0.978 0.	RVS2	5 247.5 292.5	0,003 0.004 0.006 0.003	275 n.972 1.001r	9.034	1.001.
DAY HR MIN SEC ERCE F69 1600.1 1696.5 1072.3 1 F69 1600.1 1696.5 1072.3 1 F01 10 1 1 10 1 1 1 1 1 1 1 1 1 1 1 1 1	## PROUJET TEST DATE DAY HR MIN SEC FREE ## 1 NEQ.] ## 10 PETTON ## 1	MIND-DE	1736.4 0-0	0-1:.5.x820-1=0.HIC	0.0275 0.3805 0.0957 0.3655	9955500	0,848n 0,9047	0.9993	0 0000 U	000 1.001 1.001	984 0.097 1.001	938 n.963 C.956	INBOARD	112.5 157.5	0.005 0.001	62 Inc12	0.989n 0.0807 0	20000 15000
224 HR MIN SEC	### ### ### ### ### ### ### ### ### ##	 ACODE MODE	2.3 1n72.4 110	0 519 L7 J27 E10 U3	100	0.700 0.	.8553	6 0.3809 0.381	20010 - 11010	1.001 1.001	0.587 0.958	0.943 7.944		337.5 22.5	0.010006	PD PD PD 8	4 0.9040	1
THE TOTAL OF THE PARTY OF THE P	## ## ## ## ## ## ## ## ## ## ## ## ##	DAY HR MIN SE	569 1690.1 1696.5 107	HOCK TUBE SELECT	7,094 299,77	7 0.8507 0.8764 2.259	0.8860 0.8869 9-0.8936 0.8953	0.492A 0.3842 0.	26010	1.001 1.001 1.	1.001 0.974 D.	n.055 0.955 0.	** 5348 BAADE	202.5 247.5	0.00\$ 0.010	108 13L 119	0.6272 6.3657 6.00	0.0277

-								Fis	OM C	OPY	UR	115	ED	10	DDC		-	-		-	
	TUNNEL	SCHER 1	4				0.8549	1 1	7484		1.001	1.001	956.0		137.5	0.00					PSTPIT
	ON THE	15 0. a 50	. 724.0-0.0=5	0.0530		PLEN	7741 0.	y a	6666			0.000	0.973					1.0010		1.0013	STRIS
	TRANCOLE	270 0.026	05-1 C3	1,2407		274	e e	1			1				247.5	0.00	7,1	0.9420		0.9.70	STDI. P
-	AETC PR	0.00	0-9:924	0.9652				1400	50	n-019/610-e	1	1	1.076	cs.				0.0275		0.0157	STREE PS
1	ND-UFF	0-0-0	HA-1 mik-	3800			0.905n	1	905 0.50	7	1.001	1		R CAAOS	157.5	0.01		.0027		.0431	STRDS PST
-	34	1.35.1	200	100000000000000000000000000000000000000		ESSUB	8482	1	1.000	*	3	1.096	0.961	:	112.5			9851		0.988 0	-
1	21107575	10 111	0 L1 M6 G44	0282 0	12	CONL INTERNAL PR	8529 0.	1	6.3872		-	0.00	0.93		•	0.00	9	.2697 0.		1.25e1 0.	CI3 PSTab.
1	and a	7.6 1	L7 J27 E10	701 0.	201	K1-1m00	8520 C.	1 1.	3862 6.		1.00	000.0	90		.,	500.		050		1.001 1.	PST C
1 0	E ACODE	72.4 107	14n S19 L7	0 00	0.548			1 9	3846 0.3		7 -	7 -	1			0.010		59 0.		1.0	PSTCI
	100	6.4 10		1 0.0	2.286		22	4	00		1	0.97	0.03			0.008		0.0		96	PSTC11
21.3	2 4	5.4.1	F SELECT	303.	7.847 0.8807		2 0.3472	9	A 0.3A61	:	-	000	4 4.	:	~	5 0.011		00		6 0.5805	PSTCD3
3	223	560 150	SCK TUR	3.03	8611 8611	•	0.896	PL 643	0.408	9-27	1.00	1.00	2.05	DARD BHS2		200.0 000		0.029	1	0.0576	PSTCD2
17.	9270270	3.174	LE SH	0.6177	0 649	il.	0.0000	400	4.4905	WT 604R	1	7 -	8 0.973	FING		0	-	0.0275	0000	0.0531	PSTCD1
1	14.1	-33.1	VANED VAN	0.6085	0.411	ASS. RAKE PR	0.9777	1	4004-0	•		1	24 0.078	:		1	10.	0.0530	0130	1.0515	PSTCET P
4000	S SALES	4 1050.7	BETA VANE	0.9851			0.4417	0 0 0	0.45RE			1	1		47		tat	0.1701		1.0.0	PSTCE2 PS
		. 2061 965.4	3.6 18	CUTBCAFD			CUTACA ^E D 149CA ² D		14964F0	1		400.	0.947		VE 25. EDES	000.0	F 174 SET 4	-	~		PETCE1 PS
9.0				CUT.	CUTE		CUT		101			-	-		PIVE		Lay	CuT	141	IN	Sid

### ### ### ### ### ### ### ### ### ##	PROPULCION WIND T	1.253 n.nn63 r n-1 P5-1 C3	1.271	P1543 P1573 0.81543 0.8617	P. A.	1.00. 1.00.	247.5 292.5 337.5	4 4 4 4 4 4 4 4 4 4 4 4 4 4 4 4 4 4 4	0 0.9375 1.0007 potelly potelly potelly
#EST [ATE DAY HR MIN SEC ERCODE HODE AND	4 590, usin	6 G74-2 KR-1 HIGH 0.70	100 0243 0.3401 0.0000000000000000000000000000000000	55 CUBE	04.00 01.000 0.000	7.001 1.001 1.000	110.5 157.5 202.	0.005 0.001 0.005 0.001 0.002 0.002 0.002 0.002	PSTPD2 PS
7551 1245 560 1446.0 1466.7 146 17 17 146 17 146 17 146 17 17 17 17 17 17 17 17 17 17 17 17 17	ODE MODE SET	Sie L7 J77 E10	101 57 0.0675 0.0637 0.0637	6,734 0.74 6,662 6,662 6,662	5,429 6,4300 0,4311 0,430	1372. 1 1001 1 001 0 999 1 000 0 998 1 000 0 988 0 988	317.5 22.5	9.008 -0.004 0.00 9.008 -0.004 0.00 P. P. P	1.0017 1.2564 PSTC12 PSTC13 PS
#EST PATE ##F0 VANET SHO ##F	H P IN SEC	50 1466.0 1466.7 1 THRE SELECT 1	498 W2R-F5 3.01.97 0. 3.00.91 0. 2 0. 5.0.91 0. 2.0.91	6514 0.7754 1.97 6646 6.4798 1.96 688 6.480 0.8862 0.8691	DECEMBRESSURE	1.000 1.000 1. 1.000 0.005 0. 1.00 0.976 0. 0.080 0.963 0.	202.5 247.5 29	108 1001 0 0 0 0 0 0 0 0 0 0 0 0 0 0 0 0	0.029n 0.5746 STCD2 PSTCD3 PS
10.00 0 0 0 0 0 0 0 0 0 0 0 0 0 0 0 0 0	PEYTO	SA. 0 363.1 2.495 VANED VANET SHO	65 0.6493 0.6586 83 0.4432 0.6596	28 SSU28	0,5299 0.5305 0,5299 0.5305 0,5299 0.5306	1.000	112.5 157.	104 104 104 1053 100 100 100 100 100 100 100 100 100 10	37 0.0511 0.0436 PSTCE3 PSTCD1 P

							11						ISI							
DANEL	Scuen					8624		7971		.041	.001	100.		27.5	.003					STRIS
		9.6.0.6	0.0533			101	1	0			1						1.0007	600.1	1.0035	STOI2 P
STORE STORE	F2 0.00	95-1 C3	2711				4	-							1	1	.0140		. 9177	-
		130-1	9044				1961	66				27.5	45.	1			-			Ans peto
	0.00	-1 Hike	1			645 9111	1	2. 46	044n BT		0.0.	957	CAAD			1	. 5		0630	200
_	# 2	14-2 HP	00		1 3	400	1	900.	441 -00	036			12		1			•	0	PSTP
10/24/	110	1 H6 G	10	٠ ا د		400		0 4		.001	986.	936		5.2	90	à	.00	•	0	PSTPD.
	110	7 E10 U	100	9	1 5	400	1	1	1 6	1	1	1		,	0	9 9	1.27	1		PSTC13
200	1066.	17 J	10.0			0.8551	2597	.438	1 2		200	52			1	1	1.994		1.0015	STC12
	106	140 S1	112	43	1 1		1	429		101	010	34					0.0057			STC11 P
	146	LECT			Ī	1.8972	TRE .	310	•	.001	979.	.963		7.5	111	,	3400	1	.5764	CD3
+	4	S				9864	8 2	1	01476		1	1	25H	2.5	.00	4 6	6960	940	1660	CD2 PST
7	4.	SHOCK	3573	48	9. 6		1 1	0 0	34RD P		1	1	90480		1	1	0		1	PST
- 1		VANET	1 0		6 4	11	11		100			1	00		m		1	'	6	F PSTCD1
	57.2 36	VANFO	1	1 1	•			1	"		1	1			1	1 5				PSTEES
	17. n 10	95.74	0.0		0.0	0.84		1			1	1				1 6	-	-	0.76	PSTCES
'	-	1 P+4	UTBCAGD	2001	1496469	INSCASO		14364FB		-				0146 25		1. 551	UTACATO	17. SET	INSCARD	PSTCE1
	3 Dest. Dis 15410 0/200/76 2731 11 581 26 0 0 2110/20/76 505/ -2 120/20/76 505/ -2 120/20/76 505/ -2	DAMESTED TESTO 0/30/76 231 1: 581 26	A BARTINGS, TFAIR 0.23070 2731 11 581 26 0 0 0 0 0 0 0 0 0 0 0 0 0 0 0 0 0 0	1447.n 1n57.2 76%.n 2.482 K69 1467.0 1468.1 1066.8 166.8 110 110 1171.9 0-0.0n n.ng 1.282 n.ng 1.282 n.ng 1.202 1447.n 1n57.2 76%.n 2.482 K69 1467.0 1468.1 1066.8 110 110 110 1171.9 0-0.0n n.ng 1.282 n.ng 1.202	DEFINED TESTS OF STATES TO STATE THE TESTS OF STATES THE TOTAL STATES THE TOTAL STATES TO STATES THE TOTAL S	1447.n 1n57.2 763.n 2.462 6231 11581 26 6.0 1.0 219.02176 5121 0.0 1.0 1.0 1.0 1.0 1.0 1.0 1.0 1.0 1.	1447.0 1057.0 763.0 7.482 869 1447.0 1466.1 1066.8 110 110 1171.0 0.0.0.0.0 0.0.0.0 0.0.0.0 0.0 0.0.0 0.0 0.0.0 0.0.0 0.0.0 0.	1447.0 1561.0 0.30079, 2381 1 201.0	A	10 10 10 10 10 10 10 10	### ### #### #### ####################	### #### #############################	### ##################################	### #### #############################	### ### #### #########################	### #### #############################	### ### ##############################	######################################	## 1 1 1 1 1 1 1 1 1 1 1 1 1 1 1 1 1 1	######################################

			11		PHON	COFY	PURB	ISH	10 TO	DOC	-	-	-				1	1	
TUNNEL	.700 1	5.4				.8621		0.7976		1.011	1.091	0.001		337.5	0.003				FSTP13
UIVD.	0043 0.7	3 Perceb	0.0534		PLEN	n. 8457 n.	CD C.	000		.00.	1000	1.068			0.010	100	4	1.000#	STP12
PBNPUL STON	252 0.0	N30-1 P5-1 C3 N-733+461=2-796+6=0+0=5	1.2711				tanife t	. P 492 1.		1.001	1.000	0.0 A				0 1	4.0.4	0.9377	d Hors
AETC P	0.00	0 × 30 × 0 × 0 × 0 × 0 × 0 × 0 × 0 × 0 ×	0.004				4,	5	4	1.003	000	0.673	FMS;	202.5		1 nc s		0.0.45	40.
n-0FF	0-0-0	890 1:01 029	0.3597			9057	1		0048	1.0.1	1.001	0.957	UE TUBU	157.5	0.00	120	1	1	T90 96T
TE MIND-	H 10		0263		4	6736 0 8411 0		159	*Oak!	.00.	260.	0.050	•••	112.5	. 00 0	2880	43	2	8
SETIDATE 2110/2017	110	4610-12.E	106 0268 0789 0.289	0.736	1 9	6533 0		.4253		-	100		-		0.00	W 1	•	0	13 PSTeD1
ЭДСИ	8.4 110	L7 J27 E10	197 0677 0638 0.0	992.0	7 "	8553 0.		,		1:	1	ċ			4 6	7		115 1.5	PSTCI
FRCODE		5.7	00057 0.0	0.735	• • •	9.0	0			7-	100.0	•		8	9.0.0			1.0	PSTC12
200	0.1 10	- 9	00	1.970		- 0		00		-	100	ė			700.0	1			PSTC11
HIN SEC	9.1 147		301.47	. 4764 . 4802	90710			0.4325		-	0.975	•	:		0.011		4		PSTCD3
DAY HR	9= 1	5000	3.014	. P613 n	S	00	FLOMETER.	0.5285	P12/8	1	1	•	SHH G	, ,		00	1	1 20	STC02
DATE 0,20,74	496 .		0.6573	.578 D	RESSURES PLAZO	0.0000	9, 48,	0.5285	ALT BOARD.	4-	900.0	6	DUTROAR		0.006	0.0263	1540	2	STroj P
1651	on!		0.6485	0.415	14 GM 2 -0	~ 4		0.5241	٦	1		1	:	5 112.5		409	4	=	PSTCE3 PS
PROJECT PART ROS	108	ASS SAUS	1.08A5	0.404		0.6477		5286 5386						67.		0.0477		=	PSTCE, PS
9 1 1 1 9	400							66		1.00.		n. 671		22. 40FG	-1.00.	+ 1	0	_	
F467	e.70c	= -	CUT9CAFO FARCAFO	CHTGCAFD		CUT9CA50		CUTACARD				-		9146	٠. ٠	CUTSCAFD	Curacase	INGCARD	PSTCE1

The second secon

	QNIA B		-104 n.0542	HING DIG	400	1.0008 n.7391	15	0.000 1.001		792.5 337.5 n.nna q.qua n.no6 n.on3	1.001	1.001
	inavaa :	30-1 P5-1	54 1.2694			P. B.	1.001	1.1.	1:1	707.5 247.5	0.04	54 n.9 th
-	1 T	Min-1 N	124 0.9054 567 0.9054		247	0 4 4 5 6 5 6 6 6 6 6 6 6 6 6 6 6 6 6 6 6	1.001 1.001	1 1.	00	0.00% 7.00 0.00% 7.00 0.00% 0.00	700	0632 0.0354
1		14-2 HP-1	10C 1DL 0277 0.3424 0249 0.3663	32808848	8719 0.5047 8861 0.9129		-	0 0 0 0 0 0 0 0 0 0 0 0 0 0 0 0 0 0 0	INB INB	120.5 13	-	0.949n 0.0432
	5 SET: DATE 0 2110/20/7 114-1 178-0 1	10 U1 H6 C	.0263 0.0	0.646 0.646	8520 0.	.3468	1.001	0.984 0.984 3.0.989		0.009	2146	.25en
	PCR-P-TT	L7 J27 E1	0.0709 0.040-0	647 0.700 (0.6529 0. 0.8500-01	0.3465 0.0.3495 -0.3495	1.00	0.547 0.951 0.560 0.971 0.543 0.943	1 1	337.5 22.5 0.010 0.009 0.010 0.005	24	1.0019
	PCA-1	140 519	0.0060	268 0.		0.3503	100			0.004 0.0 0.008 0.0	50	
	HIN SEC	ECT.	300.71	n.8757 2.	0.8857 0.8957	PRESSURE PL600 7 0.3498 0.3476	1.001	0.974		0.004	101	0.5824
	PA 740	Ser Tube	3.007	0.8587 0.0.0.0.0.0.0.0.0.0.0.0.0.0.0.0.0.0.0.	0.480 0.4857 0.8931	PL653 0.471 0.470	400	3	BMS2	03 000.5 04 0.004	100	0.0274
	DATE PASOTA	ANE 1	n.6117	0.473 0.409 BRESSUE	0.000	4 - 4	12	000 0 000	e Tu	112.5 157.5 0.003 0.004 0.004	7==	0.0632
	CT TEST		9.6	0.413	9 9.876	0.4714 55 9.4714		4.000		67.5 11; 0.009 C.	7 - 1	0.0514
	PCINT PROJECT	A geti	0 0.004	0.402	D 0.8109	0.4713	4	200.		22. 4763	1 1	0 0.9640
	2	V 40 1V	CUTACAFD	CUTSCAFD PABCASD	CUTACAED 14964ED	CUTBCAFD	-			2 7. 0	CUTPCASO CUTPCASO CATA SET 2	INSCAFD

TEST TATE DAT HA MIN NEC ERCODE MODE SETTEDATE MIND-OFF AETC PROPULSTON W
\$101 01 \$11 TO 0 6 \$110 \$14 \ 000 \ 01 THE
AIPPA 9FTA VANFO VANFI SMOCK TUBE SELECT 140 S19 L7 J27 E10 L1 M6 G14-2 MA-1 HTA-1 N30-1 D5-1 C3
CUTRCARD 0.9040 0.5079 0.6173 3.034 0.0059 0.0705 0.0281 0.076 0.3804 0.9653 1.2807 0.0539 1.0805 0.0539 1.0805 0.0539 0.0539
CUTACAEO 0.417 0.413 0.471 0.8586 0.8758 2.283 0.647 0.700 0.646 - TABCAEO 0.446 0.471 0.8586 0.8758 2.285 0.647 0.700 0.646 - TABCAEO 0.466 0.411 0.000 0.8586 0.8788 0.8785 0.885 0.647 0.700 0.646
0.76
59 0.4754 0.3540 0.3527 0.3523 0.3514 0.9995 0.4552 54 0.4754 0.3500 0.3520 0.3523 0.3514 0.9995 0.4552 54 0.4751 0.3500 0.3520 0.3523 0.354
130 D C
1.071 1.071 1.001
*** DITTADARD RMS2 ***
#IVG 25.505G 47,5 112,5 157.5 502.5 247.5 292.5 317.5 22.5 47.5 112.5 157.5 502.5 547.5 502.5 317.5 50.5 4.0 4 5.0
0.0775 0.0530 0.0276 0.0281 0.3504 0.0059 0.9953 1.2657 0.9848 0.0129 0.0276 0.9744 1.0011 0.0442 0.0534 0.0278 0.3623 0.0044 0.9953 1.2273 0.9898 0.9898 0.0059 0.0059 0.0059 0.0059
FURSCARD 0.0435 0.0457 0.0081 0.0244 1.0014 1.2544 0.0443 0.0454 0.0454 0.0454 0.0454 0.0454 1.0014
PSTCE3 PSTCD1 PSTCD3 PSTCD1 PSTCD2 PSTCD3 PSTcD4 PSTcD2 PSTcD1 PSTc

The state of the s

							TROM	PAG	IS V	BICST	QU!	LI:	DC DC	RACTI:	CARL	
	TUNNEL	ASC 1	540.		10	1.8551	0.7397	166	. 10	0.996		337.5	0.Cn3			PSTRIX
	ON HIND	n.6267 n.	.726.0±0.0±3	0.0541 0.0541	HIN-DIENIN	25 1	.0006	604	1.00.	0000		200.6	A.00.		1 1	10
	PROPULSTON	1.276 n.	130-1 p5-1	1.2494			0.8475 1			1.001		2.730	n. n.	0.944A		cro1,
	AETC P	0.00	0=7.739	0.0055		1 tx	24	2/0/0		1.076	RVS9	202.5	0 4	0.0276	10.00	STap. p
	"INN-OFF	0-0-0	Wang un	0.3821		4.4.4	1 - 1	-		0.956	INECAPR	157.5	0.0	9	999.0	9 200
	SET10476 %1	1 127.6 0	614-2	0.0274	PAESSUA	0.8723	0.9904	i	1	7.098	:	- 6	- 1	0.0		90.
	26711	10 11	460-1=2.114610-1=.5.482041=0.110=7	105 . 0277	0.546 0.546 WTERNAL D	.8524	3548			0.000		1	5 0.008	694		G 13
	HODE HODE	060.5 T	1 327 E	.0705 0	6 0.700 6 0.700		.3541 0 .3563 0	1	-	3 0.944		5 22.5	- 1	25	410	12
	ERCODE	069.6 1	140 519 1	712 0064 0.	69.6		526	333.4	-	946 0.946 932 0.943		1	0.010		1	Sa
-	SÉC	694.8 1	Ect 1	114 0.	2.25		572 0.	3	- 6	950 6.0			11 0.00P		!	D3 PSTC11
	NI WIN	603.9 1	JBF SEL	7.001 300 2.000 200	0.8758	1 1 4		1	-	000	29	0.5 247.5 not 0.004	- 1	100		Pet
	TE DAY	74 560 1	SHOCK TO	45.6	0.8592 0.8617		a 4	1		.005 n.084	SHR GRACE	147.5 203		100	•	PSTCD
-	-	3.1	VANET	10.0	413 0.671 410 0.609 5442 BEESSU				7	6.000 6. 0.078 0.	••• PI'Ta	112,5 15		-		STCD
-	1651	6.4 534	VANED	0.5613	66					7.074		47.5 11		0.0		0
	PROJECT	21.0.10	BET.	n. 0840	0.601	0.8412	0.4754	930				19		0.0	9.00.00	PCTCE,
	Fat Pelet	n. 85r 1601.0 1046.4 534.0	11 Pt A	CHECASE	CUTBCAFD	CLITPLASD 148(46D	CUTBCARD 1ABCARD	3410	-4.			DINC 2		CUTOCARD	CATA SET	p'eTrës

FAST BOLLS TEST TEST DATE DAY HE MIN SEC ERCOTE MODE SFILDET MINN-OF	
	F AECC PROPULSION WIND TUNNEL
P. ESF 1774.7 1444.9 104.0 2.553 469 1774.7 1775.2 1453.5 1453.1 109 110 1467.1 0-	0.00 0.00 1.715 0.0001 0.550 1
ALDEA META VANCO VANET SHOCK THAF SELECT 140 STO L7 J27 E10 L1 MF GT4-2 MA-5	2 ME-1 Hite-1 130-1 P5-1 C3
75.0	2107 0.9862 1.2811 0.0295 2028 0.9879 0.2815 0.0294
143 CP265	
CAR RAMP ERESSURES - 0.0	NETO DIO DIEN
CHIEFERD 6.9424 6.9334 6.9393 6.9408 6.9214 6.927 6.9314 6.549	9467 0.8847 0.92n4 5490 0.4764 0.9140
PRESSURE ***	CANTROL DARBNETERS
7 0.4711 0.413 0.4317 0.3593 0.3580 0.3577 7 0.4536 0.4518 0.4312 0.3577 0.3577 0.3594	0.0217 0.0141 1.0001 0.8659
81MG 22 50EG 47 E 112 E 127 E 202 E 117 E 202 E 117 E 22 E 12 E 152	ij.
1. nan 1.	1,000 1,001 1,003
1.000 1.000 1.001 1.001 0.990 0.984 0.996 1.000 6.992 0.998 0.998 0.992 0.991 0.972 0.960 0.960 0.997 0.986 0.946 0.946 0.968 0.948 0.976 0.963 0.947 0.968 0.948 0.977	1. 100. 1. 100
*** 0(1304RD BMS2 ***	DARD RVS2
BINE 29. FDEG 47.5 112.5 147.5 202.5 247.5 292.5 337.5 22.5 47.5 112.5 15 15 15 15 15 15 15 15 15 15 15 15 15	157.5 202.5 247.5 202.5 337.5 0.004 0.005 0.003 0.003 0.004 0.003 0.003
107 104 10C 10R 10L T12 PD PDP 82 1V 0.01781 0.0011	17C45 BRIN BRAX 0.0147 0.9428 1.0004 0.0140 0.5448 1.0004
0.0144 0.0295 0.0125 0.0142 0.3311 0.8924 1.2214 0.9921 0.7141 0.0740	G.0202 n.944m 1.
PETEL POTCES PSTCER PSTCOS PSTCOS PSTCOS PSTCOS PSTCOS PSTCOS PSTCOS PSTCOS	PSTRIP PSTRIP PSTRIP PSTRIP

The state of the s

	11	11	11	11	111	11	ROM C	PY	FURN	ISHI	D TO	DDC	RACTIO	TI
WIND TUNNEL	7 - 49 - 5 CHEP	6-0-0-0	0.0754		43 PLFNIH	645 600 700 61731 9998 0,7277		3 +	0.055 0.059		337.5	0.004 0.004	1.0n1n	1.0015
PBOBULSTON	100 us/ut	1 85-1 CA	1.2597			Parenet ne ne n		0	1.000		747.5	1.0.0	0.0000	0.906
AEFC	30	6-1 130	1.0018			0,7919 0.7 0,7916 0.7	0 4		2000		20.		0.037	0.0470
1Nn-0FF	## WOW	Wang Ly	10L 0.5237 0.5547		6.6604 6.8604 6.8604	9907 9.	9 1		100.0	13	-	3 0.074	0.0040	0.0064
	1-178-6- PTI- 111 1330-4	6 684-2	0.0172		0.8110 0.8110	9.00	1	1	76 0.095	:	112.	5.0	0.9792	0.9*02 0.9*02 STDD.
	774-1-17 110	1 - 11	0.0361	80	F.030 P.0.752 0	6.3199 0.324A	11	100	657 6 637		1.1		1.2597	1.2380
RCODE HODE	1072.5	S19 L7 J27	C.1002 0.6971	9.0	21026 0.7809 0.7869	6.3220 0.3220	11		9.98		1	0.013	1.0014	1.0134
EA	-2 PCA-1	140 S1	0.0047	2.641 0.651 2.637		0.3239	300	100	0.030		292.5	.010	0.00690 6.00650	STC14
HIN SEC	9.4 1700.	SELECT	351.68	8151 8202	0.8365	PRESSURE- 0.3243	1 1	9	6.929	:	247.5	6.015	100	0.8569
	11 61	OCK TUBE	3.519 7.510	7921 0	0.8312	0.5077	19/214		1	4D 9KS2	000		1	0.0442 0.0442 STCD2
PATE	3.184	2	0.7:57 0.7:57	000	8 670 0 0.0000	0.5079 0.5079	14		20000	10Fags	17	3 6.015	0.0372	0.0064
	5 536.0	VENED VAN	0.7000	0.519 0.	0.450 PB	r.5077	1 1	1	1	1	7.5 227.8		1.0770	0.0754 0.0754
PETAT PROJECT	1989	pets V	0.900	0.0	0.779	0.50BE	950	- 1			1 1	50	1	0.0079
EAST PC1.T	r. 95r 1603.4	1	CUTPCARD	CUTACASD	1285.45 1285.4	CUTBCARD PARCAGD					25 SING 25.	•	C(19645)	
												436762		

in the market of the

:	
-	
-	
•	
-	
-	
••	
EADT	
7	
-	
•	
••	
:	
•	

### ### #### #### ####################	1			15/3				211	24/76	618/ -1		TRANSONIC	10 167	39000
	1.00	V41.50	# ·	= = = = =	ECT	7	1968-2 1-02-4	714-1 7 7-619-01 82-1, 461	18-7 B	N. T.	HAH 0.2.73	3.41 122	9	TOS SE
#155 N.2 MA NSP TANG #156 N.2 MA NSP TANG #167 N.2 MAN NSP TANG #167 N	00	1,6784	1 6 6	#28 3.504	17.7	712 0.0040	101	40		1.0	1.000	25.0	10.0	
### PARESSURES *** *** COUL INTERNAL DRESSURES *** *** BLATE PLATE		2 1 2	44.000.0	2000	80	627 CP	60	CP3						
PLATE PLASS PLASS PLASS PLASS PLOSS		d= 70	PRESSURE	:			00	INTE	ORES	. v3		1:	1	1:
*** CONTROL PRESSURE *** *** CONTROL PRESSURE *** *** CONTROL PRESSURE *** *** CASTA CA	PLATE 0.72	04 - 9.450 67 1.476	مَود	0 10	640		7 8 6	.775	870	9,045 0.6404 0.5458			7410	195
*** NUTSDAR PLORY PLORY PLOSO			. 51	WMETER	RESSURE	•					PATRO	PARAL	TERS	1.
*** NUT21AP3 PT2/PT3 *** *** NUT21AP3 PT2/PT3 *** *** NUT21AP3 PT2/PT3 *** *** NUT21AP3 PT2/PT3 *** *** NUT21 1:001 1:002 1:003 1:003 1:001	1	1 1	PL682	500	300	321	329	325	acc	. 6905 9306	102	1 1	7000	1701
7.576 47.5 112.5 137.5 207.5 247.5 297.5 337.5 22.5 47.5 112.5 157.5 207.5 247.5 797.5 137.5 1601 1.00		•	OUT23AP	PT2/PT	:				1 .	VPO BR	10/0	:		
	9		" 7		1.000	5.00	1	1 1	1 1	1 1	1 1	247.5	1 1	327.5
### 107 104 105 104 106 10	4 % f		100		0.942	500	1 9	100		1 1	1 1	2000	1 1	0.020
C.03 0.073 (.103 0.073 0.053 0.074 0.004 0.013 0.055 0.005 0.003 0.004 0.003 0.004 0.003 0.005 0	1 20		40=T440	-55H2-6						+	6518			
7.00	1		739	1	975	200	1	3:	3.0	10	600	2.60.0	0.003	
1 107 104 105 105 109 101 112 PD PDP P2 Inciz Incis Dulv Dulv Dulv District Control Co	- 1	1	, ,	•		.011	200	0.0	3 0.	00	6.0	0.000	0.004	
0.0572 0.0750 0.0315 0.0442 0.5541 0.0040 1.0007 1.2559 0.9401 0.0003 0.0315 0.9341 1.0003 0.9401 0.0003 0.0315 0.9044 1.0020 0.95541 0.0045 0.0044 1.0007 0.9792 0.0989 0.0521 0.9034 1.0007 0.3074 0.0777 0.0949 0.0442 0.0044 0.0044 1.0007 0.0401 0.0401 0.0401 0.0041 0.0020 0.0521 0.0040 0.0051 0.0040 0.0051 0.0040 0.0051 0.0040 0.0051 0.0040 0.0051 0.0051 0.0051	-		105		IDL		PD	PDP	20	Incaz	10045	1	×4.0	1
0.0007 0.0777 0.0899 0.0889 0.8845 1.0140 1.2374 0.9792 0.0989 0.0521 0.0134 1.0007 0.0974 0.0989 0.0521 0.0134 1.0007 0.0974 0.0974 0.0974 1.0007 0.0974 0.0974 0.0047 0.0027 0.0027 0.0047 0.0027 0.	·	!	0.0315		0.5541			1.2550	0.9401	-	0.015		60.	
- sires - ssrep - ssrep, astrop astrop astrop astrop astrop astrop astrop astrop			(# 0	.038	ac ab		1.0140	1.2374		00	. 0 F 2	0.0034	1.0007	
7.25 7.17 0.00 0.00 0.00 0.00 0.00 0.00 7.75			1.	3 5	STEED B	1	1			\$100p	STEPS		21013	1019

UNVEL	SCHEN	s s				:	573 F017		701		900	926		3.05 9.09	900			257818
161	9	A.C=0.L	IPA	0.0714		PLENIN	nec	45 ···	009 099		1	0.030		0.005 0.00		1.0024	200	Stale as
ST.OSNYE	74/41 007.	- 55-1 FS	90	.2501		1 376	1.7	ARACTE	7729 - 0.99		1	0.075		100	E	9000	9750	130 10130
460 00 TE	HAM TO	2.733.	Pr	0013				ONTROL P	99 0.77	2/PT0	1	0.091	-83-65-	0.000	400	0.557	1 -	- 1
-966	N. WAR	-1=0. HL 0=		5411 1.		:	345 6597 6638	3	PL79	JARD PT	1 1	0.00	3044G	0.004	• .	0 6900	0050	SO PSIAN
76 (18)	PTI NCN	6,4820		0.0257 0.		RESSURES	015 P. 8912 6.		PL702	avi	200	953	*	0.003	200	.9755 0.	90	STORE OF
2:10/24/7	1 TTB-ñ	6-		0.0467 0.0	6.739	ERNAL D	795 C.		93 999 041		67.5	0.935		0.003	5	1	md	3 PSTAD
900×	8-2 TIA-	37			0.768 C	COAL INT	A7A 0.7		92 PL6 994 0.3		1.00		'	3.008	1.004	117 1.2591	11.5	651613
ERCOBE 0	CA-1 PC	519 t7		46 0.0967	CP155 0.737	:	PL07		1 PL6		m	0.953		0.003	0.01	1		051610
37	PTR-2 PC	Rado	54 112	130	2.273		6.3	3E	PL69		10.5m		1	0.003	-	00.0	1 1	15154
6: 46: 3	PTA-1 P	E 65LE07	1	7 350.67	7446		P149	PRESSUR	PL690 7 0.4025	TO	1.00	000	•	3 0.013	0	90	5 0.8410 3 0.5423	P\$1c03
5 273:	=	3920		1.507	7. P.	5	PL489	OWMETER .	PL683 0.545 0.543	D P72/P		44	0	mo	-	0.046	0.0196	PSIch
9/23/7	REY10-6	14.53	45-100	9.7450	0.302	PRESSURE	PL 470 9.7541	14	PL542 6.5456 0.5440	0UT304R	77	70 0.904	947	3 0.0n3		0.0257	0.0958	PSIcal
TF 410	2000	14.76 14	2534	0.7463	75 0.503	da Va	91450 0.8448		9.5448 7.5448	:	.010 -112.5	1	1	1	10.014	0.0714	0.0736	P\$1553
P417-124	9	0.006 18	35	1.975	0.484	:	PL 415 0.7075 0.7009		0.5449		400.00		1	, -	107	3.0043	0 4	SSTARS D
421 7 P41T-02A	F. 4. 104.	3.0		IN 3CACD	CUT MER ^C D		1196450		CUTSCAFD		alve 25.				, Ser	7.5	101	SETCES B

Tanaci e	SCHED	S=0				:	. F029-		.7889		337.5 1.001	1	0.003	0 1			PSTRIP.
10 167	MT NB	26.0=0.	101	0.0711		C PLENUM	7749	FBS	200		1.000	030	1.00	200	1.0015	1.0012	24.05
THANSON	TP/ 44 dd7	3. HL 1=2.7	9.0	1.2580		74	ā : c	PARAUET	1751	:	7.7.5	0.07 9.04	5.0	0.13	Pulv.	0.9054	4 10.30
•	34%	0=2.73		1.0015	2			CONTROL	757 PL 7973 6.	PT2/PT0	2000	981	3,000	0.00	0.0214	0.0474	3.85
14n-0F6-	NEN KAE	20-1=0.H.		0.5576		v3.	P. 045 0.6405 0.0649	:	9849 0.7 0523 0.7	NPCARD	11.00.1	4 4 4	0.00	0.00	0.007	1.1	35
24/76 6	TB-ñ PT1	1 - 5 . AB	Inc	0.0256		PRESCUE	9.615 0.8226		20.0	:	12.5	cc	3 0.003	2.00	0.9754	1.	24.35 139
2:10/	114-1 TTB	=2.1, AP10-	104	0.0461	S CP355	INTERNAL	FL030 6.7811 6.7772		PL693 0.4062 0.4066		22.5 67. 9.000-1.001	00	103 0.00		PDP 1.2589	1.2403	PSICIA PS
0 0	19701	7. RC0-1=	InT	0.0975	SS CP25	1×00	PL020 0.7883 0.6010		FL692 0.4614 0.4043		1.001 1.0		003 0.00	013 0.0	1.0015	1.0132	0.00
	PCA-1	140 ST	T12	0.0055	2 CP1			:	PL691 0.4064 0.4023		292.5 3. 1.001 1		0.003 0.000	.011	712 0.0085 0.0055		PSICI, PS
30: 1	1 PT9-2	erect	HZA-FS	350.28	AVG . #1952.		P. 400 0.6398 0.6477	ESSURE	PL690 0.4555 0.4048	:	1.000	0.945	0.6n3	600	10L 0.5010 0.5576	0.8380	9SIC03 PS
273: 74	71 PTA-1 558 147215	4-TUBE 5	HOR	1.503	7 T	:	P. 480 0.6158-	METER PR	PL683 0.5461 0.5448	PT2/PT0	1.00.1		0.00.0	0.011	0.0460	0.0192	O.O.
9/20/16	PEX10-6	S 6	ME 4100	0.7538	0.502 - 0.8	ESSURES.	PL470	*** FLOW	PL642 4.5:61-	OUTBOARD	1.001	3	737	0.011	105 0.0254	0.0056	Stepi BS
16410	1000	18.70 14.5	2:34		0.512 0. 0.501 0.	EAVP PR	PL450 0.6467 0.6317		21641 0.5454 0.5464	:	112.5	5.4	6000	5.3	104	0.0736	6.65
5 P41T-724		-0.001 18.	50	0.975	475 0.485 0.485	:	PL215 0.7006 0.8005		0.5643		1.601 1.001	1 1		r.nnk 6.n12	0.0675	0.1047	7.40
454 ° 841T-124	1. 1. 1. 1. 1. 1. 1. 1. 1. 1. 1. 1. 1. 1	3.0 -0.		INSCARD	Cut geafe INSCARD		TAPEAED INCERED		CUTECARB -		PING 22		10.5.00	•	CALASTI CHITOCAES INBCAES	CUTRCA SET 2	7.87

						1			FR		COP		KN	LSHED	101	U	-				
WIND TUNNEL	T MB SCHED	6.C=0.U=S	1DA 0.0734		PLENUY	PL57	690 0.9017	45 ···	00 P1701	97.11		.5 377.	985 1.00	25		0.003	0.00	XYnd	1.0021	1.0015	States giarac
TRANSONIC	TPP WA/WT	3, HL 1=2.72	dud.		270	1 10 1	6.0	PASAVETE	712 017	7767	:	2.7.5	600	1.959		0.00.0	0.00	NIAG	ח. פחגה	1.907	Tory of
1 FPC	PAN	14-1-N30	1.000	-				· CONTRO		-	PT2/5T0	202		1 0.691	4459	2000	0.0	-	0.0553	0.0474	P8790
WIND-OFF	NON	820-1=0.	101	5	UPES	P. 045	0.04	:	1702	. 0534	INDOART	.5 15		37 0.944	Ť.	n63 0.0n3	0	0.00	0.000	0.3951	2.50
T: D: TE	110 n pri	0-12.5,A	170	33	AL PRESS	P. 045				c	:	7.5 11	100	936		003 n.	003 n.		0.9754	0.9789	PSTOD!
0 2:	2 114-1 7	7 610 UT	1DR 0.0353	55 CP3	WL INTERN	PL030	7		PL693	4		r	100	0.010		7.00 M 0.			1.2556	1.2407	PSICIS
ERCOPE-MO	PCA-	S10 47-32	101	155 CP	00	PL020	900		PL692	3 0.434		1		0.954	;	0.003	015	4	1.0009	1.0129	PSICIP
	PTR-2 PCA-1	140 BB0	S 712	2.87			9	:	PL691	2 0.402		282		0.038		0.0	0.01		0.0036	1	PSICIA
7: 34: 46	114	E SELECT	850x9	45 8216		PL490	6 0.847	PRESSUR	PL690	4 0 5	10	24		0.945		0	00		0	3 0.834	PSTCD3
6 273:	560 143	SHOCK TUB!	1,2R	SP	:: 5	PLARO	0.641	LOWMETCR	P1 6P3	7 0.546	4D PT2/P	5	-	75 n. 049	1	00.0 200		1	3 0.0463	0.030	PSICO
9 9/20/7	REX11-6	4.53	*	1.00	Bagesile	01470	0.745		PL682	0.545	OUTBOA	112.5 157		0.073 0.092 9.648 0.975	04110		7.013 0.0		0.625	0.0951	PST CO.
7651	3 2 3 3	VANES VANEI-	, FB2		d^ 7	1	P. 6317		PL681		•	67.5 11					0.012		90.000	0.0734	633250
PC +T PG0JECT	1484.9.986;P	. 0 . 0 . 0	£2.	11		PLATS			0.910			. DEG		1		נו בניים		1 107	0.0675	1,0064	7.47
475	1	3.0	Cerses C	CUTOCAPO INSCAPO		900000	1. acard			INSCARD		81 NE 22		•		,	. 41	EATA SET	0,706,1	Curacasa	7.83

		-									THIS	OOF	Y FU	RN	ST QU	TO	DDC	-				
FUNE	SCHED	San	11.				:	573	6 2		1701		337.5	1.000	0.957	1	0.013	6.00				sterse
151	2	726.C=0.U=	IDA	0.071			C PLENUY	543	7690 ".	F25	700 P		1.000.	200	954	1	9.00 e		XYHO	1.0022	1.0013	1
TALVENTE	TPP WA/WT	3. HL 1:2.7		1.2504			70	14		PARAMET	7740 01	:	7.7.5	. 4	00	1	0.00	0.0		1.915k	0.9070	=
1	30	0=2.73	6	1.0009						CCNTROL	707 PL 7919 n.	PT3/cT0	200.	-		453	20.00	0	17045	0.0260	0.0471	4
623/ -1	NCN MAR	20-1=0.H	17.	0.543			••• >30	045	0.0640	:	702 PL 9646 n. 9533 n.	INDOARD	1 1.001	1	00	6-1	400		1012	0.0084	0.0046	4
124/76 6	119 1177.5	12. 6. 4B	170	0.026			L PRESSU	0	0.8713		95.5	:	112.	9	5.03		0n3 n.ng3		25	0.9756	0.9764	26 100130
0 2:10	114-1 17	A 210	108	0.0462	S CP3SS	;	INTERNAL	1030	0.7767		PL693 0.4042		00 1.001	10	0.0	1		6	PDP	1.2556	1.2408	3
-	PCB-2	. RCO-1=2.1	-	0.0990	S CP25		1×00	1020	0.8006		F.692 6.4034 0.4052		337.5 22				500		04	1.000	1.0129	4
	PCA-1	-140-519 RBC-1=7	112	0.0038	NW	243	-			:	PL691 0.4071		292.5 33	- 1	- 1		0.033 0.0	011	:	0.0038		PSICLY PS
38: 54	1 PTB-2		KOR-FS	352.35	. 00	212		1490	0.6463	essure .	PL690 0.4063 0.4059	:	1.000-1	1050	. 936		0.003	600	tol	0.5404	0.8302	3
273: 7:	17 PTA- 560 14714	K TUBE-S	HON T	1.523	4	281 0.	:	480	0.8407	METER OR	PL683 0.5483	P72/P73	1.002	3 6		2	0.003	0.011	2 5	0.0462	0.0791	1
9120176	REX10-6	FI- SHOCK	MFR:00	0.7581	NS 41		Papsyged	C .	0.7449	*** 510%	PL682 0.5489	OUTBOARD		7	0.605	##0#1# 9	0.005	0	100	0.0260	0.0946	4
76410		74 14.53	VFB2			0.502.0	440	05010	4.8308		0.5481	•	117.5	- 1	66		1	2 0.n13		n.071	0.0730	a
	1 1 1 1 1 1 1 1 1 1 1 1 1 1 1 1 1 1 1	-0.001 18.74 14.53	60	1.9754	85%	6.4.9	:	PL 435	0.700;		0.5477			. 1	61 0.054	1	0.03	0.012	101	0000.0	0.0000	ત
426 . P417-524	· ** · · · · · · · · · · · · · · · · ·	3.0 -0.	9.10.50		1	INBCARD			149C4FD		Cureca60		BING 22. EDEG	1	100.0	9 70 3710	1	,000	CATA SET	TA SCAFD	CUTRCARD	4

APPENDIX C

LIST OF COMMON SYMBOLS AND CONVENTIONS

```
d
     shock tube diameter
IDA
     average distortion index
IDC total circumferential distortion index
IDL stall margin allocation ratio
                                               see Table 5.1
IDR total radial distortion index
IDT total distortion index
     Mach number
PSi overpressure at i'th claw probe (i=1,2,3)
     shock overpressure at blast arrival (scaled to 1 atm. ambient
     pressure conditions)
     pressure
     pre-blast tunnel ambient pressure
     total pressure
Pto
     re-blast tunnel total pressure
Pt<sub>2</sub>
     average engine face total pressure (psf)
     average engine face total pressure for inboard inlet (nondimensional)
R2I
R20
     average engine face total pressure for outboard inlet (nondimensional)
     distance from end of shock tube
r
     fan stall margin (Sec. 8.3)
SM
     pre-blast tunnel total temperature (OR)
TT
W2
     engine-face weight flow
W2R
     engine-face weight flow corrected to standard conditions (for
     full scale inlet (1b/sec)
= W2x(TT/519) 1/2 / (P<sub>t</sub> /2116)
side-slip angle
W2R
     side-slip angle
     polar angle from shock tube axis
     angle between shock tube axis and wind tunnel axis
     blast intercept angle (between a normal to the blast
     front and the inlet longitudinal axis)
```

Notes:

In most pressure plots in this report the ordinate label designates the variable measured and the vertical scale is either pressure/ p_t or pressure/ p_o , the latter being designated by an asterisk after the label.

All blast pressure values in this report designated as Δp are scaled to a tunnel ambient pressure of one atmosphere. The actual test values can be obtained by dividing Δp by the ambient pressure in atmospheres (obtained from P in Appendix B).

Inlet mass flow rates in this report are always expressed in terms of full scale inlet conditions. To obtain model values divide by 100.

A separate table of symbols is provided for Appendix B in that appendix.

DISTRIBUTION LIST

DEPARTMENT OF DEFENSE

Assistant to the Secretary of Defense Atomic Energy ATTN: Executive Assistant

Defense Documentation Center 12 cy ATTN: DD

Defense Nuclear Agency

ATTN: SPAS
ATTN: DDST
ATTN: STSP
4 cy ATTN: TITL

Field Command Defense Nuclear Agency ATTN: FCPR

Livermore Division, Fld. Command, DNA Lawrence Livermore Laboratory ATTN: FCPRL

Commandant NATO School (SHAPE)

ATTN: U.S. Documents Officer

Under Secy. of Def. for Rsch. & Engrg.
ATTN: Strategic & Space Systems (OS)
ATTN: Strategic & Space Systems, M. Atkins

DEPARTMENT OF ARMY

Harry Diamond Laboratories
Department of the Army
ATTN: DELHD-N-NP
ATTN: DELHD-N-P, J. Gwaltney

U.S. Army Ballistic Research Labs. ATTN: DRXBR-BLE, W. Taylor ATTN: DRDAR-BLV, J. Meszaros

U.S. Army Materiel Dev. & Readiness Cmd.
ATTN: DRCDE-D, L. Flynn

U.S. Army Nuclear & Chemical Agency ATTN: Library

DEPARTMENT OF THE NAVY

Naval Material Command ATTN: MAT 08T-22

Naval Research Laboratory ATTN: Code 2627, Tech. Lib.

Naval Surface Weapons Center ATTN: K. Caudle

Naval Weapons Evaluation Facility ATTN: L. Oliver

Office of Naval Research ATTN: Code 464

Strategic Systems Project Office ATTN: NSP-272

DEPARTMENT OF THE AIR FORCE

Aeronautical Systems Division, AFSC ATTN: ENFT, R. Bachman 4 cy ATTN: ENFTV, D. Ward

Air Force Aero-Propulsion Laboratory
ATTN: M. Stibich

Air Force Materials Laboratory ATTN: MBE, G. Schmitt

Air Force Weapons Laboratory
ATTN: DYV, A. Sharp
ATTN: SUL
ATTN: DYV, G. Campbell

Foreign Technology Division, AFSC ATTN: PDBF, Mr. Spring

Strategic Air Command/XPFS
Department of the Air Force
ATTN: XPFS, B. Stephan

DEPARTMENT OF DEFENSE CONTRACTORS

Aerospace Corp.
ATTN: W. Barry

Avco Research & Systems Group ATTN: J. Patrick ATTN: P. Grady

Boeing Co.
ATTN: R. Dyrdahl
ATTN: S. Strack
ATTN: E. York

Boeing Wichita Co.
ATTN: R. Syring

Calspan Corp.
ATTN: M. Dunn

Effects Technology, Inc. ATTN: E. Bick ATTN: R. Parisse ATTN: R. Wengler

General Dynamics Corp.
ATTN: R. Shemensky

General Electric Co.-TEMPO Center for Advanced Studies ATTN: DASIAC

General Research Corp.
ATTN: T. Stathacopoulos

Kaman AviDyne
Division of Kaman Sciences Corp.
ATTN: N. Hobbs
ATTN: R. Ruetenik
ATTN: E. Criscione
ATTN: R. Smiley

Kaman Sciences Corp. ATTN: D. Sachs

DEPARTMENT OF DEFENSE CONTRACTORS (Continued)

Los Alamos Technical Assoc., Inc. ATTN: P. Hughes

McDonnell Douglas Corp. ATTN: J. McGrew

Prototype Development Associates, Inc. ATTN: C. Thacker ATTN: J. McDonald

R & D Associates
ATTN: C. MacDonald
ATTN: J. Carpenter
ATTN: F. Field
ATTN: A. Kuhl

Rockwell International Corp. ATTN: R. Sparling ATTN: R. Moonan

DEPARTMENT OF DEFENSE CONTRACTORS (Continued)

Sandia Laboratories ATTN: Doc. Con. for A. Lieber

Science Applications, Inc. ATTN: D. Hove

Science Applications, Inc. ATTN: J. Dishon

SRI International ATTN: G. Abrahamson